UC San Diego

UC San Diego Electronic Theses and Dissertations

Title

Fluid origins, paths, and fluid-rock reactions at convergent margins, using halogens, Cl stable isotopes, and alkali metals as geochemical tracers

Permalink

https://escholarship.org/uc/item/7xj422dq

Author

Wei, Wei

Publication Date

2007

Peer reviewed|Thesis/dissertation

eScholarship.org Powered by the California Digital Library
University of California

UNIVERSITY OF CALIFORNIA, SAN DIEGO

Fluid Origins, Paths, and Fluid-Rock Reactions At Convergent Margins, Using Halogens, Cl Stable Isotopes, and Alkali Metals As Geochemical Tracers

A dissertation submitted in partial satisfaction of the

requirements for the degree Doctor of Philosophy

in

Earth Sciences

by

Wei Wei

Committee in charge:

Professor Miriam Kastner, Chair
Professor Neal Driscoll
Professor Joris Gieskes
Professor David Hilton
Professor Arthur Spivack
Professor Mark Thiemens

2007

©Copyrights

Wei Wei, 2007

All rights reserved

The dissertation of Wei Wei is approved, and it is acceptable in quality and form for publication on microfilm:

_____

_____

_____

_____

_____

_____

Chair

University of California, San Diego

2007

TABLE OF CONTENTS

LIST OF FIGURES

LIST OF TABLES

ACKNOWLEDGEMENTS

First and foremost, I would like to express my deepest gratitude to my research advisor, Professor Miriam Kastner, for her never-ending support, both financially and emotionally, ingenious guidance and cordial encouragement throughout my PhD education at Scripps. Dr. Kastner is a scientist from whom I have not only learned the intriguing geologic and geochemical process on Earth, but also an enthusiastic, diligent and meticulous scientific attitude and a sincere, honest and confident professional approach. Dr. Kastner's more than three decades of pioneering research in geological and geochemical science has been constant inspirations for me. Never can I thank enough the other members of my supervisory committee. Arthur Spivack, Professor at Graduate school of Oceanography, University of Rhode Island, showed great kindness and generosity to invite me to use the Mass Spectrometer in his lab many times for the past seven years. I am also indebted to him for his warm accommodations and the enlightening conversation. Joris Gieskes gives me constant jovial and insightful guidance, from whom I can always seek help. David Hilton is always prompt for any of my questions and provided me very precious samples collected during his fieldtrip, which is integral to my research on Cl isotope cycling in arc volcanoes. Neal Driscoll contributes to the understanding of convergent margins from a geophysicist perspective, along with many laughs and joyous spirits. Mark Thiemens, Professor at Chemistry and Biochemistry department and Dean of Division of Physical Science, kindly agreed to serve on my committee despite his very busy schedule. They have given me far-reaching edification and stimulating counsel.

Very special thanks go to Prof. Lui-H Chan, Professor at Department of Geology and Geophysics, Louisiana State University, for her Li isotope analysis. During the collaboration, she showed me a meticulous and honest attitude toward even the most tedious lab work. I am also indebted to Robert Rosenbauer at U.S. Geological Survey at Menlo Park and Yishai Weinstain at Department of Geography, Bar Ilan University, Ramat Gan, Israel, for their tremendous help and guidance on the hydrothermal experiment projects.

Many special thanks also go to Gustaf Arrhenius, who provided me unconditional caring and support in many aspects of my research progress. I would also like to thank Professor Pat Castillo, Doug Macdougall, Gunter Lugmair to teach and allow me to use the Mass spectrometer for Sr isotope analysis, Chris MacIssac for his help in laboratory, Jim Hawkins for providing me precious samples and broad petrology background, Bruce Deck and Evelyn York for the assistance on the instruments at Analytical Facility, and Andrew Dickson for his scientific and partial financial support during my time working at Analytical Facility.

My endless thanks also go to the best co-workers one could wish for: Gretchen Robertson, Evan Solomon, Annette Deyhle, Barbra Ransom, for their friendship and altruistic assistance.

I would never have completed my Ph.D. degree without the constant and friendly support from the faculty and staff at Scripps Institution of Oceanography, and the financial support from National Science Foundation and the Academic Senate of the University California, San Diego.

Finally, I must end with the people whose love and support are unconditional and unreserved, my father Jin-he Wei, my mother Zhi-zhen Shi, my sister Jing Wei, my brother-in-law Zhou-xin, Shen, and more recently, my husband, Chao Zheng.

Chapter 2, in part, has been submitted for publication as it appears in *ODP Leg 195 Scientific Results*. Wei Wei, Miriam Kastner, Annette Deyhle, Arthur J. Spivack (2005). Geochemical cycling of halogens and boron and its implications for fluid-rock reactions in the non-accretionary Mariana supra-subduction zone. 23 pages. The dissertation author is the primary investigator and author of the paper.

Chapter 2, in part, will be submitted to Earth and Planetary Science Letters, Wei Wei, Miriam Kastner, Arthur J. Spivack. Chlorine stable isotopes and halogen concentrations in convergent margins with implications for Cl isotope cycling. The dissertation author is the primary investigator and author of the paper.

Chapter 3, in part, will be submitted to Earth and Planetary Science Letters, Wei Wei, Lui H. Chan, Miriam Kastner, Robert Rosenbauer, Yishai Weinstein. Alkali elements mobility, Li and Sr isotope exchanges in hydrothermal experiments: implications for reaction temperatures and fluxes at ridge crests and subduction zones. The dissertation author is the primary investigator and author of the paper.

VITA

EDUCATION

Ph.D. Earth Sciences

University of California, San Diego (UCSD) - Scripps Institution of Oceanography,

March, 2007

B.S. Chemistry

Peking University (Beijing, China), 1999

PUBLICATIONS

Wei Wei, Miriam Kastner, Arthur J. Spivack. Chlorine stable isotopes and halogen concentrations in convergent margins with implications for Cl isotope cycling. *To be submitted to EPSL, March 2007.*

Wei Wei, Lui H. Chan, Miriam Kastner, Robert Rosenbauer, Yishai Weinstein. Alkali elements mobility, Li and Sr isotope exchanges in hydrothermal experiments: implications for reaction temperatures and fluxes at ridge crests and subduction zones. *To be submitted to EPSL, March 2007.*

Wei Wei, Miriam Kastner, Arthur J. Spivack (2005). Chlorine stable isotopes in three subduction zones, with inferences for serpentinization and fluid flow. *Eos Trans. AGU* Abstract. *V51B-1482*.

Wei Wei, Lui H. Chan, Miriam Kastner, Robert Rosenbauer, Yishai Weinstein (2005). Li concentration and isotope cycling in the ocean - an experimental study. *Eos Trans. AGU* Abstract. *V41F-1533.*

Wei Wei, Miriam Kastner, Annette Deyhle, Arthur J. Spivack (2005). Geochemical cycling of halogens and boron and its implications for fluid-rock reactions in the non-accretionary Mariana supra-subduction zone. *ODP Leg 195 Scientific Results*. 23 pages. (http://www-odp.tamu.edu/publications/195_SR/106/106.htm)

Wei Wei, Miriam Kastner, Arthur J. Spivack (2005). Chlorine stable isotopes in two subduction zones: Nankai trough and Mariana, and implication for fluid-sediment interactions and fluid flow. *Abstract and oral presentation. Goldschmidt Meeting 2005.*

Wei Wei, Miriam Kastner, Robert Rosenbauer, Yishai Weinstein, Lui H. Chan (2004). Cycling of Li, K, Rb, and Cs at subduction zones and ridge crests, with

implications for ocean chemistry: hydrothermal experiments at 35-350°C and 600 bars. *Eos Trans. AGU, Fall Meeting Suppl.*, *Abstract 85:1450.*

Wei Wei, Miriam Kastner, Arthur J. Spivack (2003). Halogen concentrations and stable isotopes (O, Sr, and Cl) in the Nankai Muroto Transect and their implication for fluid-sediment interactions and fluid flow. *Eos Trans. AGU, Fall Meeting Suppl., Abstract 84:1459.*

Wei Wei (1999). Separation, analysis and application of Chinese tradition medicine by HPLC. *B.S. Thesis. Peking University.*

Miriam Kastner, Evan Solomon, Wei Wei, Lui H. Chan, Ola M. Saether (2006). Chemical and isotopic compositions of pore fluids and sediments from across the middle America Trench, Offshore Costa Rica. *ODP Leg 205 Scientific Results*, in press, 21 pages. (http://www-odp.tamu.edu/publications/205_SR/208/208.htm)

ABSTRACT OF THE DISSERTATION

Fluid Origins, Paths, and Fluid-Rock Reactions At Convergent Margins, Using Halogens, Cl Stable Isotopes, and Alkali Metals As Geochemical Tracers

by

Wei Wei

Doctor of Philosophy in Earth Sciences

University of California, San Diego, 2007

Professor Miriam Kastner, Chair

Aqueous fluids play a major role in the physical and chemical evolution of subduction zone systems and profoundly impact the elemental and isotopic composition of the atmosphere, crust, mantle, and seawater. Chlorine stable isotope ratios ($\delta^{37}Cl$) and halogen concentrations (*e.g.* Br/Cl) in pore fluid samples and solid samples from three subduction zones, the Nankai Trough, Costa Rica, and Mariana Forearc, provide critical information on fluid sources, flow paths, and reaction conditions at subduction zones. At the Nankai and Costa Rica subduction zones, the $\delta^{37}Cl$ values of pore fluids are significantly more negative (up to -7.8 ‰, $2\sigma \pm 0.3$‰) than seawater value (0 ‰) and the Br/Cl ratios are higher than seawater value (1.5×10^{-3}). Both $\delta^{37}Cl$ and Br/Cl show lateral seaward evolution along the transects. The

data indicate the existence of a deep-sourced fluid, originated from high temperature hydrous mineral formations that preferentially incorporate the heavier Cl isotope (^{37}Cl), but exclude Br.

In contrast, the δ^{37}Cl values in the pore fluids at the Mariana mud volcanoes range from +0.3‰ to +1.8‰ and the Br/Cl ratios are lower than the seawater ratio. The positive δ^{37}Cl values in the pore fluid and the high content of Cl with positive δ^{37}Cl values (+1.2 to +6.0 ‰) in the serpentines, support that the origin of the upwelling pore fluids is the dehydration of the subducting serpentinized crust. These upwelling fluids, together with ridge crest hydrothermal fluids, having δ^{37}Cl of +2.4‰ to +4.1‰, constitute the positive ^{37}Cl fluxes into the ocean that compensate the negative δ^{37}Cl fluid flux at subduction zones.

In an approach to estimate geochemical fluxes at mid-ocean ridges and subduction zones, hydrothermal experiments were conducted and the alkali metals (Li, K, Rb, and Cs) are used as tracers of fluid-rock reactions. The alkali concentration ratios together with Li isotope ratios may be used as approximate geothermometers. Hence, alkali elements could assist Cl isotopes and halogen concentrations to identify the temperature range and fluid-rock reactions at the fluid source in convergent margins.

CHAPTER 1

INTRODUCTION

1.1 The importance of fluids at convergent margins

Fluid is present throughout the Earth's crust and mantle and it plays a critical role in the major geological processes. The main important internal fluids at convergent margins are: (1) pore fluids of the sediment and oceanic crust, present at all depths, and expelled from the sediments by compaction and porosity reduction during plate subduction or accretion. In the incoming sediments, the porosity is approximately 50 ± 10 % and reduced to < 5-10 % at great depths (i.e. (Kastner et al., 1991) and references within); (2) fluids derived from diagenetic and metamorphic dehydration reactions, such as smectite (~15 wt% interlayer water and ~6 wt% structural water) to illite (a total of 8.5% water) transition at 50-150 °C in the upper crust. The change of physical properties of the solid phases localize shear and form planes of weakness and may control the up-dip limit of seismicity (e.g. (Vrolijk, 1990; Hyndman et al., 1993); (3) fluids from phase transformation (>200 °C) (O'Hanley, 1996) of high temperature hydrous minerals, such as serpentines, which contain ~13 wt% H_2O and are estimated to compose 10-20% of oceanic crust (Carlson, 2001). The stable-sliding serpentine or the brittle to ductile temperature transition may control the down-dip limit of the seismogenic zone (e.g. Hyndman et al., 1997; Peacock, 1993).

The expelled fluids from these different processes are estimated to be ~7.0 × 10^{12} kg/yr (Kastner et al., 1991; von Huene et al., 1991), assuming that the entire ocean is recycled through the subduction zone in every 200 million years. The expelled fluids are being returned to the ocean mostly via channelized fluid flow, some via diffusive flow, or involved in arc volcanism, rehydrating the upper mantle to produce serpentine diapirism, or being carried by the subducting plates into the mantle. The fluids carry distinct geochemical and isotopic compositions, which are critical for evaluating the types and extent of fluid-rock reactions, and fluid mixing. Fluid cycling at subduction zones represents Earth's deepest hydrologic cycle and has an impact on the chemistry of seawater, arc and back-arc volcanism, and serpentinization of the shallow lithospheric mantle, hence plays an important role in global geochemical cycles (e.g., (Hubbert et al., 1959; Carson et al., 1990; Kastner et al., 1991; Spivack et al., 2002). Fluid flow also transports large amounts of heat, thus are vital in the deformational and thermal evolutions of convergent margins (von Huene, 1984; Moore et al., 1990; Kastner et al., 1993).

At divergent plate boundaries, i.e., ridge crest, fluid flow is as well very important. Here thermal gradients drive convection of seawater through oceanic crust and extensive fluid-rock reactions occur. The reacted fluids carry distinct chemical and isotopic signals, such as higher than seawater Ca and alkali metals concentration, zero Mg, and lower than seawater Li and Sr isotope ratios (Edmond et al., 1979; Mottl et al., 1994; Elderfield et al., 1996). The flux of the hydrothermally altered fluid greatly influences seawater chemistry and impacts these elemental and isotope oceanic cycles. One of the key problems is the uncertainty of the relative importance of axial

ridge axis and ridge flank in the oceanic hydrothermal fluxes, because chemical fluxes through ridge flanks are poorly constrained due to the wide range of crustal conditions and lack of studies at ridge flanks (Mottl et al., 1994; Elderfield et al., 1996). The most critical parameter for characterizing crustal condition is temperature, which can be inferred, in turn, from profiles of sediment pore fluid chemistry (Mottl et al., 1994).

An addressed important question in this thesis is: how to distinguish between a fluid sampled at depth that was solely produced by *in situ* fluid-rock reactions, or consists of a mixture of the *in situ* fluid with a fluid from a different source, such as fluid advected from greater depths, or simply with seawater. How can they be differentiated and their paths identified? An additional important question is what are the temperatures at the fluid-rock reaction sites?

Geochemical tracers, such as Cl and Br, and Cl stable isotope ratios are mostly not involved in low to moderate temperature retrograde reactions (except in evaporite formation), but are probably reactive during high temperature hydrous mineral formation or dehydration, thus preserve the original fluid-rock reaction signatures during fluid transport. Therefore they were selected and emphasized in the thesis.

The alkali metals (Li, K, Rb, and Cs) have a strong affinity to the fluid with increasing temperature (50-350 °C), and the variations in alkali concentrations in the fluids are sensitive to the temperature of the fluid-rock reactions, thus could potentially be used as approximate geothermometers, assist in identifying the temperature of the fluid rock reactions.

Furthermore, because the concentration of the alkali metals (Li, K, Rb, and Cs) and isotope ratios of Cl, Li and Sr become highly altered relative to seawater values in

the fluid during fluid-rock reaction with increasing temperature, the fluxes through subduction zones and hydrothermal vents are important for their global geochemical cycles.

1.2 Geochemical tracers for fluid flow and fluid rock reactions

1.2.1 The Halogens (F, Cl and Br) and Cl stable isotope ratios

Fluorine, chlorine, and bromine have long been identified as excess volatiles via outgassing of the mantle or from a late accretion of volatile-rich material (Rubey, 1951; Anderson, 1974; Schilling et al., 1978; Schilling et al., 1980; Wanke, 1981; Jambon, 1994). Despite their abundances and widespread distributions, the geochemical cycles of F, Cl, Br are, as yet, not well constrained (Deruelle et al., 1992; Jambon, 1994) and only limited data exist for the Cl concentration or Cl isotope composition of most sea floor rocks, sediments, and minerals, much less about their Br and F concentrations.

The halogens are excellent tracers in the fluids because their geochemical behaviors are dominated by strong partitioning into the fluid phase. Chloride is the most abundant anion in seawater, and fluids in crust and sediments that are subducted. The two stable isotopes of chlorine are ^{35}Cl and ^{37}Cl, with natural abundance of approximately 76% and 24%, respectively. Their relative mass difference, 5.7%, is similar to the relative mass differences between the isotopes of C or S. Therefore, the stable isotopes of Cl can significantly fractionate, and can be exploited to solve geological problems.

Previous studies have shown that marine sedimentary pore fluids, especially in subduction zones, have stable Cl isotopic compositions that are distinct from seawater, with δ^{37}Cl (defined relative to modern seawater) values ranging from -0.9 ‰ to -7.8 ‰ at Nankai and Barbados (e.g. (Ransom et al., 1995; Spivack et al., 2002)), indicating significant fractionation of Cl isotopes in the source regions or along their flow paths. The generation of these isotopically light fluids is consistent with hydration reactions in igneous oceanic crust resulting in positive δ^{37}Cl values, e.g. in amphiboles and smectite samples (~+8 ‰), such as those reported by Magenheim *et al.* (Magenheim et al., 1995; Wei, 2005). The higher temperature hydrous minerals, such as serpentines and amphiboles, often contain hundreds to thousands of ppm Cl (Sharp et al., 2004) and this study) whereas smectite, a lower temperature mineral, on average contains 20-30 ppm Cl ((Magenheim et al., 1995) and this study). Hence, despite the smaller fractionation factors at higher temperatures, because of the high Cl concentrations, formation of hydrous minerals deeper in the subduction zone could have greater impact on the Cl and ^{37}Cl compositions of the pore fluids and the ocean than reactions which occur at shallower depths and lower temperature.

Fluorine is the smallest ion of the halogen group and has no naturally occurring isotopes. Its ability to form complexes with certain transition metals, such as U and Th, may lead to increase the solubility of such trace elements in the pore fluid.

Bromine is associated with organic matter diagenesis (Price et al., 1977). The increasing ionic sizes of fluorine, chlorine, and bromine in the halogen group determine the different partitioning of the halogens during fluid-rock reactions. During hydrous mineral formation, such as serpentines, talc, chlorite, and amphiboles, which

contain hundreds of ppm of Cl, but < ~5ppm of Br, Cl (^{37}Cl) is preferentially incorporated into the mineral structure to replace OH, while Br may be excluded due to its larger ionic size. Thus the residual fluid would be depleted in ^{37}Cl/^{35}Cl and Br/Cl ratios. Consequently, during hydrous mineral dehydration, the Cl enriched in ^{37}Cl/^{35}Cl and water released would increase the δ^{37}Cl value and Cl/Br ratios of the fluids. Therefore, in addition to δ^{37}Cl, the halogen ratios, such as Br/Cl, may also be used diagnostically to fingerprint fluids that have been formed by specific reactions (Magenheim et al., 1994; Ransom et al., 1995; Spivack et al., 2002).

Selected published data of F, Br, and Cl concentrations, and Cl isotope ratios in solids, fluids, and gases are listed in Table 1.2.1, representing their natural trend and range of concentrations and Cl isotope ratios. As shown, the natural range of δ^{37}Cl values of pore fluid and solid is significant (> 15‰).

1.2.2 Alkali Metal Concentrations (Li, K, Rb and Cs) and Li Isotope Ratio

At low temperatures, the alkali metals (Li, K, Rb and Cs) are preferentially partitioned into the solid phases, whereas at moderate to elevated temperatures they are preferentially released into the fluid phase. The threshold temperature for release into the fluid phase for each is as yet not well constrained, but could occur at as low as 50 ^{o}C (i.e. You et al., 1994; Seyfried et al., 1984, 1998, and references therein). A detailed study of the alkali metal concentrations as a function of temperature may set better constraints on the threshold temperatures. If each has a different threshold

temperature and fluid affinity with increasing temperature, they could be considered as potential geothermometers. The enrichments of alkali metal concentrations in the fluid with increasing temperature (50 to 350 ^{o}C) can also provide critical information on their fluxes through hydrothermal ridge crests or through ridge flanks, and the nature the reacting solid phases as sediments are more enriched in alkali metals than oceanic basement, thus the involvement of sediments in arc volcanism (Hart, 1969; Hart et al., 1982; Palmer et al., 1989; You et al., 1996; Seyfried et al., 1998).

The two isotopes of lithium (^{6}Li and ^{7}Li), with abundance of 7.52% and 92.48%, respectively, have a large relative mass difference of 14.4%, greater than those of C and S isotopes, and can significantly fractionate in nature. The seawater δ^{7}Li value is 32.4‰ (Chan et al., 2000).

1.2.3 Sr Stable Isotope Ratios

The relative mass difference of ^{87}Sr and ^{86}Sr is only 1.1%, therefore Sr isotopes hardly fractionate and provide a signal of the source material involved in the reactions, such as terrigenous continental source (highly radiogenic) versus arc volcanic or oceanic basement source (non-radiogenic). The ^{87}Sr/^{86}Sr ratio of modern seawater is 0.709172 ± 0.000010 (Hodell et al., 1990).

1.3 Outline of the thesis

The main objectives of the thesis were to establish a critical data-base for halogen concentrations and Cl stable isotopes, to be used as effective geochemical tracers capable of differentiating the volatile components released *in situ* from those transported from a source at greater depth, probably from the up-dip or down-dip of a seismogenic zone; to determine what controls the halogen elemental (F, Cl, and Br) and Cl isotopic systematics in subduction zone fluids, and use this information to constrain fluid sources, transport, fluid mixing, fluid-rock reactions, and mass transport into the ocean and mantle.

In order to characterize the partition behavior of the major and trace elements in different types of fluid-rock reactions, and constrain the threshold temperatures for elemental releases into the fluid phase, hydrothermal experiments were conducted to mimic the natural system, to monitor the mobilities of elements, with emphasis on alkali metals (Li, K, Rb and Cs), as well as on Li and Sr isotope exchanges, from 35 to 350 ˚C at 25 or 50˚C increments. The reactivities of the solids from 35 to 350 ˚C were also investigated. The results of the hydrothermal experiments help to evaluate the alkali elemental and Li isotope cyclings in the ocean.

The thesis consists of the following chapters:

Chapter 1 introduces the importance of fluids at subduction zones and the main geochemical tracers used in the study.

Chapter 2 presents a systematic study of halogen concentrations and stable chlorine isotopic ratios ($\delta^{37}Cl$) of selected pore fluids and mineral phases in marine systems, with a focus on subduction zones. The Cl isotopic data acquired in this thesis work help to identify the fluid-rock reactions at source. In addition, the fluid paths and fluid mixing are estimated at each subduction zone. The serpentines are important hydrous minerals due to their abundance in oceanic crust and high contents of water (13 wt%) and Cl. Therefore, different forms of serpentine were selected from various locations for analysis. The Cl isotope flux and cycle in the ocean is estimated on the basis of the analyzed data in pore fluids, serpentines, and hydrothermal fluids.

Chapter 3 consists of results of element (Mg, Ca, Si, Sr, Li, K, Rb, and Cs) concentrations and Li and Sr isotopes of both reacted fluids and solids in the hydrothermal experiments from 35 to 350 °C, using a rocking autoclave apparatus located at US geological Survey, Menlo Park. The alkali metal concentrations (Li, K, Rb, and Cs) are shown to increase dramatically with temperature and the concentration-temperature profile of each alkali metal is distinct, *i.e.* each has a characteristic temperature-dependant partition between the fluid and solid phases. It implies that alkali concentration ratios together with Li isotope ratios may eventually be used as approximate geothermometers. The experimental data are applied to estimate the approximate temperature of the deep-sourced fluid at the Costa Rica subduction zone. The experimental results and mass balance calculations also suggest

that the ridge flank environment is an important source for Cs, Sr and Li isotopes to the ocean.

Chapter 4 is a conclusion chapter and also presents several broader implications on Cl isotopes of natural hydrothermal fluids, Br element and isotope ratios, and geothermometry.

Table 1.2.1 Summary of selected published halogen concentrations and $\delta^{37}Cl$ values

	Samples	F (ppm)	Br (ppm)	Cl (ppm)	$\delta^{37}Cl$ (‰)	Reference
Solids	Meteorites (CI-type)	8-64	0.18-3.91	580-849	+ 2.7	(Driebus, 1979)
	evaporites (200Ma)	--	--	--	-0.58 to +0.24	(Eggenkamp et al., 1994; Eggenkamp, 1995)
	MORB	89-388	--	40-170	+3.0 to 7.2	
	amphibolite	53-241	--	100-3000	+0.4 to 3.4	(Magenheim et al., 1995)
	smectite	150-397	--	21-23	+4.0 to 7.5	
Gas	gas condensates (volcanic Island)	700-39000	--	12400-28900	-0.61 to +0.29	(Musashi et al., 2000)
		(μM)	(μM)	(mM)		
Fluids	seawater	86	840	559	0	By definition
	pore fluids	0-105	800-1574	188-1090	-1.97 to -8.5	(Ransom et al.,1995; Spivack et al., 2002) (Gieskes, 2000)
	HT fluids	0-452	533-1832	338-1090	+4.6- 6.9 -0.03 ± 0.06	(Chung et al.,2002; Bach et al., 2002; Bonifacie et al., 2005) (Hurwitz et al., 2005)
	ground water	--	--		-2 to +2	(Long et al., 1993)
	rivers	--	--	0.07	< ±1.0	(Holland, 1978)

CHAPTER 2

CHLORINE STABLE ISOTOPES AND HALOGEN CONCENTRATIONS IN CONVERGENT MARGINS

2.1 Introduction on Cl stable isotope and halogens

The stable isotopes of Cl (^{35}Cl and ^{37}Cl) are expected to significantly fractionate and to solve geological problems. The method developed by (Taylor et al., 1969) precisely measures Cl isotope ratios of methyl chloride by gas mass spectrometry. With modifications (e.g. (Kaufmann et al., 1984; Eggenkamp et al., 1994)) the methyl chloride method has been successfully used for groundwater; mineral; whole-rock, including evaporites; and organic compound studies with a precision of 0.24 ‰, demonstrating significant natural Cl isotope variations.

Despite these successes, use of this method has been limited to relatively Cl-rich samples (>1 mg Cl for a single analysis). Thus, it precludes analysis of many geological samples or environments of limited supply or of low Cl abundance. A high sensitivity method (μg of Cl), suitable for stable Cl isotopic analysis of samples with low-Cl abundance (<100 ppm), by which the $^{37}Cl/^{35}Cl$ ratio is measured by positive ion thermal ionization mass spectrometry (TIMS) with a reproducibility of 0.23‰, was developed by Xiao and Zhang (1992) (Xiao et al., 1992) and Magenheim (1994) (Magenheim et al., 1994) and recently refined by Numata (2001) (Numata et al., 2001). This method has been used successfully for Cl stable isotope measurements of

seafloor basalt glasses and altered oceanic crust, silicate minerals from layered intrusions, chondritic meteorites, marine sediment pore fluids, atmospheric aerosols, and organic compounds (e.g. (Magenheim et al., 1994; Magenheim et al., 1995; Ransom et al., 1995; Boudreau et al., 1997; Stewart et al., 1997; Volpe, 1998)). Recently it has been used to analyze hydrothermal fluids ((Bach et al., 2002; Chung et al., 2002) and this thesis).

Because of the abundance of Cl, thus its long residence time and conservative behavior in the water column, seawater is the standard for Cl isotopes ('Standard' Mean Ocean Cl: SMOC). Numerous analyses of the seawater Cl isotope ratio (Kaufmann et al., 1984; Godon et al., 2004) confirm the constancy of seawater Cl isotopic composition. In contrast, marine pore fluids, especially in subduction zones, demonstrate stable Cl isotopic compositions that are distinct from seawater, with $\delta^{37}Cl$ values ranging from -8.20 ‰ to -0.89 ‰ at Nankai and Barbados, (e.g. Ransom et al., 1995; Spivack et al., 2002), indicating significant fractionation of Cl isotopes in their source regions or along their flow paths. The generation of these isotopically light fluids is consistent with hydration reactions in the volcanic oceanic crust resulting in positive $\delta^{37}Cl$ values of amphiboles and smectite samples, such as those reported by Magenheim et al. (1995), as well as serpentine values reported by Sharp (2004) (Sharp et al., 2004). It has also been noted that resultant isotopically light fluids may be recycled during subduction and possibly be involved in arc-magma genesis. Dehydration reactions involving serpentine or other high temperature hydrous phases, on the other hand, generate $^{37}Cl/^{35}Cl$ enriched fluids. A few preliminary $\delta^{37}Cl$ analyses of hydrothermal fluids ((Bach et al., 2002), by SIMS; (Chung et al., 2002), by TIMS,

in abstracts only) show positive (+4.6 to 7.7‰) values, and appear to corroborate this assumption.

In addition to the few existing data mentioned above, it is necessary to establish a database for Cl, F, and Br concentrations and Cl stable isotopes in fluids and solids at convergent margins, in order to study the fluid origins, paths, and fluid-rock reactions, thus to constrain their oceanic cycles.

2.2 Geologic background of study areas

The Nankai, Costa Rica, and Mariana subduction zones were chosen as the study areas because of their contrasting geologic characteristics. The Nankai Trough subduction zone has a significant accretionary prism whereas at the Costa Rica and Mariana subduction zones all sediments are underthrust.

The main Geologic characteristics of the three subduction zones are summarized in Table 2.2.1 and discussed below.

2.2.1 Nankai Trough

The pore fluid and sediment samples are from a transect of drill sites across the trench shown in (Fig. 2.2.1, Fig. 2.2.2 and Fig. 2.2.3). ODP Site 1173 is in the trench's outer-margin, 10.5 km seaward of the deformation front. Site 1174 is located 1.8 km arcward of the deformation front and 1.6 km east from Site 808, the most arcward site. Most of the sediments are accreted, with only 25-30% of the section, mainly hemipelagic sediments, underthrusted (Fig. 2.2.3). The subduction rate is 20-40 mm/yr and the geothermal gradient is high, ~110°C/km, due to the relatively young age (15 Ma) of the subducting plate (Moore et al., 2001).

The most interesting and distinct feature of the pore fluid Cl-depth profiles from Site 1173, through Site 1174, to Site 808, the east to west Muroto transect, is a broad low-Cl zone situated in the lower Shikoku Basin unit (Fig. 2.2.4). Other important characteristics are: (1) the extent of Cl dilution relative to seawater, in the low Cl zone, differs systematically among the sites; it evolves from 8-9 % at Site 1173, to 16-17 % at Site 1174, and to 20-21 % at Site 808; (2) all three sites have numerous local extrema, while in general, the profiles are increasingly smoothed seaward from Site 808 to Site 1173; (3) the vertical structures of local extrema are similar at Sites 808 and 1174 in the lower Shikoku Facies (Fig 2.2.4).

One of the key objectives of ODP Legs 131 and 190 was to differentiate the fluids evolved by local *in situ* processes from those advected from greater depths by chemical and isotopic data analyses. Chlorine stable isotopes are thus used to help to decipher the origin of the low-Cl fluid along Sites 1173, 1174, and 808 transect, in

particular to determine the relative contributions to the low Cl and other volatiles of a deep-sourced fluid transported laterally from the seismogenic zone versus *in situ* smectite dehydration (e.g. (Kastner et al., 1993; Underwood et al., 1993; Saffer et al., 1998; Henry et al., 2004)).

2.2.2 Costa Rica

The main objective of drilling the Costa Rica transect, ODP Leg 170, Sites 1039, 1043 and 1040; and ODP Leg 205, Sites 1253, 1255 and 1254 was to investigate the active fluid flow regime across the Costa Rica margin and its implications for the seismogenic zone and subduction geochemical cycling (Kimura, 1997; Morris, 2003) (Fig. 2.2.5). The décollement and underthrust sediments were penetrated at Site 1043 (1255), located ~0.5 km arcward from the trench and at Site 1040 (1254), 1.6 km arcward from the trench (Fig. 2.2.6). There is no accretionary prism and the underthrust section is lithologically identical to the reference site section (Sites 1039 (1253), ~1.5 km seaward of the trench); it is thinned from ~380 m (~160 m of siliceous hemipelagic sediments overlying ~220 m of pelagic carbonates) at the reference site to ~285 m (~110 m of hemipelagic sediments overlying ~175 m of pelagic carbonates) at Site 1040 (1254). The wedge sediments above the décollement consist mostly of silty clay with volcanic ash (Fig. 2.2.7). The subduction rate at Costa Rica is 85 mm/yr and the geothermal gradient is ~10°C/km (Table 2.2.1) (Kimura, 1997).

Pore-fluid chemistry was used to identify the presence of a distinct and active fluid flow regime along the décollement, clearly shown in the Cl depth-profiles (Kimura, 1997; Chan et al., 2000; Silver et al., 2000). The fluid is characterized by lower than seawater concentrations of Cl, Na, K, and Mg, and elevated Ca, Li, and Sr concentrations, and is enriched in C_3-C_6 hydrocarbons, non-radiogenic $^{87}Sr/^{86}Sr$ and $^{7}Li/^{6}Li$ isotopes. Based on laboratory experiments (i.e. (Seyfried et al., 1984; You et al., 1996; Seyfried et al., 1998)), these data indicate that the fluid originates from mineral-fluid reactions at a temperature of greater than 150ºC while the temperature at the décollement is ~2-4ºC at this site (Chan et al., 2000; Silver et al., 2000).

2.2.3 Mariana Forearc

On the Mariana intra-oceanic subduction zone, cold (~2 °C) springs with fluid salinity lower than that of seawater have been observed associated with serpentine mud volcanoes (Fig. 2.2.9). The subduction rate is 40mm/yr (Table 2.2.1) (Salisbury, 2002). Water released from the downgoing Pacific Plate, venting from a depth of 27-29 km, hydrates the overlying mantle wedge and convert depleted harzburgite to lower-density serpentinite. The resulting serpentinite mud, containing variably serpentinized harzburgite clasts, ascends buoyantly along fractures and extrudes at the seafloor, where it forms large (30 km in diameter, 2 km high) mud volcanoes along the outer Mariana forearc, in a band that extends from 50 to 120 km behind the trench axis (Fryer et al., 1985; Fryer et al., 1992; Fryer et al., 1995; Fryer et al., 2000; Mottl, 2003).

Conical Seamount was drilled during ODP Leg 125 (Fryer et al., 1992). Numerous cruises and submersible and remote control coring operations in the area have recovered similar material from other seamounts (e.g. Bluemoon Seamount (Fryer et al., 1995; Fryer et al., 1999)). Carbonate chimneys with brucite, blue amphiboles, phengite, and hydro-garnets were also recovered. The South Chamorro Seamount, located on the southern Mariana forearc ~85 km arcward from the trench (Fig. 2.2.9), was drilled on ODP Leg 195, Site 1200. It exhibits the second most highly-altered fluid signal relative to seawater yet detected in the Mariana system (Mottl, 2003). This is the only known site of active blueschist mud volcanism in the world. Hole 1200E is located within 10 m North of Hole 1200A (Fig. 2.2.10) where a cold seep was identified. Hole 1200B is ~20 m east of Holes 1200A and 1200E. Holes 1200F and 1200D are ~20 and 80 m north of Hole 1200E, respectively, forming a transect northward from the seep at Hole 1200A (Fig. 2.2.10).

Relative to seawater, the deep upwelling fluids in South Chamorro Seamount (ODP Leg 195) and Conical Seamount (ODP Leg 125) have higher sulfate, alkalinity, pH, Na/Cl, K, Rb, B (Fig. 2.2.11), light hydrocarbons through C_6 (mainly thermogenic), and NH_4^+ concentrations, $\delta^{18}O$, and δD values; and lower Cl, Mg, Ca, Sr, Li, Si, and phosphate concentrations, and Sr and B isotopic ratios (Mottl et al., 1992; Benton, 1997; Benton et al., 2001; Mottl, 2003).

Our study focuses on characterizing the systematics of the halogen concentrations and Cl isotopic behavior in the pore fluids and serpentines at the South Chamorro seamount, as well as of serpentine samples from three other adjacent serpentine seamounts.

Table 2.2.1 Main Geologic characteristics of the three subduction zones

	Plate boundary	Fate of incoming sediments	Subduction rate	Age of subducting plate	HF	Temp Gradient
			mm/yr	Ma	mW/m^2	$^oC/km$
Nankai Trough	Philippine-Eurasian	most sediment accreted	20-40	15	125-130	110
Costa Rica	Cocos-Caribbean	no accretionary prism; all sediments subducted	85	24	10-30	~10
Mariana	Pacific-Philippine	no accretionary prism	40	>34	13-99	9.2 (HoleE, Site 1200) to 72 (HoleF, Site 1200)

Note: HF = Heat Flow. Data are from ODP Leg 190, 170/205, and 195 Initial Reports (Kimura, 1997; Moore, 2001; Salisbury, 2002; Morris, 2003).

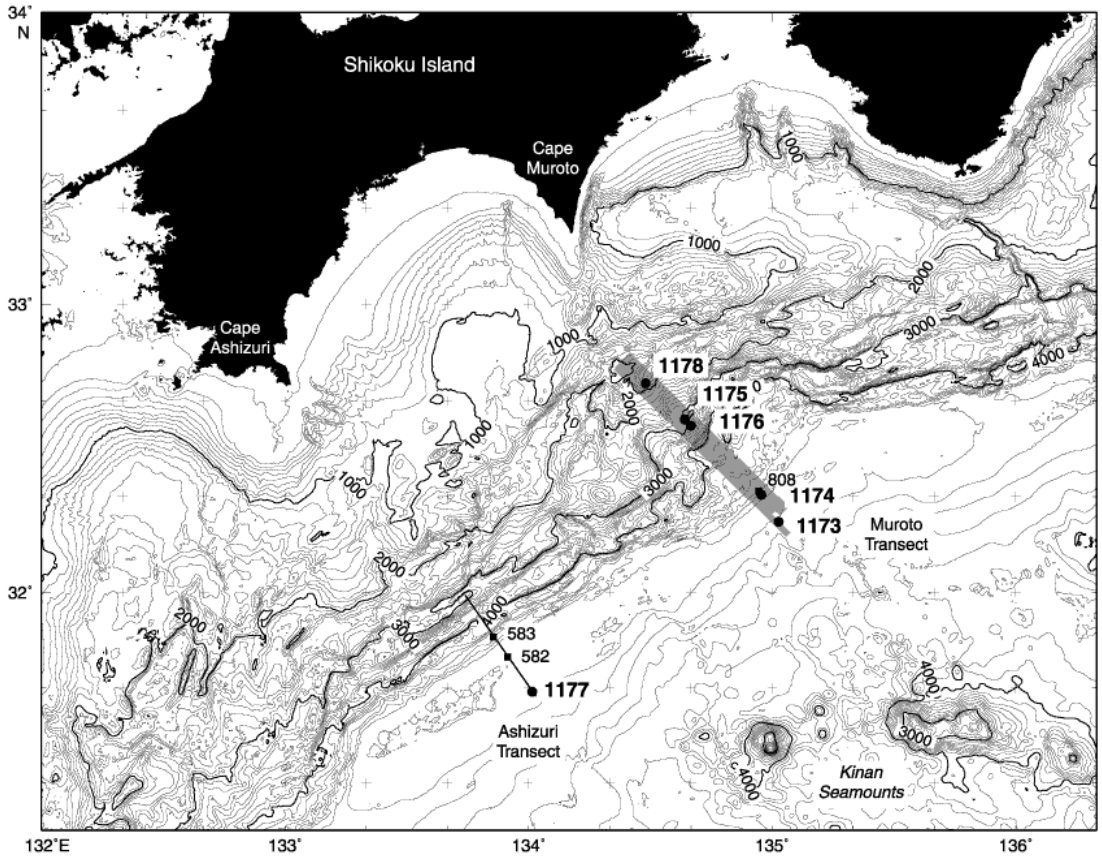

Figure 2.2.1 ODP Leg 190 (solid circles) in the Nankai Trough. The shaded outline shows the 3-D seismic survey of Bangs et al. (1999) and Moore et al. (1999). Contour interval = 100 m. Figure is from Leg 190 Initial Reports (Moore, 2001).

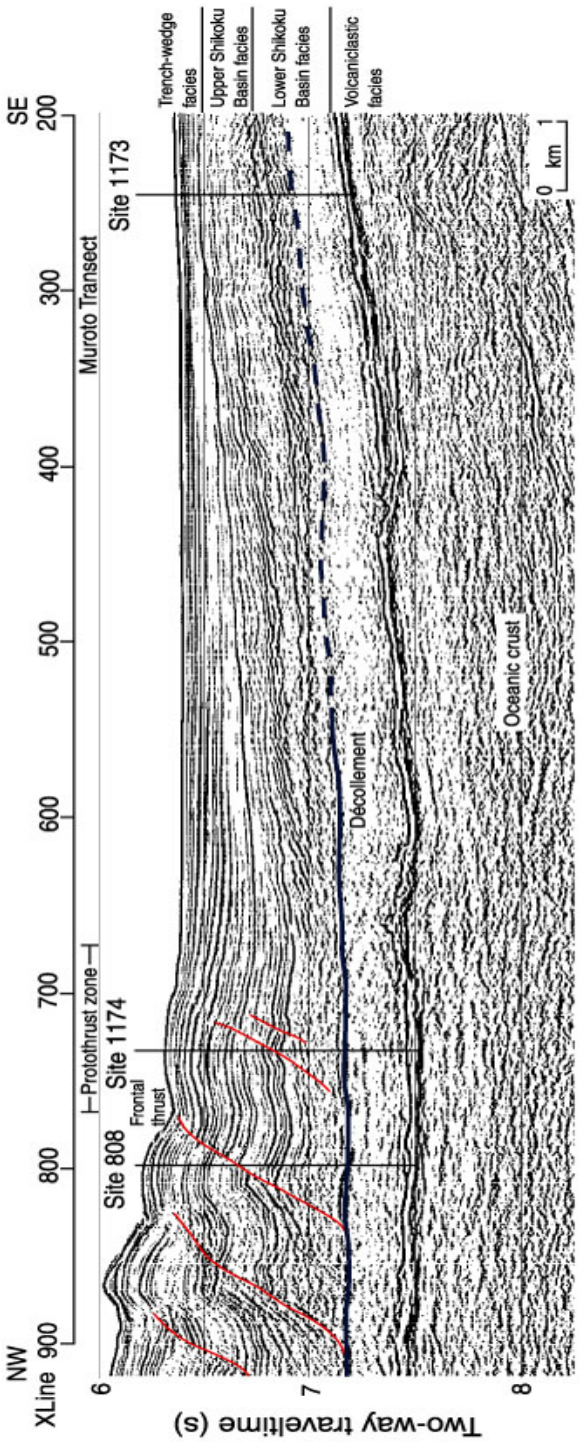

Figure 2.2.2 Seismic reflection profile of the Muroto transect at Nankai Trough, showing locations of Ocean Drilling Program (ODP) Sites 808, 1174 and 1173. Figure is from Leg 190 Initial Reports (Moore. 2001).

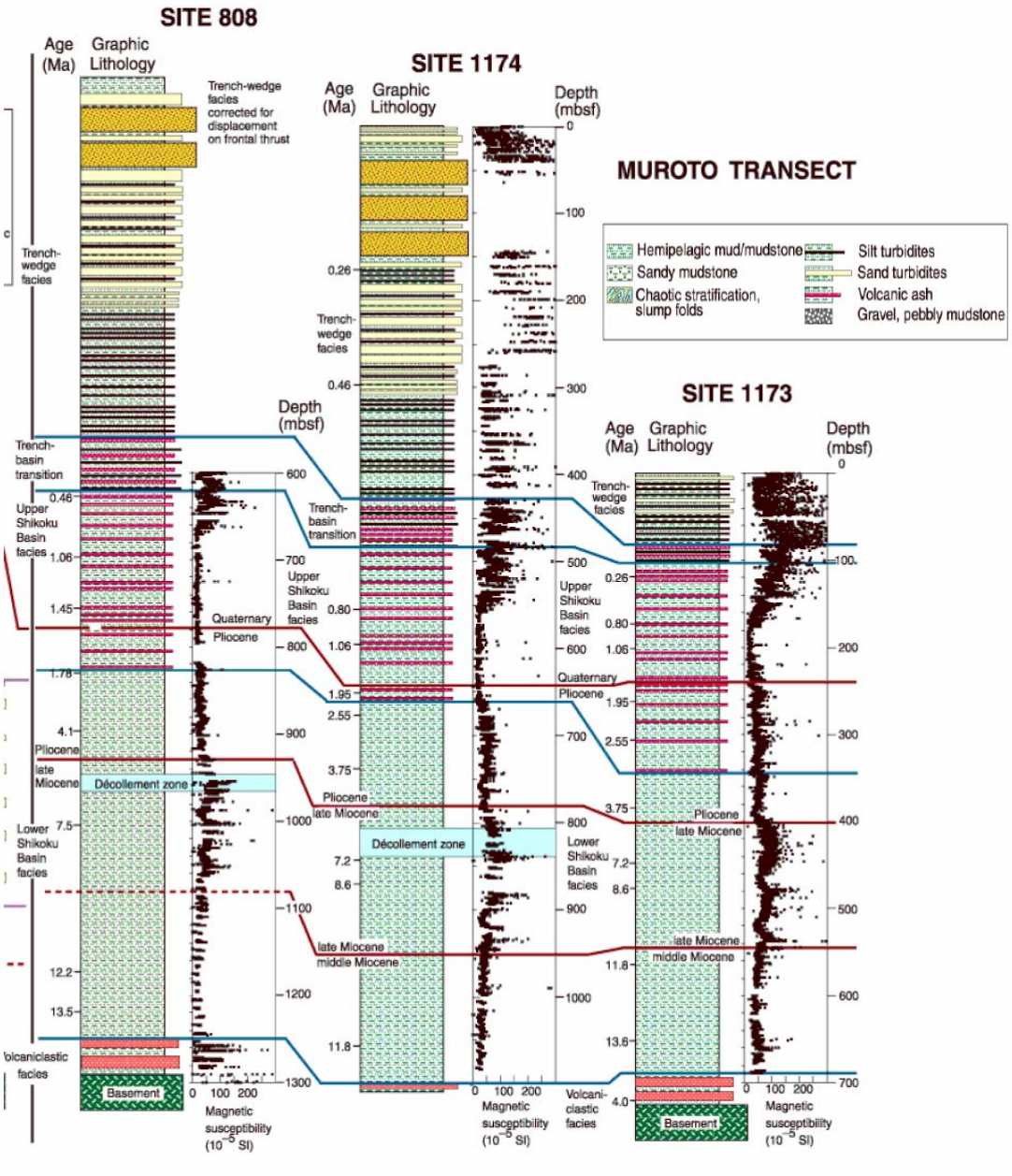

Figure 2.2.3 Correlation of facies units, magnetic susceptibility, and major time boundaries within stratigraphic successions of the reference and prism toe sites at the Muroto Transect at Nankai margin. Time boundaries are in red (solid line). Facies boundaries are in blue (Muroto Transect) (Moore, 2001).

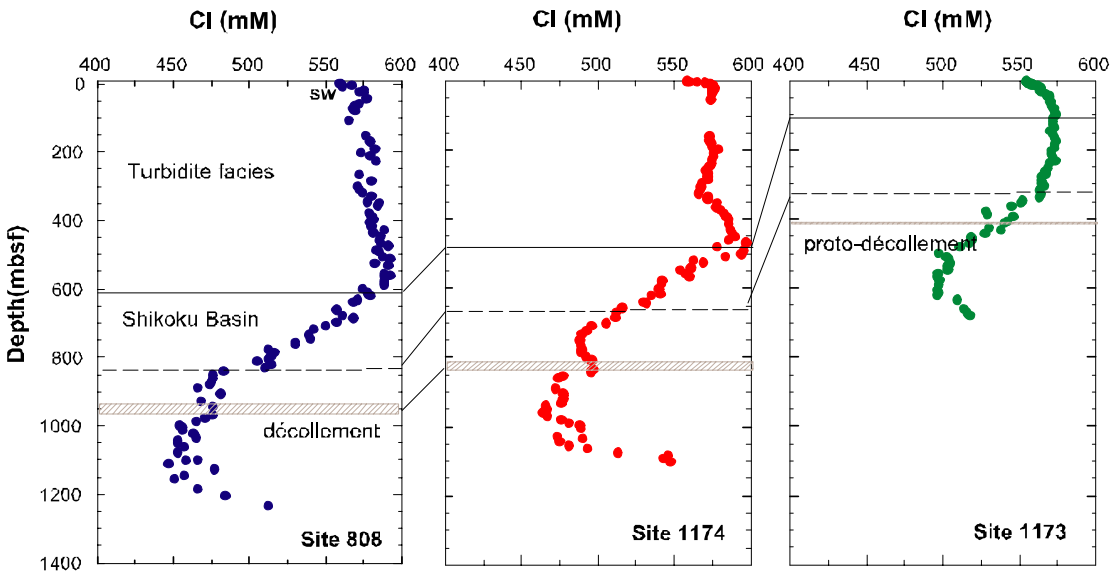

Figure 2.2.4 Cl concentration (mM)-depth profiles along the Muroto transect at Nankai Trough. Data are from ODP Leg 190 Initial Reports (Moore, 2001).

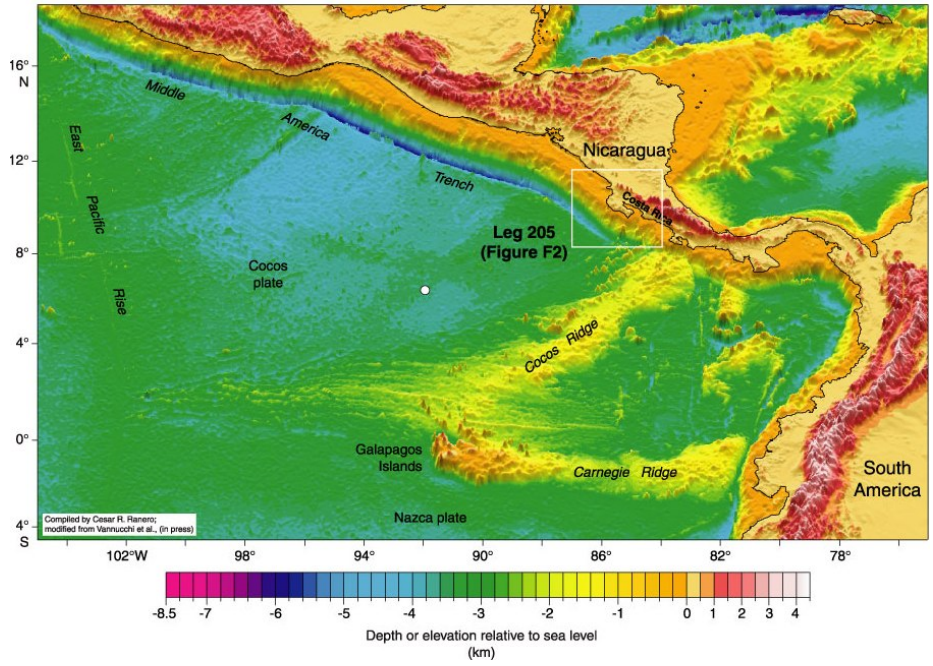

(A)

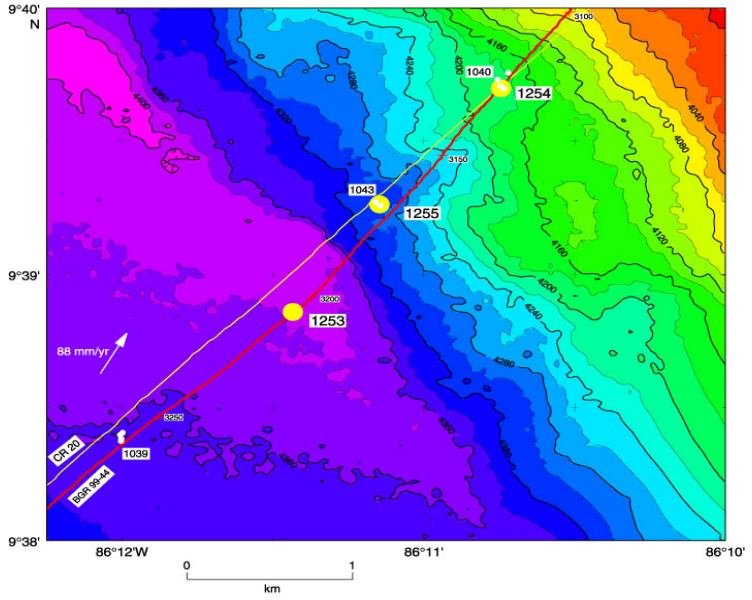

(B)

Figure 2.2.5 (A) Location map of Leg 205 and 170; (B) Bathymetric map of Leg 205 and 170 drill sites. Figure is from ODP Leg 170 and 205 Initial Reports (Kimura, 1997; Morris, 2003).

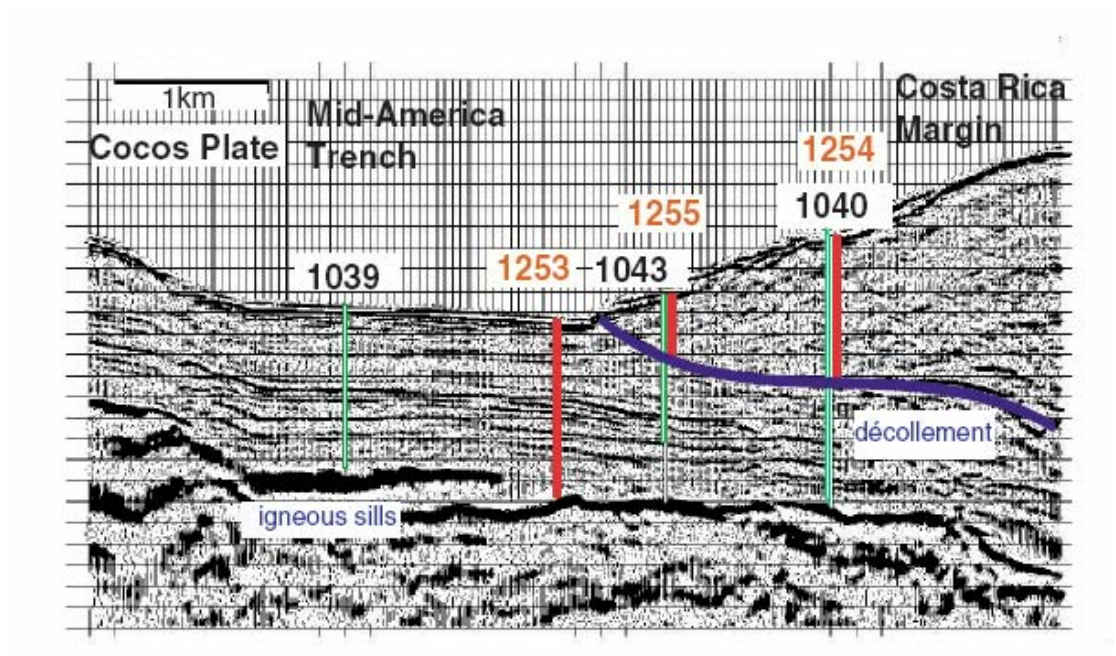

Figure 2.2.6 Seismic reflection profile of the Costa Rica Transect off shore Nicoya Peninsula, showing locations of ODP Sites 1039/1253, 1043/1255, 1040/1254. The vertical green and red lines indicate the depth of drilling on ODP Legs 170 and 205, respectively; the blue line indicates the décollement. Figure is from ODP Leg 170 and 205 Initial Reports (Kimura, 1997; Morris, 2003).

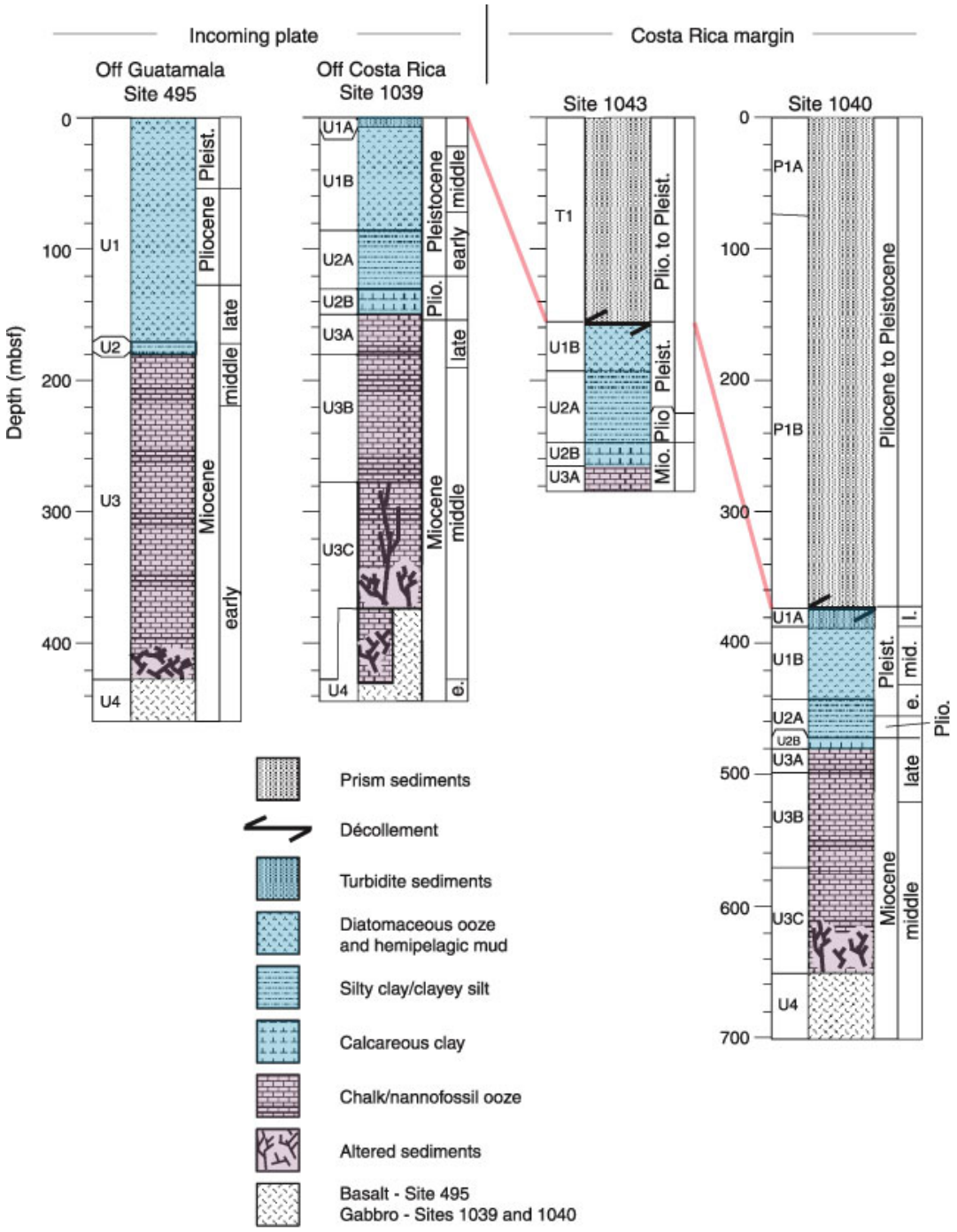

Figure 2.2.7 Summary of recovered lithology at drill sites on the incoming plate offshore Guatemala (Deep Sea Drilling Project Site 495) and Costa Rica (Site 1039) as well as on the Costa Rica margin (Sites 1040 and 1043). Note the similarity of incoming sediment sections at Sites 1039 and 495, as well as the repetition of the Site 1039 section below the décollement at Sites 1040 and 1043 (Kimura, 1997).

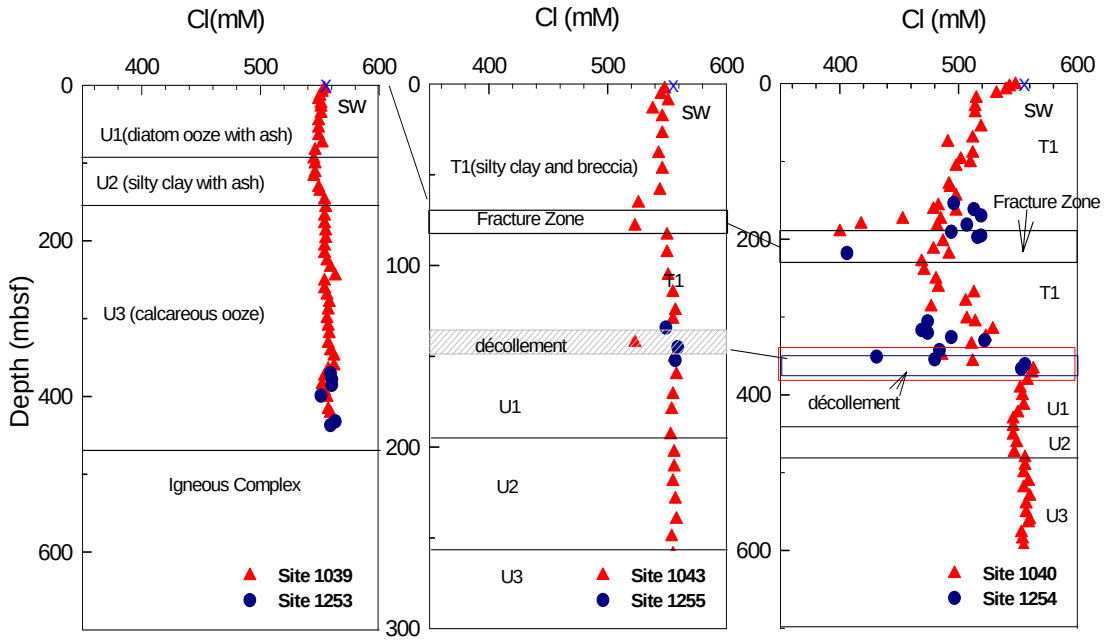

Figure 2.2.8 Cl concentration depth profiles at the Costa Rica transect. Data are from (Kimura, 1997; Morris, 2003)

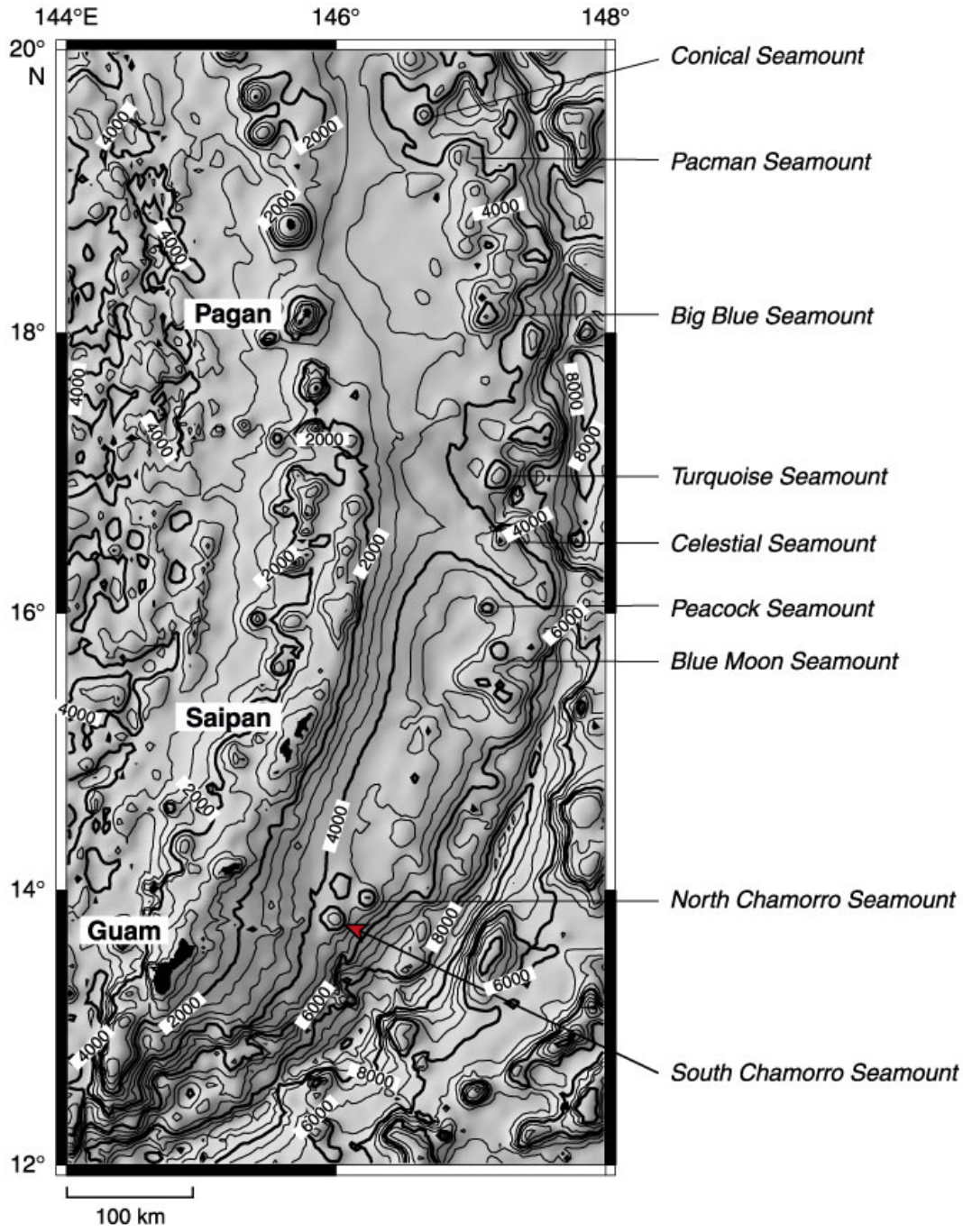

Figure 2.2.9 Location map of seamounts at Marina subduction zone. ODP Site 1200 was drilled on the summit of South Chamorro seamount. Figure is from ODP Leg 195 initial Reports (Salisbury, 2002).

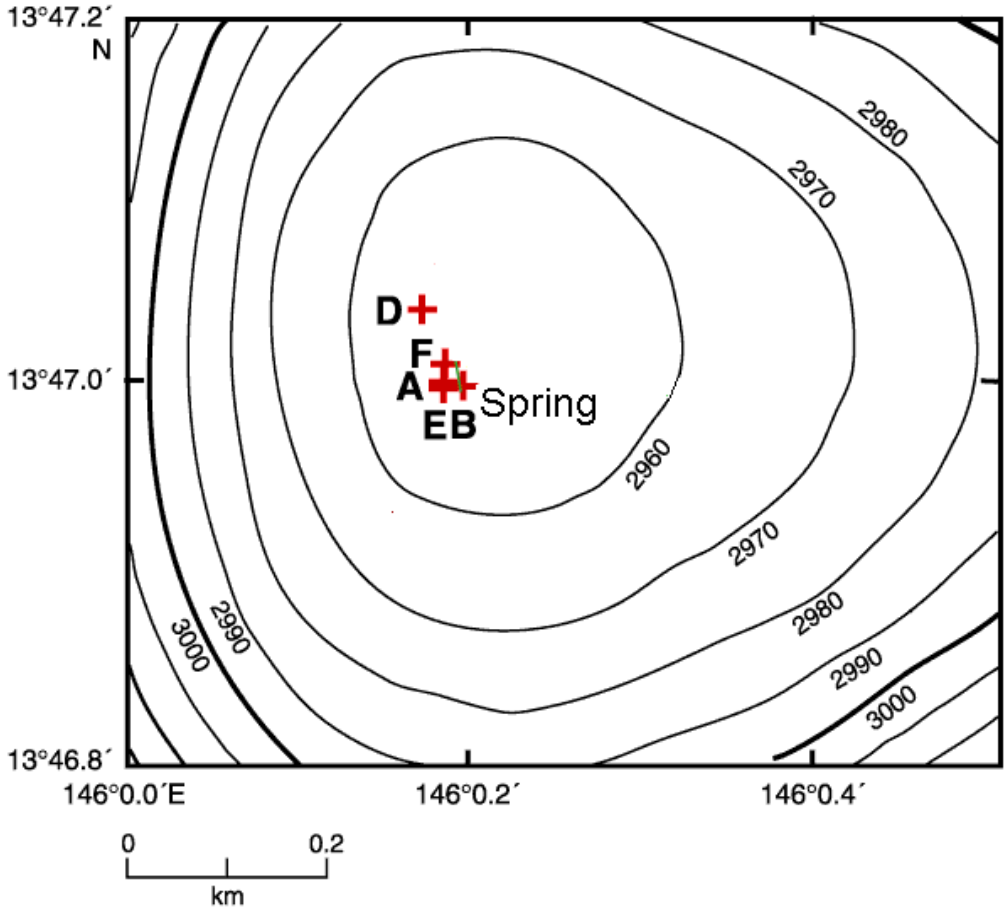

Figure 2.2.10 Map of drilled holes A, B, D, E, F, and of the spring at ODP Site 1200. Figure is from ODP Leg 195 initial Reports (Salisbury, 2002).

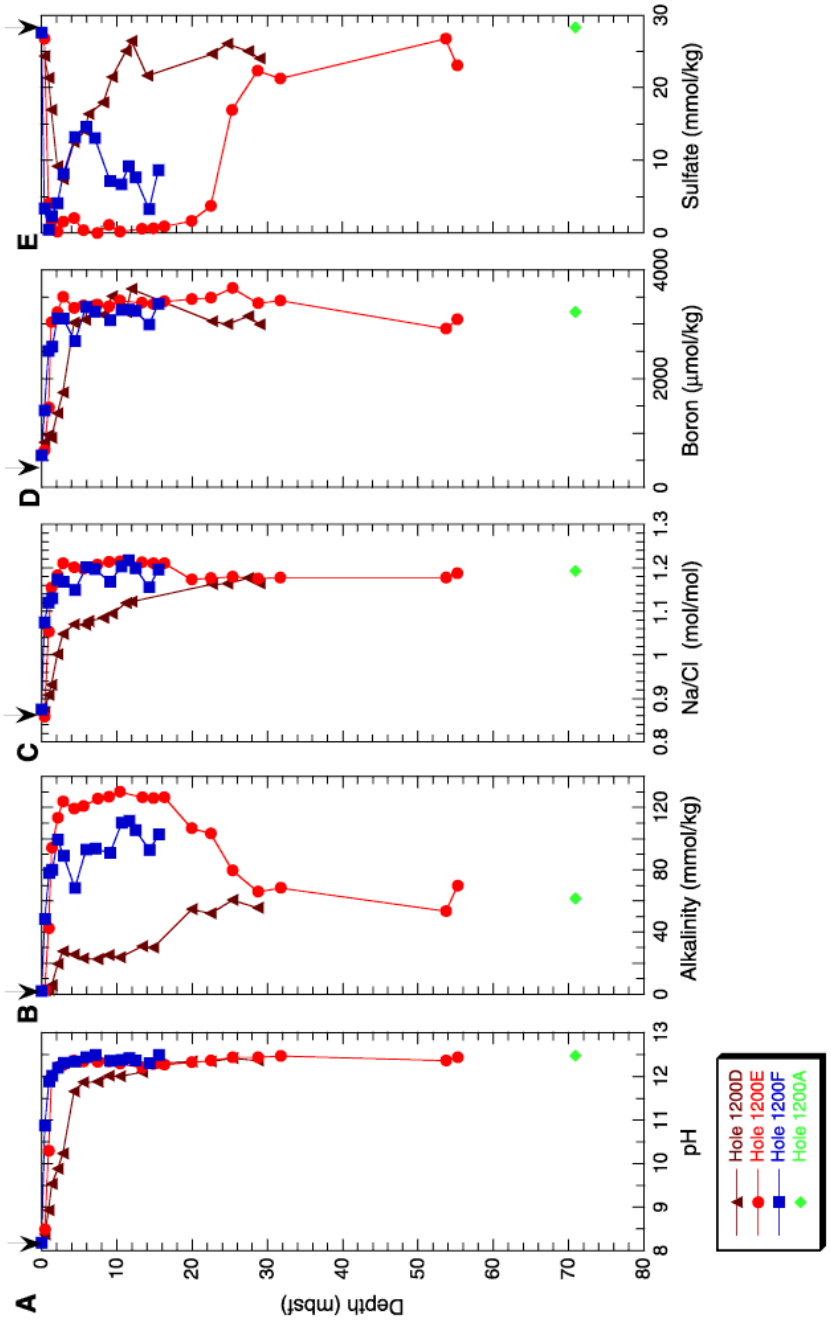

Figure 2.2.11. Pore water composition vs. depth curves for Holes 1200D, 1200E, and 1200F. A. pH. B. Alkalinity. C. Sodium/chloride. D. Boron. E. Sulfate. Hole 1200E is closest to the vent community on the summit of South Chamorro Seamount; Hole 1200D is the most distant. Arrow = seawater value. The figure is from (Salisbury, 2002).

2.3 Analytical Methods

2.3.1 Halogen concentration analysis

Chloride concentrations of pore fluid samples were determined by titration with $AgNO_3$ (precision 0.1% based on duplicate analyses of samples and standards). Fluoride and Br concentrations were determined by eluent-suppressed ion chromatography (I.C.) with a Dionex DX-120 (external precision is ~ 3%). Fluoride concentrations of pore fluids at Site 1039 at the Costa Rica subduction zone were also analyzed by Saether (Kastner, 2006), using an ion-selective electrode, with a precision of ~3.6 %. Bromide concentration of pore fluid at Site 808 has been analyzed by colorimetric methods (You et al., 1993) and the results obtained by two methods agree with each other.

2.3.2 Chlorine isotope analysis

Chlorine isotopes were analyzed by thermal ionization mass spectrometry (TIMS) using a VG 336, by the Cs_2Cl^+ method described in (Magenheim et al., 1994; Xiao, 1995; Numata et al., 2001). Daly detection was utilized with a gain of $\sim 10^{13}$. Two μg of Cl was used per analysis, equivalent to ~0.1 μl seawater.

$^{37}Cl/^{35}Cl$ ratios are reported as $\delta^{37}Cl$ values as per mil (‰) deviations from seawater ('Standard' Mean Ocean Cl: SMOC), expressed as:

$$\delta^{37}Cl = [(^{37}Cl/^{35}Cl)_{sample}/(^{37}Cl/^{35}Cl)_{smoc} - 1] \times 1000, \quad (2.1)$$

The standard was filtered seawater collected from the scientific pier at Scripps Institution of Oceanography, San Diego. The typical in run precision for a single analysis is 0.15‰ and the external reproducibility (1σ) is 0.3‰ based on 160 standard analyses from 2001 to 2005.

For solid samples, halogens were extracted from silicates by the pyrohydrolysis method (Magenheim et al., 1994). The method involves inductively heating a sample to temperatures of 1300-1400ºC in a platinum boat and extracting the sample's volatile constituents with H_2O vapor. This vapor is collected in a quartz condenser. After extraction the system is flushed with milli-Q. water which, together with the sample washing solution, provides quantitative recovery of halogens from the solid, thereby eliminating extraction-induced isotopic fractionation artifacts. Procedural blanks were established for Cl for each sample analyzed and the blanks were collected using the same procedure as for the solid. Our Cl blank is less than 0.1μg/ml of solution, which is less than 1% of the amount of Cl that was extracted from samples with Cl concentrations of >20 μg (30-800 ppm). Cl concentrations in fluids extracted from solid samples are determined by eluent-suppressed anion chromatography with a Dionex DX-120 (external precision is ~ 3%).

For Cl stable isotope analysis, solutions extracted from solid samples are purified before Cs-column exchange, to prevent interference from other anions on the mass spectrometer. The method is adopted from Numata *et al*. (2001) (Numata et al., 2001) and has been modified in our laboratory. To purify solutions, we add an

appropriate amount of 1M HNO_3 and 30mM $AgNO_3$ solution to the extracted fluid, based on solution Cl concentration. This completely precipitates the Cl. For a complete reaction, solutions are kept for 2 hours at room temperature in the dark. The solution is then centrifuged and the supernatant discarded. The AgCl precipitate is washed twice with 500 µl 0.01 M HNO_3 and once with 50 µl H_2O. To dissolve AgCl, 50 µl of 1M NH_3 is added. About 1 mg of Mg powder is also added to remove Ag^+ ion. This reaction lasts ~1 hour. The solution is then centrifuged and the supernatant recovered. The precipitated material is washed twice with 1 ml milli Q water, followed twice with washes of 100 µl milli Q. water. These supernatants are then combined. If there is any organic contaminant, which may prevent ionization in the mass spectrometer, it is removed from the eluent by adding activated charcoal powder (1mg, GL Sciences GX-60). The final solution is evaporated to dryness under a heat lamp. The residue (NH_4Cl+ $MgCl_2$) is then dissolved in 200 µl water. The yield and pureness of Cl is tested by ion chromatography for every sample to make sure the yield is >99.9%.

2.3.3 Column Exchange Preparation for Chlorine Isotopic Analysis

In pore fluids, Cl is the dominant anion and the interference from other anions for mass spectrometry is generally negligible (Xiao et al., 1992). Therefore, the pore fluid samples are directly converted to CsCl solution using a Cs-form of AG50-X4 resin in a short (~4 cm high) ion exchange column. Because some pore fluid samples

from Mariana have relatively high alkalinity, before the Cs-column exchange, these samples are passed through an H^+-form resin to neutralize OH^- and CO_3^{2-}.

For solids, the solution obtained from the chemical purification procedures (Section 3.2) is first loaded into a short H^+-form resin to remove excess CO_3^{2-} and OH^-. The residual solution should consist primarily of HCl, and is directly loaded onto a column with Cs-form cation exchange resin (DOWEX 50w x8, 200-400 mesh). The column is rinsed with milli Q water until the pH is 7. After the column exchange, the yield and total amount of Cl are determined by ion chromatography. The yield for the above column procedure is 100 ± 5%, thus eliminating any possible isotope fractionation during sample preparation (Chan et al., 1992). The solution is evaporated almost to dryness and an appropriate amount of dissolved Cl is loaded onto the filament.

2.3.4 Sr concentration, Sr and B isotope analysis

Sr concentration was analyzed by ICP-OES, with error of 3%. The $^{87}Sr/^{86}Sr$ ratios were measured at SIO in Drs. G. Lugmair and P. Castillo's laboratory, with an internal error < 5.5×10^{-6} and external error <0.002‰) based on repeated measurements of IAPSO seawater standard. The average $^{87}Sr/^{86}Sr$ of IAPSO seawater standard is 0.709186.

B isotope ratios of the pore fluids were determined by negative thermal mass spectrometry, and the $^{11}B/^{10}B$ ratios of the solids were measured by TIMS, at GEOMAR, Kiel (Germany) by Annette Deyhle, with internal precision of 0.05 ‰

2σ mean on average and external precision of 0.5‰ (Deyhle, 2001). The B isotope ratio is reported as $\delta^{11}B$ in permil (‰) deviation from the standard (SRM-951 boric acid) as follows: $\delta^{11}B = 1000\ (^{11}B/^{10}B_{sample}/\ ^{11}B/^{10}B_{standard} - 1)$. The seawater $\delta^{11}B$ value is 39.5‰.

2.3.5 Mineral Separation

X-ray diffraction (XRD) was used to determine sample mineralogy before and after sample preparation procedures. All samples were scanned at 1º 2θ/min, using CuKα radiation. Selected clay minerals were physically separated using standard mineral separation methods based on grain size, into < 2μm and > 2μm size fractions (Jackson, 1973).

Minerals of different densities were separated by heavy liquid Sodium Polytungstate ($3Na_2WO_4.9WO_3.H_2O$). A mixing chart was used to get the target density. The detailed sample preparation procedure is as follows:

- Slightly disaggregate and grind sample
- Sonicate the sample to disperse the grains
- Put the sample in the heavy liquid, and sonicate
- Decant the lower density samples through the filter to collect mineral grains
- Collect the heavy fraction on a filter
- Wash the separated mineral repeatedly with milli Q using sonication to remove $Na_2WO_4.9WO_3.H_2O$ from the mineral surface

- X-ray each fraction. Based on XRD results, if needed, repeat procedure 2-4 times. Grind and wash sample before repeating.

2.3.6 Thermal Gradient-Differential Scanning Calorimetry (TG-DSC)

After completion of washing, the serpentine samples are examined by Thermal Gradient-Differential Scanning Calorimetry (TG-DSC) analysis to identify the three forms: lizardite, chrysotile, and antigorite (Deer, 1978). Approximately 10 mg sample is pulverized and loaded to an aluminum cup, which is placed in the chamber of the TG-DSC instrument. The isotherm ramp is set at 30 °C for 2500 seconds to fill the chamber with Helium gas, thus preventing any possible oxidization reaction for the minerals. Then the temperature is increased from 30 to 550 °C at the rate of 30 °C/min. It is stabilized at 550 °C for 5 minutes. In order to capture the endothermic peak from 550 to 800 °C, the temperature is increased at 10°C/min, a lower rate because the most important dehydration reactions, i.e., the release of the structurally bound water, occur during this interval. At the end, it is cooled down from 800 to 30 °C at 30°C/min. The whole run for each sample lasts ~2 hours.

This technique unequivocally identifies three forms of serpentines, as antigorite has an endothermic peak at ~750-780˚C, while chrysotile and lizardite have peaks between 680-750˚C. Lizardite also has an endothermic peak at 550˚C, which can be used to distinguish it from chrysotile (Figure 2.6.6).

2.4 Nankai Trough

2.4.1 Results

Most of the $\delta^{37}Cl$ data of the pore fluids at Site 808 were published in (Ransom et al., 1995). The newly acquired data points, together with the new pore fluid $\delta^{37}Cl$ data for Sites 1173 and 1174, provide a 2-D across-trench section through the Nankai Trough Muroto transect (Fig. 2.4.1). These data allow the analysis of the geochemical evolution from the most arcward Site 808 to the reference Site 1173. This is the first high resolution, chlorine isotope transect for a subduction zone (Fig. 2.4.1).

The pore fluid $\delta^{37}Cl$ values show that $\delta^{37}Cl$ values are significantly more negative than the seawater value and exhibit the largest range observed in any environment yet studied (Fig. 2.4.1). The $\delta^{37}Cl$ profiles also show a systematic evolution along the three sites. In the lower Shikoku Basin Facies, at stratigraphically equivalent depths below the décollement at Sites 808 and 1174, or the proto-décollement at the reference Site 1173, $\delta^{37}Cl$ values decrease to a minimum of -7.8 ‰ at the most arcward Site 808, to -7.1 ‰ at Site 1174 and to -5.8 ‰ at Site 1173. One possible explanation of the low-Cl in the pore fluid in this transect is *in situ* smectite dehydration. Based on cation exchange capacity (CEC) measurements (Henry et al., 2004), the low-Cl concentrations in the pore fluid observed at Site 1174 was explained primarily as a dilution effect from clay interlayer water release during smectite to illite transformation. Given that the *in situ* porosity is ~35%, the average solid density is ~2.65 g/cm^3, the bulk sediment contains ~15 % smectite (15wt% interlayer H_2O

(Kastner et al., 1993)) and ~20% illite (6wt% K_2O) (Underwood et al., 1993); (Underwood, 1996), assuming that all the illite is authigenic, mass balance calculation indicates that a complete transformation from smectite to illite (20% of bulk solid), could account at most for ~13% dilution of Cl concentration in the pore fluid, whereas 19% of Cl dilution was observed, and would require an uptake of ~800 mM potassium from the pore fluids; this is ~80 times higher than the measured potassium depletion of ~10 mM (Underwood et al., 1993).

In addition, smectite dehydration alone does not explain the observed negative $\delta^{37}Cl$ signature because dilution does not fractionate the Cl stable isotopes. Assuming a similar positive $\delta^{37}Cl$ value of ~+8‰ in the authigenic illite as in smectite (Magenheim et al., 1995), with the measured Cl concentration of ~20-30 ppm in the 16 analyzed *in situ* bulk sediments at Sites 808 and 1174 (Fig. 2.4.1), at ~35% porosity and density of ~2.65 g/cm^3, mass balance calculations indicate the above mentioned *in situ* clay mineral reaction, can only decrease the pore fluid $\delta^{37}Cl$ from the seawater value to -0.1‰, compared to the $\delta^{37}Cl$ value of -7.8‰ observed. Hence, the pore fluid negative $\delta^{37}Cl$ observed in the lower Shikoku Basin cannot be derived by just *in situ* dehydration reactions, but requires mixing with a deeply sourced fluid having a negative $\delta^{37}Cl$ signature of $\leq$ -7.8‰ that originated from greater depths where higher temperature (Sharp et al., 2004) fluid-rock reactions (such as serpentine or other hydrous mineral formation) take place and fractionate Cl isotopes.

The high resolution, seaward evolved $\delta^{37}Cl$ - depth profiles suggest that a deep-sourced fluid is laterally advecting from arc to sea through Site 808, 1174, and probably to Site 1173. Based on Cl concentration gradients, fluid velocities within these horizons have been estimated to be 13 ± 5 cm/year (Spivack et al., 2002).

In the turbidite section of the uppermost 600m of the prism, at ~260 mbsf (Fig 2.2.4 and 2.4.1) at all three sites, the Cl concentration increases by ~3% and $\delta^{37}Cl$ shows negative values of ~-5.5 to -6 ‰. At the same depth, $\delta^{18}O$ decreases from seawater value (0 ‰, SMOW) to ~-3.0 ‰ and $^{87}Sr/^{86}Sr$ decreases from seawater value (0.7092) to 0.7080 (Kastner et al., 1993; Wei, 2003). These data clearly indicate volcanic ash diagenesis to clay minerals and zeolites (Kastner et al., 1993), which consumes water, ^{37}Cl and ^{18}O, and releases non-radiogenic $^{87}Sr/^{86}Sr$. The bulk solid, including volcanic ash, has ~600 ppm Cl (Fig. 2.4.1). It is premature to calculate mass balance for the observed negative $\delta^{37}Cl$ value, as the Cl concentration and $\delta^{37}Cl$ data of the unaltered volcanic ash are not known. Separating the pristine ash for analysis is impossible from this horizon because it is altered and mixed with the rest of the sediment.

The higher bromide (Br) concentrations in the shallow turbidite section are attributed to organic matter diagenesis (Price et al., 1977), where organic matter is more abundant (TOC >1.0%) (Moore, 2001). This leads to Br/Cl ratios that are higher than the seawater value. At all these sites, Br concentrations decrease with depth in the Shikoku Basin but Br/Cl ratios do not return to seawater value, neither below the turbidite section nor below the décollement; the ratios are 0.2 to 0.4 $\times 10^{-3}$ higher than

the seawater value of 1.5 $\times 10^{-3}$ below the décollement, at the Cl concentration minimum depth (Fig. 2.4.2), with Br concentration of ~800 μM, slightly lower than the seawater value. Organic matter is mostly absent in the lower Shikoku Basin at 100 °C (Moore, 2001) thus could not affect Br concentration. Pore fluid dilution by smectite dehydration alone does not fractionate Br and Cl, nor change the Br/Cl ratio. Unlike the smaller Cl, the Br ion is excluded from the high temperature hydrous minerals, as indicated by the fact that the Br concentrations were too low (< ~5 ppm) in all solid samples from Nankai to be detected on I.C. by the pyrohydrolysis procedure. Thus, it suggests that in addition to fractionating Cl isotopes, the formation of hydrous minerals at greater depths, at elevated temperatures, also fractionates Br from Cl, thus increasing the Br/Cl ratios in the fluid, as observed.

Fluoride concentrations in the pore fluids remain at the seawater value throughout the turbidite facies, increase dramatically in the upper Shikoku basin pore fluids, and reach maximum values in the lower Shikoku Basin section (Fig. 2.4.3). The maximum F concentration decreases from 3320 μM at Site 808, to 2568 μM at Site 1174, to 2111 μM at Site 1173 as compared to 86 μM in seawater. These values are significantly higher than previously reported values from other ODP sites (e.g. (Froelich et al., 1991; Gieskes et al., 2002)). The sediments exhibit similar F concentration-depth profiles as the pore fluids; they are close to constant and low through the turbidite facies, gradually increase and reach maxima at the boundary between the upper and Lower Shikoku basin facies: 1000 ppm at Site 808 and 870 ppm at Site 1174. The behavior of fluoride is different from Cl and Br due to its small

ionic size. The same shape of depth profiles of F concentration in sediments and pore fluids, and the much higher concentration of F in the solid than in the fluid, suggest that F concentrations in the pore fluids are controlled by lithology. The solubility product K_{sp} of fluorite (CaF_2) increases with temperature, determines that F concentration in the pore fluid is also a function of temperature.

The lithology control on the fluid composition is also shown in the Sr concentration and Sr isotopic ratio - depth profiles at the three sites (Fig. 2.4.4 and 2.4.5). Possible fluid sources can be evaluated through a mixing diagram between Sr isotopic composition and 1/Sr of the pore fluids ((Kastner et al., 1993) and Fig. 2.4.6). From ~100 to 150 mbsf to the boundary between upper Shikoku basin and lower Shikoku basin, which is at ~820 mbsf at Site 808, at ~670mbsf at Site 1174, and at ~340 mbsf at Site 1173, Sr concentration increases steadily and $^{87}Sr/^{86}Sr$ ratios decrease with depth. At the boundary between the upper and lower Shikoku basins, $^{87}Sr/^{86}Sr$ reaches the most non-radiogenic value of ~ 0.7071 where fluoride reaches the maximum concentration. Below the upper and lower Shikoku basin, both Sr concentration and $^{87}Sr/^{86}Sr$ ratios increase, indicating the mixing with a different fluid source, which is Sr rich and highly radiogenic, probably terrigenous. At Site 808 and 1174, the more radiogenic maxima below the décollement, which coincide with the Cl minima depths, most likely reflect transformation reactions of predominantly detrital minerals having radiogenic terrigenous Sr isotopic composition. Close to the basement, the Sr-rich and $^{87}Sr/^{86}Sr$ non-radiogenic signal reflect a third oceanic basement source (Fig 2.4.4 and 2.4.5).

The above geochemical tracers demonstrate that the pore fluid composition is influenced by both *in situ* reactions (shown by F concentration and Sr isotope ratios) and mixing with a deep source fluid (shown by Cl isotope and Br/Cl ratios). The relative contributions of the two are calculated in the next section based on Cl concentration and Cl isotope ratios of the pore fluids.

2.4.2 Fluid mixing: *in situ* fluid and deep sourced fluid

The depth-profiles of Cl concentrations and stable isotope ratios, together with other reported geochemical tracers (Kastner, 2006) indicate that a deeply sourced fluid is laterally advected seaward at Nankai subduction zone. The contributions of the *in situ* and deep-sourced fluids at the sites analyzed are estimated using the following Cl concentration and stable isotope mass balance equations:

$$[Cl]_m = [Cl]_{in\ situ}\, f_{in\ situ} + [Cl]_{deep\text{-}sourced}\, f_{deep\text{-}sourced} \quad (2.2)$$

$$\delta^{37}Cl_m[Cl]_m = \delta^{37}Cl_{in\ situ}[Cl]_{in\ situ}\, f_{in\ situ} + \delta^{37}Cl_{deep\text{-}sourced}\, [Cl]_{deep\text{-}sourced}\, f_{deep\text{-}sourced} \quad (2.3)$$

[Cl] is the Cl concentration and $\delta^{37}Cl$ is the Cl stable isotope composition of the analyzed fluid (m), which is the mixed fluid produced from the *in situ* diagenetic and deep-sourced fluids. The f is the fraction of the *in situ* fluid and/or of the deep-sourced fluid. Diffusion can be ignored if the characteristic length scale for diffusion (d) is less than the width of the low chlorinity anomaly or the width of the gradient zone ($d= 2(Dt)^{1/2}$, in which d is diffusion distance, D is diffusion coefficient of Cl in

sediment, and t is time) (Henry et al., 2004). It is valid for Nankai subduction zone (d = 250m with t=500 kyr and $D=1.4\times10^{-9}$ m^2/s (Henry et al., 2004)).

At the Cl concentration and $\delta^{37}Cl$ minimum depth (~1100 mbsf), the mixed fluid Cl is 450 mM and the $\delta^{37}Cl$ is -7.8 ‰ at Sites 808; at Site 1174 (~900 mbsf), the mixed fluid Cl is 470 mM and the $\delta^{37}Cl$ is -7.1‰. $[Cl]_{in\ situ}$ is estimated to be ~480mM at Site 808, based on the ~ 13% dilution by smectite dehydration with porosity of 30-35% and ~510mM at Site 1174, following a similar calculation with a higher porosity of ~40-45%. In order to produce the minimum $\delta^{37}Cl$ value observed in the pore fluid at Site 808, Cl of the deep sourced fluid has to be ≤ 450 mM and $\delta^{37}Cl$ has to be ≤ -7.8‰. Applying these maximum values to equation (2) and (3) , the pore fluid sample at Site 808 represents mixing of ~0% of the *in situ* derived fluid with 100% of the deep-sourced fluid; and ~30% *in situ* fluid with 70% of the deep-sourced fluid at Site 1174. The $\delta^{37}Cl$ of the deep sourced fluid at Site 1174 is ~-10‰, ~2‰ more negative than at Site 808. Because the deep sourced fluid is the same for both sites, this is an unlikely scenario. Thus, in order to have the same Cl concentration and isotopic value in the deep sourced fluid for both sites, the mixing ratio has to be ~50:50 between the *in situ* fluid and the deep-sourced fluid at Site 808 and ~55:45 at Site 1174. Accordingly, the Cl concentration of the deep sourced fluid is ~410 mM and $\delta^{37}Cl$ is ~-16.9‰.

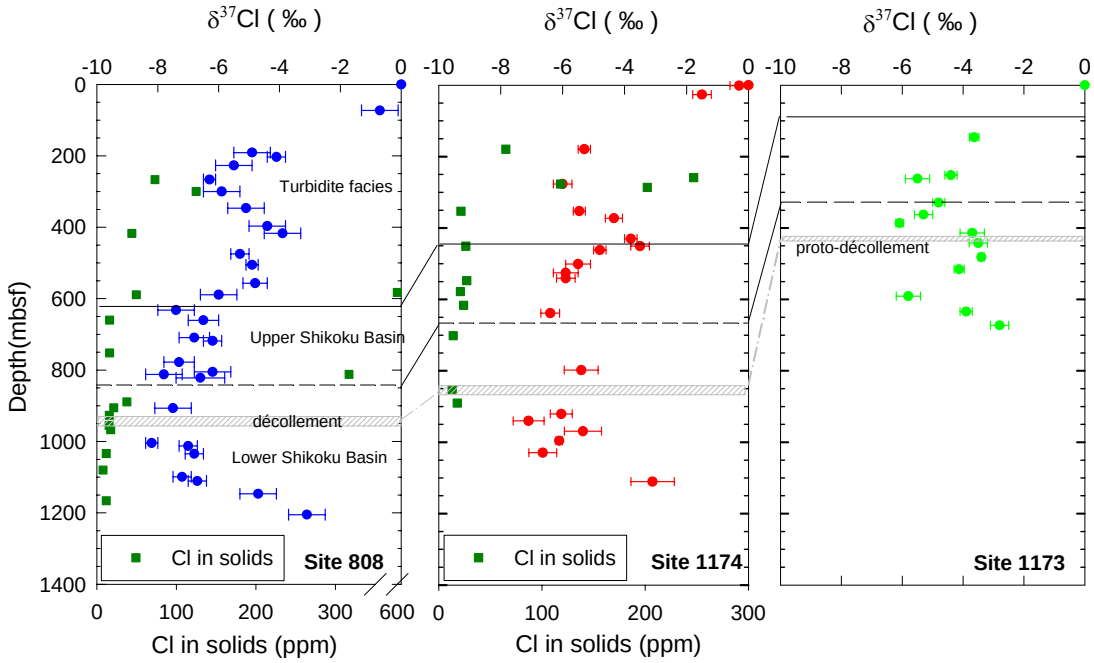

Figure 2.4.1 $\delta^{37}Cl$ (‰)-depth profiles in pore fluids (solid circles) and Cl concentrations of corresponding solids (■) at the Nankai Trough transect. The décollement is situated in the lower Shikoku Basin. Seawater value is by definition 0 ‰ therefore not shown. The error bars represent external errors.

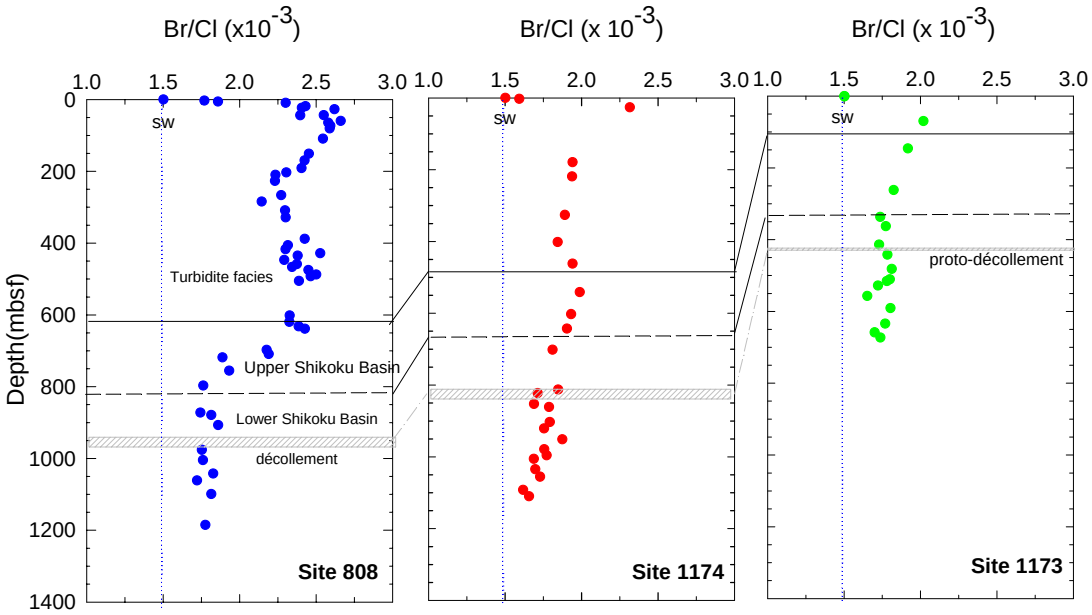

Figure 2.4.2. Br/Cl molar ratio-depth profiles in pore fluids at the Nankai Trough. Seawater value is denoted by the vertical dotted line.

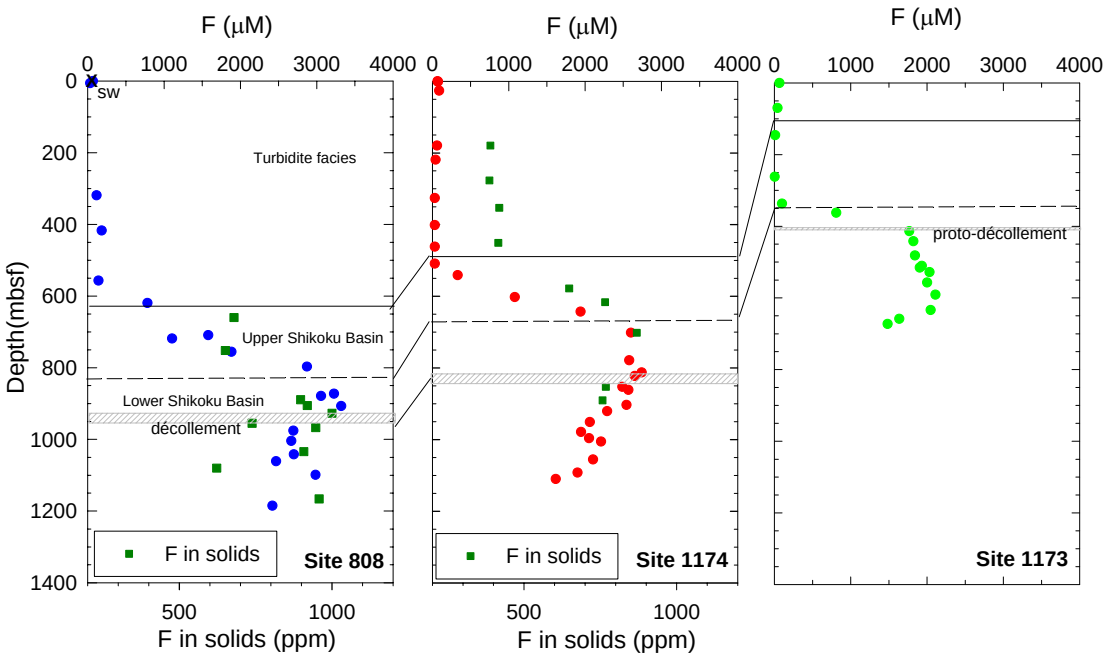

Figure 2.4.3. F concentration depth profiles in pore fluids (solid circles) and in solids (■) at the Nankai Trough. Seawater value is denoted by "x".

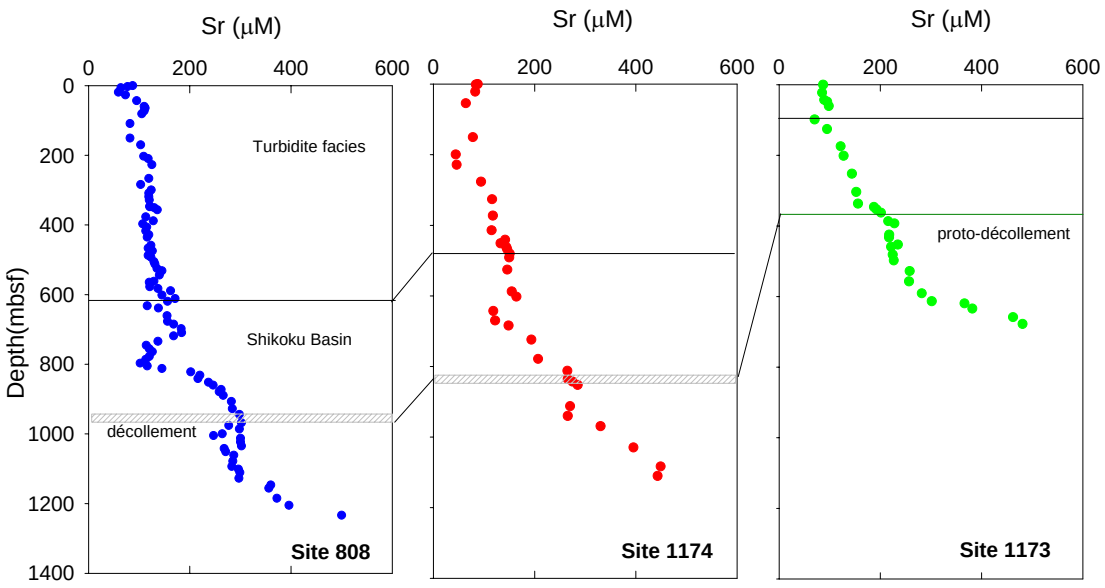

Figure 2.4.4. Sr concentration depth profiles of pore fluid at the Nankai Muroto transect.

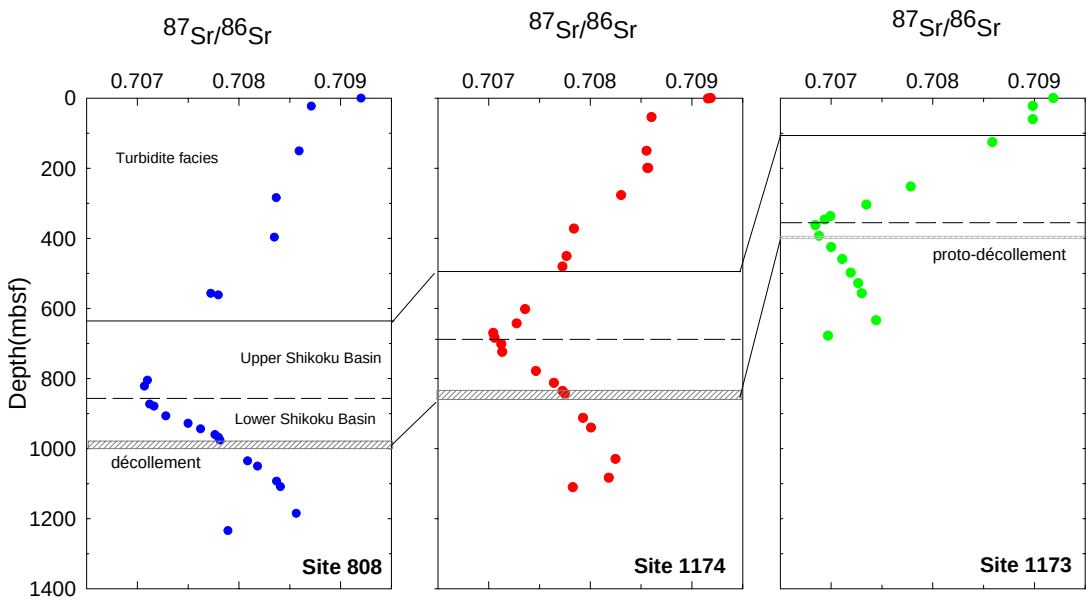

Figure 2.4.5 $^{87}Sr/^{86}Sr$ depth profiles of pore fluid at the Nankai Muroto transect.

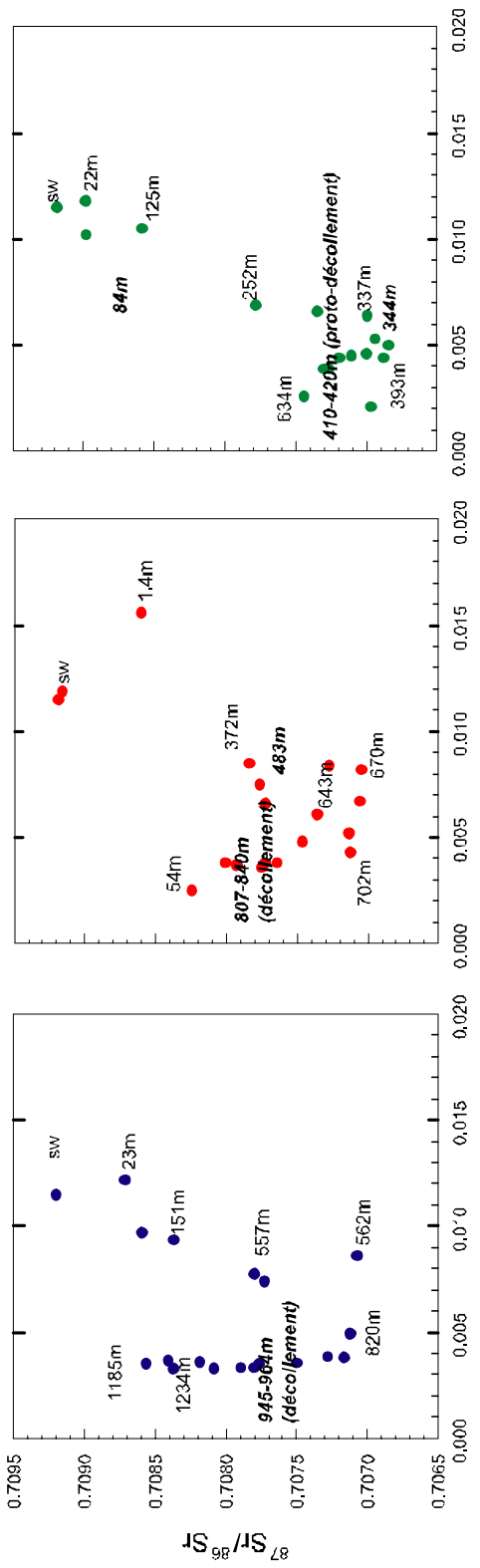

Figure 2.4.6 Mixing relationships between $^{87}Sr/^{86}Sr$ ratios and 1/Sr at the Nankai Muroto transect. The numbers indicate burial depths.

2.5 Costa Rica Subduction Zone

2.5.1 Results

At the reference Site 1039/1253, $\delta^{37}Cl$ values of pore fluids are within ± 0.5 ‰ of the seawater value throughout the sediment section (Fig. 2.5.1). Arcward across the trench, at Sites 1043/1255 and Site 1040/1254 (Fig. 2.5.1), $\delta^{37}Cl$ values at the fracture zone show minima of -3.0 ‰ and -3.2 ‰, respectively. The fracture zone is situated at 90m above the décollement at Site 1043/1255 and 150m above the décollement at Site 1040/1254. Similarly, at the décollement zone of both sites, $\delta^{37}Cl$ minimum values are -3.0 ‰ at Site 1043/1255, and -5.5 ‰ at Site1040/1254 (Fig. 2.5.1). In both the fracture zone and décollement, the $\delta^{37}Cl$ minimum values are more negative at the more arcward site. This arcward trend of Cl depletion and ^{35}Cl enrichment, together with the anomalies of other geochemical tracers (such as Li and Sr concentration and isotope ratios), indicate vigorous fluid advection within the décollement and fault zones that transports species generated at temperatures of > ~150°C (Chan et al., 2000; Silver et al., 2000; Kastner, 2006), thus, at greater depth arcward. The negative $\delta^{37}Cl$ signal of the deep-sourced fluids also implies that similar to that at Nankai subduction zone, high temperature formations (> ~150°C) of hydrous minerals that uptake Cl and fractionate Cl isotopes, also occur at greater depth at the Costa Rica subduction zone. Below the décollement, where the underthrust sediment section is lithologically equivalent to that of the reference Site 1039/1253, $\delta^{37}Cl$ values of the pore fluids are close to the seawater value, within ± 0.5 ‰.

The Br/Cl ratios at the fracture zone and décollement also increase arcward. At the more seaward Site 1043/1255, Br/Cl only shows a slight increase to 2.8 $\times 10^{-3}$ at the fracture zone and 1.8 $\times 10^{-3}$ at the décollement, compared to the value of ~1.5 $\times 10^{-3}$ in the sediment section above the fracture zone and below the décollement, whereas at the more arcward Site 1040/1254, the maximum value is 5.8×10^{-3} at the fracture zone and 5.5×10^{-3} at the décollement (Fig. 2.5.2). Between the fracture zone and décollement at Site 1040/1254, the approximate constant and higher than seawater Br/Cl value of ~3.8 $\times 10^{-3}$, suggests advection of or diffusion from the higher Br/Cl fluid at the décollement and the fracture zone. The high Br/Cl ratios observed at Costa Rica support the conclusion that high temperature hydrous mineral formation fractionates Br and Cl, as at the Nankai subduction zone.

The maximum fluoride concentration values are 1300 μM at the fracture zone and 1400 μM at the décollement at the most arcward Site 1040/1254 (Fig. 2.5.3). These maximum values at Costa Rica are lower than at the Nankai subduction zone (2000-3000 μM), most likely due to the different F concentration in the source solids: 400-500 ppm at Costa Rica and up to 900 ppm at Nankai. At the seaward Site 1043/1255, the F concentration maximum values are considerably lower, ~125 μM at the fracture zone and the décollement. Similar to the Br/Cl ratios, between the fracture zone and the décollement, F concentrations are higher than the seawater value but lower than adjacent maxima, implying diffusion/advection of the high F fluids from the fracture zone and décollement. Above the fracture zone and below the

décollement, F concentrations are constant with seawater value; the fluoride concentration-depth profiles simply resemble that at the reference Site 1039/1253.

Sr concentration and isotope ratios are strongly affected by diagenetic reactions and tend to depart from seawater values with depth in most marine sediments, especially in calcareous volcanic-rich sediments (Baker et al., 1982). At the fracture zone and décollement of Site 1040/1254, the $^{87}Sr/^{86}Sr$ ratios reach minimum values (0.7076 and 0.7073, respectively), suggesting the deep source fluid carries a less radiogenic signature and is probably influenced by volcanic ash (Fig. 2.5.4 and 2.5.5). At Site 1039/1253, from 0 mbsf to ~300 mbsf, Sr concentration increases from seawater value of 87 μM to ~300 μM, and Sr isotope values become less radiogenic due to volcanic ash influence (Fig. 2.5.4 and 2.5.5). Below 300 mbsf, both trends reverse and approach modern seawater values in the basal sections. This is driven by a fluid flow system in the upper igneous complex and/or basement that governs the transport of heat at this section of the down-going slab (Kastner, 2006). Based on Sr concentration and isotope ratios at Site 1039, Silver et al. (Silver et al., 2000) have estimated that the basement formation water is younger than 20 ka.

In summary, a chemically distinct fluid originating at greater depth arcward is laterally injected along fracture zones and décollement. Relative to seawater, this fluid has a low Cl concentration, negative $\delta^{37}Cl$, high F concentration and Br/Cl ratio. Similar to the Nankai subduction zone, at Costa Rica, the source fluid indicates a high temperature source arcward. Because of dilution with *in situ* pore fluids, the signal is weaker seaward along the décollement from Site 1040/1254 to Site 1043/1255.

2.5.2 Fluid flow modeling at the décollement, using Cl concentration and isotope ratios

The halogen concentrations, Cl isotope and Sr isotope ratios of pore fluids at Costa Rica indicate that there is a deep source fluid advecting along the décollement and the fracture zone and the fluid-rock reaction at the fluid source is similar to that at Nankai Trough. At the Costa Rica subduction zone, the geothermal gradient is low and temperatures remain less than 5°C at the fracture zone or the décollement, therefore, the smectite-illite transition does not contribute to the *in situ* Cl freshening at the fracture zone and décollement at Site 1043/1255 and 1040/1254, located just 0.5 km and 1.6 km from the deformation front. The fresher than seawater pore fluid along the décollement and fracture zone represents a mixed fluid involving a fluid advected from the underthrust sediments where Cl concentration is close to the seawater value, and a deeply sourced fluid flowing along the décollement (Saffer et al., 2003). The difference in the diffusion coefficients of ^{35}Cl and ^{37}Cl in the fluid from the underthrust sediment may cause Cl stable isotope fractionation at the décollement (Eggenkamp et al., 1994; Saffer et al., 2003). Solving the transient advection-diffusion equation in one dimension for the underthrust section (Crank, 1975):

$$D_L \frac{\partial^2 C}{\partial x^2} - v_z \frac{\partial C}{\partial x} = \frac{\partial C}{\partial t} \tag{2.4}$$

Where

C = solute concentration

x = distance from source

T = time since the introduction of the solute

D= diffusion coefficient

v = average fluid velocity

L= total length of the system

Initial condition: $C(x, 0)= 0$ for $0 \le x \le L$

Boundary condition: $C(0, t)=0$ for all t,

$C(L, t) = C_0$ for $t>0$

Solving the equation (Al-Niami et al., 1977),

$$\frac{C(x,t)}{C_0} = \frac{\sinh(\,vx\,/\,2D)}{\sinh(\,vL\,/\,2D)} \exp\left[\frac{v(x-L)}{2D}\right] + \frac{2\pi D}{L^2} \exp\left[\frac{v(x-L)}{2D} - \frac{v^2 t}{4D}\right]$$
$$\times \sum_{n=1}^{\infty} \frac{(-1)^n \cdot n \cdot \exp[\,-Dn^2\pi^2 t\,/\,L^2]}{Dn^2\pi^2\,/\,L^2 + v^2\,/\,4D} \sin\,\frac{n\pi x}{L}$$

(2.5)

An alternative condition which allows some dispersion to occur at the boundary which may be more realistic is: $\frac{\partial C}{\partial x}(0,t) = \frac{v}{2D}(0,t)$.

Solution can be obtained in a similar manner to equation (2.5) (Al-Niami et al., 1977):

$$\frac{C(x,t)}{C_0} = \frac{\cosh(vx/2D)}{\cosh(vL/2D)}\exp\left[\frac{v(x-L)}{2D}\right] - \frac{\pi D}{L^2}\exp\left[\frac{v(x-L)}{2D} - \frac{v^2 t}{4D}\right] \quad (2.6)$$
$$\times \sum_{n=0}^{\infty} \frac{(-1)^n (2n+1)\exp[-0.25\,D(2n+1)^2\pi^2 t/L^2]}{D(2n+1)^2\pi^2/4L^2 + v^2/4D} \cos\frac{(2n+1)\pi x}{2L}$$

For the Costa Rica subduction zone, based on F and Br concentration profiles between the décollement and fracture zone, dispersion seems to occur, thus equation (2.6) was used in the modeling of Cl stable isotope ratio fractionation of the pore fluid caused by diffusion, in the underthrust section.

The isotopic separation factor S, which is approximately equivalent to δ^{37}Cl (‰), can be expressed as:

$$S = \left(\frac{35C^0\,37C}{37C^0\,35C} - 1\right)\times 1000 \text{ (Desaulniers et al., 1986)} \quad (2.7)$$

With the ratio of diffusivities of Cl (D_{37Cl}/D_{35Cl}=0.99857) (Richter et al., 2006) of the fluid in the underthrust section, the δ^{37}Cl value of the *in situ* fluid was calculated to be by equation (2.6) to be ~-1‰ at both Sites 1040/1254 and 1043/1255, assuming no mixing with the deep-sourced fluid, as shown in Fig. 2.5.6. Following similar explanations to those used for the Nankai subduction zone, the observed δ^{37}Cl values of -3.2 to -5.5 ‰ along the Costa Rica décollement indicate that the *in situ* pore fluid having Cl concentration of ~559 mM and δ^{37}Cl of ~-1‰, is as well a mixture

with a deep-sourced fluid, assumed to also originate from high temperature hydrous mineral formation.

Following the calculation at Nankai, assuming ~0 % of the *in situ* measured fluid is from advection/diffusion from the underthrust section, and ~100% consists of the deep sourced fluid, Cl concentration and isotopic ratio of the deep sourced fluid are equal to the measured values of the pore fluid at the décollement at ODP Site 1040; hence, its Cl concentration would be 480 mM with δ^{37}Cl of -5.5‰. In such a case, at the more seaward Site 1043, the calculated fluid mixing is 40% and 60%, respectively. Using this mixing ratio, the calculated δ^{37}Cl of the deep sourced fluid is -5.4‰, only 0.1‰ less negative than that assumed at Site 1040. The difference in the two values at the two sites is within the Cl isotope ratio analytical error of ±0.3‰, suggesting that this scenario is plausible. If, however, the difference of the δ^{37}Cl value of the deep sourced fluid at both sites is reduced to 0.0‰, the mixing ratio between the *in situ* fluid and the deep-sourced fluid at Site 1040 is ~30:70 and ~55:45 at Site 1043, with the Cl concentration of the deep sourced fluid of ~450 mM and δ^{37}Cl of ~-7.9 ‰.

The decreasing percentage of the deep sourced fluid along the décollement from the more arcward Site 1040 to the more seaward Site 1043 is also reflected in the Br and F concentrations.

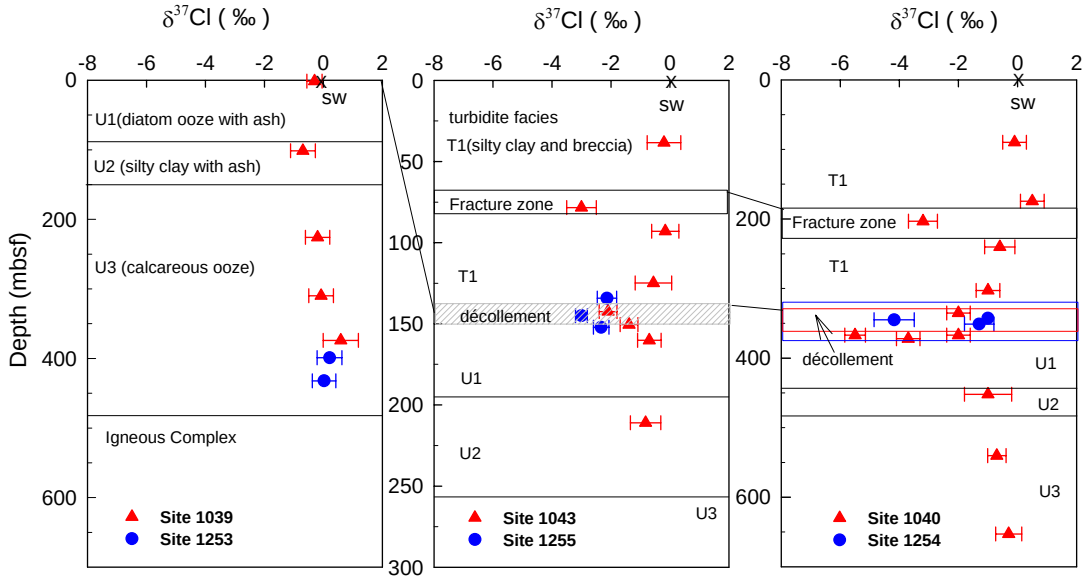

Figure 2.5.1 δ^{37}Cl (‰)-depth profiles in pore fluids at Costa Rica subduction zone transect. Note the different depth scales at the three sites. Seawater value in A, B, and C is denoted by "×". U1, U2, U3, and T1 indicate lithostratigraphic units. U1: diatom ooze with ash; U2: silty clay with ash; U3: calcareous ooze; T1: silty clay and breccia.

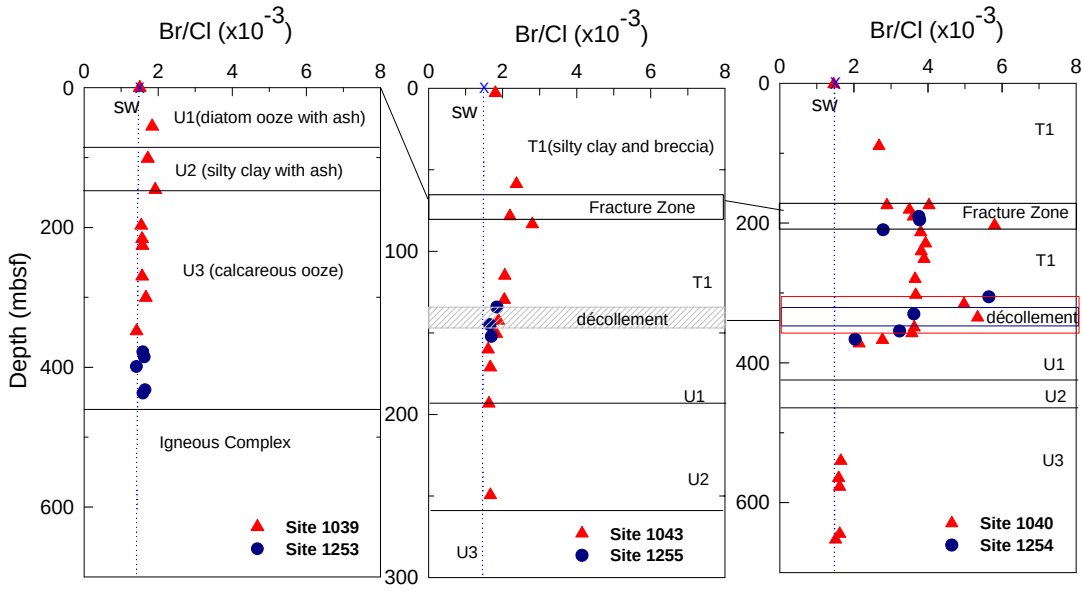

Figure 2.5.2 Br/Cl molor ratio-depth profiles in pore fluids at the Costa Rica subduction zone transect. Seawater value is denoted by dotted line. Seawater value in A, B, and C is denoted by "×". U1, U2, U3, and T1 indicate lithostratigraphic units. U1: diatom ooze with ash; U2: silty clay with ash; U3: calcareous ooze; T1: silty clay and breccia.

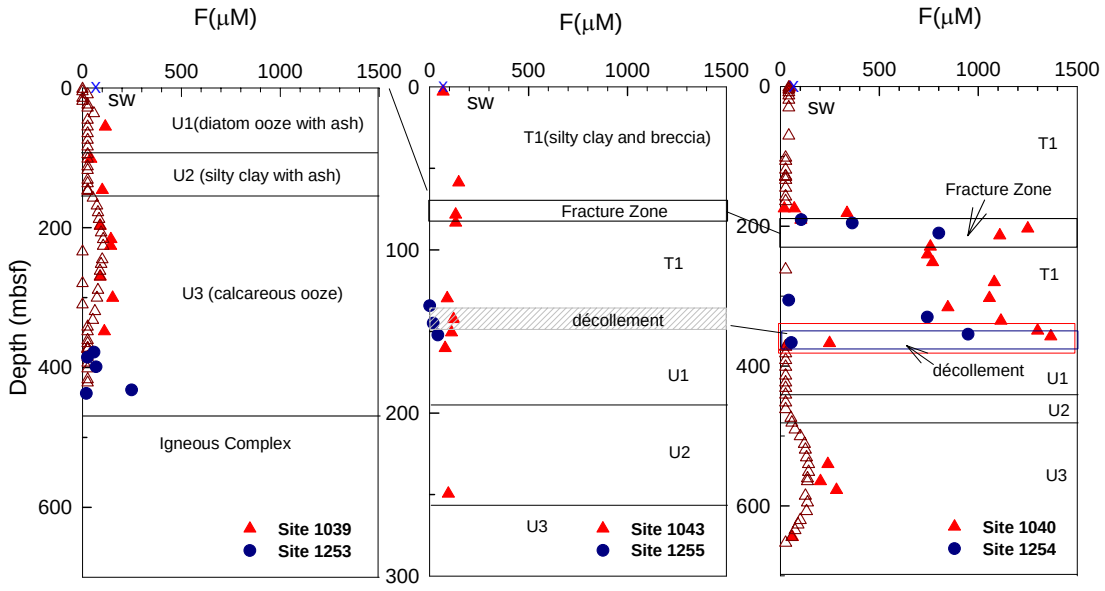

Figure 2.5.3 F concentration depth profiles in pore fluids at the Costa Rica subduction zone transect. The open triangles (Δ) indicate data analyzed by Saether using ion-selective electrode (personal communication). Seawater value in A, B, and C is denoted by "×". U1, U2, U3, and T1 indicate lithostratigraphic units. U1: diatom ooze with ash; U2: silty clay with ash; U3: calcareous ooze; T1: silty clay and breccia.

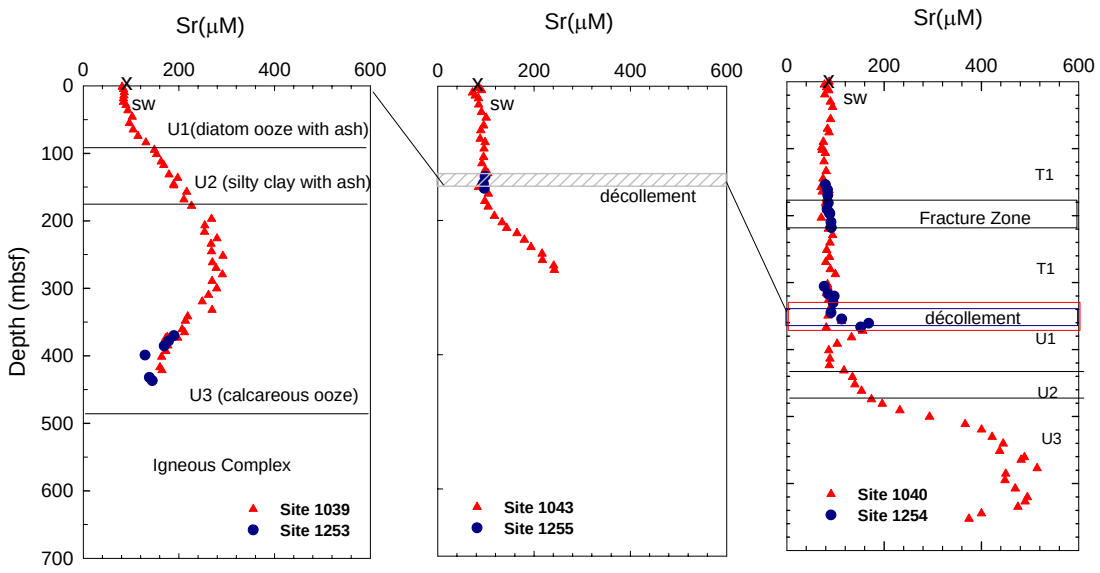

Figure 2.5.4 Sr concentration depth profiles of pore fluid at the Costa Rica subduction zone. Seawater value is denoted by "×". U1, U2, U3, and T1 indicate lithostratigraphic units. U1: diatom ooze with ash; U2: silty clay with ash; U3: calcareous ooze; T1: silty clay and breccia.

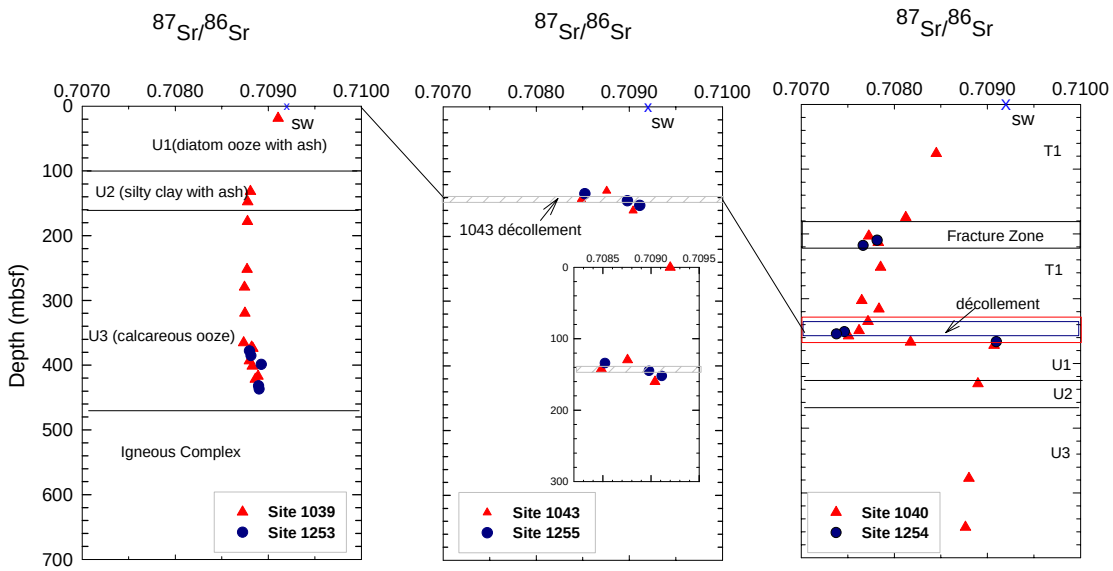

Figure 2.5.5 $^{87}Sr/^{86}Sr$ depth profiles of pore fluid at the Costa Rica subduction zone. Seawater value is denoted by "×". U1, U2, U3, and T1 indicate lithostratigraphic units. U1: diatom ooze with ash; U2: silty clay with ash; U3: calcareous ooze; T1: silty clay and breccia.

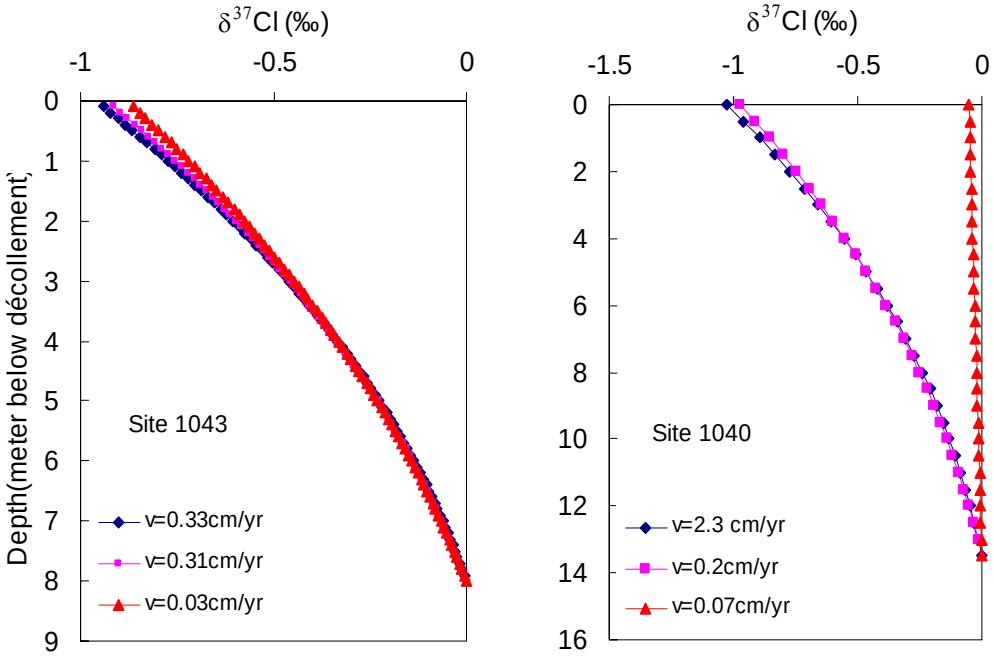

Figure 2.5.6 Modeled $\delta^{37}Cl$ fractionation at the décollement caused by advection-diffusion at Site 1043 and Site 1040, Costa Rica subduction zones, under different possible fluid advection velocities, indicated by different symbols. Diffusion time t=8.7 kyr at Site 1043 and t=13.5 kyr at Site 1040.

2.6 Results and Discussion of Mariana Mud Volcanoes

2.6.1 Results

Halogen concentrations and Cl stable isotope

Chloride concentrations in the pore fluids from all holes drilled at South Chamorro Seamount are lower than in bottom seawater by as much as 7% (Morris, 2003). In contrast to the negative $\delta^{37}Cl$ values in the pore fluids at Nankai and Costa Rica subduction zones, pore fluid $\delta^{37}Cl$ values at ODP Sites 1200, serpentine mud volcanoes at Mariana, range between 0.3 ‰ at 0.9 mbsf, to +1.8 ‰ at the deepest uncontaminated sample obtained at just 70 mbsf in Hole A (Fig. 2.6.1). It is important to note that the maximum drilling depth (70 mbsf) at Mariana is much shallower than at Nankai (1200 mbsf) or Costa Rica (700 mbsf). The observed positive $\delta^{37}Cl$ (up to +1.8 ‰) suggests that the fluid-solid reactions, which affect Cl isotope ratios at depth at the Mariana *versus* at the Nankai and Costa Rica subduction zones, are distinct.

In the associated serpentinite mud samples from Hole 1200 E, Cl concentrations range from 110 to 200 ppm and the $\delta^{37}Cl$ from +1.0 to +4.2 ‰ (Fig. 2.6.1 and Table 2.6.1). The serpentinized igneous basement samples from Holes 1200 A and B are similar; both are enriched in Cl up to 400-500 ppm, with $\delta^{37}Cl$ value of +1.7 ‰ (1200 B, Table 2.6.1). The serpentinite from Bluemoon Seamount contains 521 ppm Cl and the $\delta^{37}Cl$ value is +1.9‰. The $\delta^{37}Cl$ values in serpentines from the Mariana seamounts are close to the theoretical estimate of $\delta^{37}Cl$ of 2-3 ‰ in silicates formed in equilibrium with seawater of $\delta^{37}Cl$ equal to 0‰ (Schauble et al., 2003). The

Cl content variations in the serpentines may be due to the different forms of serpentines having different partition coefficients. One brucite sample separated from a calcite chimney at Conical Seamount has a Cl concentration of 428 ppm and a $\delta^{37}Cl$ value of +8.4‰, being the most positive $\delta^{37}Cl$ value analyzed so far in any Cl-containing mineral reported (Table 2.6.1). The high $\delta^{37}Cl$ value in the brucite separate sample probably reflects a difference in the vibrational zero-point energy in brucite and serpentines.

At high temperature and pressure when hydrous mineral dehydrate, in addition to water, Cl with enriched $\delta^{37}Cl$ is also released into the fluid phase. The above mentioned observed positive $\delta^{37}Cl$ in the pore fluids supports the suggestion by Mottl et al (Mottl, 2003) that at the Mariana subduction zone, the origin of the upwelling pore fluids is the dehydration of the subducting serpentinized crust.

Fluoride concentrations in pore fluids were determined on board (Shipboard Scientific Party, 2002). Generally, our IC results show similar trends to those obtained from the ion selective electrode method (ISE) (Fig. 2.6.2). In Hole 1200D, the farthest from the spring, fluoride concentrations decrease sharply within the uppermost meter below the seafloor, from 68 μM to almost 0 and then rebound to ~50 μM at 30 mbsf. At the spring and close to it in Hole 1200E, fluoride first increases to ~110 μM above 20 mbsf, then decreases to 50 μM at greater depth, and in Hole 1200F, fluoride concentration is ~40 μM at the seafloor and increases to ~80 μM with depth. F/Cl vs. depth profiles (Fig. 2.6.2) indicate that at shallow depths (<20 mbsf), the values in Holes 1200E and 1200F are higher than in seawater, whereas in Hole 1200D, F/Cl

ratios are much lower. At greater depth (>20 mbsf), F/Cl ratios merge to the seawater value, with the deepest sample in Hole A having greater than seawater value, implying that F and Cl released by the solids have slightly higher F/Cl ratios than seawater.

Bromide concentration-depth profiles are similar to those of Cl (Fig. 2.6.2). The values are also lower than the seawater value and exhibit a steep depletion in concentration within the uppermost 4.5 meters below seafloor (mbsf); deeper they remain approximately constant. The Br profile at Hole 1200 F has the typical convex-upward shape and steep near-surface gradient, indicative of upwelling at 1-10 cm/yr (Mottl et al., 2003).

All bulk solid samples contain <100 ppm F, except at depths of 10 to 15 mbsf in Hole 1200E, fluorine is enriched up to 400 ppm (Table 2.6.1). XRD analysis of this solid sample Hole 1200E 3H1 has shown that it contains ~40% aragonite. A fluoride peak is also observed in the F concentration-depth profiles of the pore fluids at the same depth (Fig. 2.6.2-B and D). No bromine was detected in any of the solids by I.C. method; therefore, Br is not shown in the table.

The pore fluid Br/Cl *versus* 1/Cl data from all ODP Site 1200 holes fall on a straight line (Fig. 2.6.3), indicating mixing between two end-member fluids; an ascending fluid and bottom seawater. In general, Br/Cl ratios in Hole 1200D are higher and closer to the seawater value than in Holes 1200E, 1200F and 1200A. At Hole 1200D, which is farther away from the spring, fluid upwelling is less intense, thus the deep fluid signal is more diluted by mixing with seawater as compared with Holes E, F and A that are closer to the spring. All 1/Cl values are higher than that of seawater because of Cl depletion with depth. Below 5 mbsf, the lower than the

seawater Br/Cl values indicate the depletion of Br relative to Cl due to dehydration/dechlorination of hydrous minerals releasing Cl enriched in ^{37}Cl and water, but not Br. In contrast, at the Nankai and Costa Rica subduction zones, where hydrous mineral formation influences the pore fluid Br and Cl concentrations and the Cl isotopic compositions, the pore fluids have negative $\delta^{37}Cl$ values and higher than seawater Br/Cl ratios. Another interesting observation is that the maxima in Br/Cl ratios observed at the fracture zone and décollement at the Costa Rica subduction zone sites 1040 and 1043 are higher than those at the Nankai subduction zone, suggesting a higher organic carbon content in the fluid source region at the Costa Rica subduction zone than at Nankai.

Boron concentration and isotope ratios in pore fluids

B isotope fractionation between solids and fluids is thought to relate to the preferential incorporation of ^{10}B-rich $B(OH)_4$ into silicate minerals and is strongly influenced by pH and temperature (Spivack et al., 1987; Palmer et al., 1998; Sanyal et al., 2000). B isotope ratios and concentrations may provide evidence for serpentine formation and clay alteration at depth (Spivack et al, 1987; Palmer 1996; Benton et al., 2001). At seafloor temperatures, B partitions preferentially into serpentine (Spivack and Edmond, 1987; Bonatti et al., 1984). When serpentine forms, B uptake is high and isotope ratios ($^{11}B/^{10}B$) in the residual fluid increase (Benton et al., 2001) because of preferential uptake of ^{10}B by solids. At low temperatures, the reversible adsorption of B also occurs and the adsorbed species is as well predominantly the light isotope ^{10}B (Spivack et al, 1987; Palmer 1996). In general, at greater depths, B gets enriched in

fluids by processes such as desorption from clays, mineral dehydration reactions, increasing temperature and alteration of volcanic or igneous rocks (Seyfried et al., 1984; Spivack et al., 1987; You et al., 1996; Palmer and Swihart, 1996).

At Site 1200 at the Mariana subduction zone, boron concentrations in pore fluids increase sharply from seawater value of 416 μM to ~3500 μM immediately within 5 meter below seafloor (mbsf) and remain constant with depth to the deepest uncontaminated sample at 70 mbsf (Fig. 2.6.4 A and B). B/Cl ratios at depth (Fig. 2.6.4 A) are about six times seawater value, indicating that the upwelling fluids are greatly enriched in boron. The high B concentration is also observed in the pore fluid dataset from Conical Seamount (Mottl et al., 1992; Benton, 1997; Benton et al., 2001).

Boron isotope signatures in the pore fluids are significantly depleted relative to the seawater value of 39.5 ‰ (Spivack et al., 1987) (Fig. 2.6.4 C). Even the pore fluid sample from closest to the seafloor in Hole 1200E, sample 1H-1, has a value of 20‰, much lower than the sea water value of 39.5‰. $\delta^{11}B$ values gradually decrease with depth to 16‰ at 71mbsf. The gradient is higher at shallower depths (21‰ to 17‰ from 0.95 to 15 mbsf, then to 16‰ from 15 to 71 mbsf). The cross plot of $\delta^{11}B$ vs. 1/B (Fig. 2.6.5) shows that $\delta^{11}B$ evolves from the lowest value of 16‰ in the deepest sample to 20‰ in the shallowest sample, having relatively constant but much higher (~3 to 8 times) than seawater B concentration throughout the depth range analyzed. This implies mixing even at the shallow depth; if we assume the sample (1500 μM B with $\delta^{11}B$ = 21.5‰) at 1 mbsf is a mixture of seawater (416 μM B with $\delta^{11}B$ = 39.5‰) and upwelling fluid (3500μM B with $\delta^{11}B$ = 16‰), the calculation shows that the

seawater accounts for ~65% and the upwelling fluid for ~35% at 1 mbsf, while below 5 mbsf, upwelling fluid constitutes greater than 99% of the fluid analyzed.

Boron concentration and isotope ratios in solids

In Hole 1200E, B concentrations in solids (Fig. 2.6.4 B) are ~70-80 ppm (twice the pore fluid value of 1.4 to 3.6 mM; [~16 to 39ppm]) in the upper 10 mbsf and decreases sharply to a constant concentration of ~40 ppm (slightly higher than the pore fluid value of 3.5 mM, [38.5ppm]) below ~10 mbsf. The B isotope value is 13‰ in the surface sample and decreases to 7 ‰ at depth (Fig. 2.6.3 C). In Hole 1200A, the solid sample from 18.8 mbsf shows B concentration of ~66 ppm and isotopic ratio of 15.5‰, higher than at the equivalent depth in Hole 1200E (Fig. 2.6.4 B). High heterogeneity and different mineral composition might have an influence on differences in B contents.

The B signatures in the solids, are a result of chemical exchange with upwelling pore fluids containing ~3600 μM B (Moore et al., 1992; Benton et al., 2001)(Fig. 2.6.4 B). It is inferred from the $\delta^{11}B$ of the solids that the upwelling slab fluid has a $\delta^{11}B$ of about +13‰ (Benton et al., 2001), representing the lower limit of $\delta^{11}B$ in pore fluids, because the high pH of the pore fluids should minimize fluid-mineral isotopic fractionation, as B speciation in solution is strongly dependent on pH, at pH ~12, essentially 100% of pore fluid B will be speciated as tetrahedral $B(OH)_4^-$.

As indicated by other geochemical tracers, dehydration of minerals must be occurring at depth during subduction (Mottl et al., 2003). The $\delta^{11}B$ difference between

B in pore fluids (+16‰) and structurally bound B in subducted sediments (–4‰ to +3‰) (Spivack et al., 1987), ranges from 13 ‰ to 20 ‰. Peacock and Hervig (1999) (Peacock et al., 1999) have shown that subduction-zone metamorphic rocks have a $\delta^{11}B$ –11 to –3 ‰, decreasing $\delta^{11}B$ of the subducting solids by 1 ‰ to 14 ‰ (–4 ‰– (–3) ‰ to 3 ‰– (–11) ‰). This suggests that slab dehydration reactions significantly lower the $\delta^{11}B$ values of subducted oceanic crust and sediments and enrich the pore fluid in ^{11}B.

Boron concentration in seawater has been nearly constant over the past 25 Ma, approximately one residence time, implying a close balance of inputs and outputs for B (Spivack et al., 1993). The proposed outputs of B in the ocean are uptake during low- temperature weathering of the oceanic crust, adsorption on clastic sediments, and co-precipitation in carbonates (Spivack et al., 1987) and the inputs are rivers, hydrothermal vents, and fluid expelled from accretionary prisms in subduction zones (Lemarchand et al., 2000). The data from Mariana forearc show that the fluids from non-accretionary prisms can also contribute significantly to the B cycle. The estimates of B budgets indicate that the output flux (2.5×10^{10} mol/yr) is far more than the input flux (0.6×10^{10} mol/yr) (Spivack et al., 1987; Vengosh et al., 1991; Smith et al., 1995). Based on the data from Nankai, You et al. (1993) suggested that the fluids expelled from Earth's subduction process contributes 0.2×10^{10} mol/yr as reflux, balancing only 10% of the seawater budget. The most likely “missing” boron input source is associated with volatilization associated with island- arc magma genesis, derived from subducted slab and/or sediments (You et al., 1993). The data in the

Mariana subduction zone support this suggestion. The deeper fluids, which are released by dehydration and expelled by advection, are enriched in B up to 3 to 4 mM, with upwelling rates of 1-10 cm/yr. Assumed that the total area of the South Chamorro Seamounts is 707 km^2 ($\pi \times [30/2]$ km^2 based on a seamount diameter of 30 km), the fluid flux is up to 0.07 km^3/yr and the B flux is calculated to be 0.03×10^{10} mol/yr. Based on the nine identified active seamounts at Mariana which are assumed to have similar B concentrations and flux rates (as indicated by the data from Conical Seamount and South Chamorro Seamount), the total B flux is ~0.3×10^{10} mol/yr. This is only a minimum estimated fraction of the total B flux in one non-accretionary subduction zones. Therefore, the B reflux during plate subduction seems to be a critical part that may complete the B cycling in the ocean.

2.6.2 Serpentine Mineralogy

Serpentine, $Mg_3Si_2O_5(OH)_4$, has three different forms: lizardite, chrysotile, and antigorite (O'Hanley, 1996). Reactions that form serpentine, such as: $2Mg_2SiO_4$ (olivine) + $3H_2O \rightarrow Mg_3Si_2O_5(OH)_4 + Mg(OH)_2$ (brucite) are exothermic and consume H_2O. The three forms of serpentines form at different temperature and pressure: hydration of forsterite produces antigorite and brucite at higher T and P (H_2O); chrysotile and brucite at intermediate T and P (H_2O); and lizardite and brucite at lower T and P (H_2O) (O'Hanley, 1996).

To better understand the origin and structure of serpentine, it is important to distinguish its three different forms: lizardite, chrysotile, and antigorite. It is almost impossible to identify the three forms of serpentines with an unaided eye because they all have similar colors, habits and occurrences (Wicks, 1988). X-ray Diffraction (XRD) method has been used to help characterize the forms (Whittaker et al., 1956; Page et al., 1967; Wicks, 1988), but the results in many cases have shown that the "diagnostic peaks" are non-reliable because of the low intensities. Therefore, Thermal Gradient- Differential scanning Calorimetry (TG-DSC) is used to serve the purpose.

The three pure forms of serpentines from different locations were used as standards to identify the temperature at which the endothermic reaction (releasing water) occurs. Antigorite gives an endothermic peak at ~ 730 °C, whereas for chrysotile and lizardite, the peak occurs at ~640-690°C and ~600-630°C, respectively. Another peak at 550°C is also associated with lizardite, which is used to differentiate from chrysotile (Fig. 2.6.6). Therefore, TG-DSC is a powerful tool to distinguish the antigorite, lizardite, and chrysotile.

By this means, serpentine samples from seamounts in Mariana were analyzed and identified to be mainly chrysotile and lizardite. Some samples also contain brucite, which gives an endothermic peak at 450°C, and calcite or aragonite, which gives a peak at 760-800°C. The brucite and calcite (or aragonite) are further identified by XRD analysis. Only one sample from Bigblue Seamount has been detected to contain antigorite.

By identifying the different forms of the serpentine, various concentrations of incompatible elements, such as Cl, may be explained by the slightly different mineral

structures. Of the fibrous serpentine forms, chrysotile and lizardite, chlorine concentration is higher, in the range of 260-415 ppm; when they transform to the more massive antigorite structure, Cl is expelled and decreases to ~140 ppm. The chlorine content in serpentines is discussed in detail in the next section.

Table 2.6.1 Fluorine and chlorine concentrations (ppm) and $\delta^{37}Cl$ (‰) values in serpentines, analyzed in this study

Serpentine	Location	Sample Description	F (ppm)	Cl (ppm)	$\delta^{37}Cl$ (‰)[2]
Antigorite	N. California	>95% serpentinized Dunite(ol) and Harzburgite (ol+opx)	47	140	2.2
Chrysotile	from S. Africa	>95% serpentine	0	415	2.3
Serpentine muds Site 1200 Hole E	Marianna				
Core 3H1, 11.4 mbsf	S. Chamorro seamount	Serpentinized peridotite with aragonite	430	186	3.2
Core 5H1, 17.7 mbsf	S. Chamorro seamount	Serpentinized harzburgite	30	200	1.4
Core 7H1, 27.0 mbsf	S. Chamorro seamount	Serpentinized mylonite	27	146	4.2
Core 10H2, 54.9 mbsf	S. Chamorro seamount	Serpentinized harzburgite	78	127	1.2
Site 1200 Hole B[1], Core 2W2, 33.2 mbsf	S. Chamorro seamount	Altered igneous basement rock	5	400	1.7
Serpentine bulk sample	Bluemoon seamount	>95% serpentine	56	521	1.9
Brucite Separate from Calcite	Conical Seamount	Carbonate chimney at Conical Seamount	244	428	8.4
Serpentine bulk sample	Hess Deep (ODP Leg 147 Site 895)	>95% serpentinized from harzburgites and dunites; only washed outside without crushing	12-109 (n=4)	445-745 (n=4)	-0.1 to +1.8 (n=2)
Serpentine powdered	Hess Deep (ODP Leg 147 Site 895)	powdered to fine grains	92-100 (n=2)	290 (n=1)	+6.0 (n=1)

[1] Serpentines from Hole 1200A and 1200B are both altered igneous basement rocks; $\delta^{37}Cl$ value of 1200 A is not available.
[2] Error is 0.6‰ (2σ).
n=number of samples analyzed.

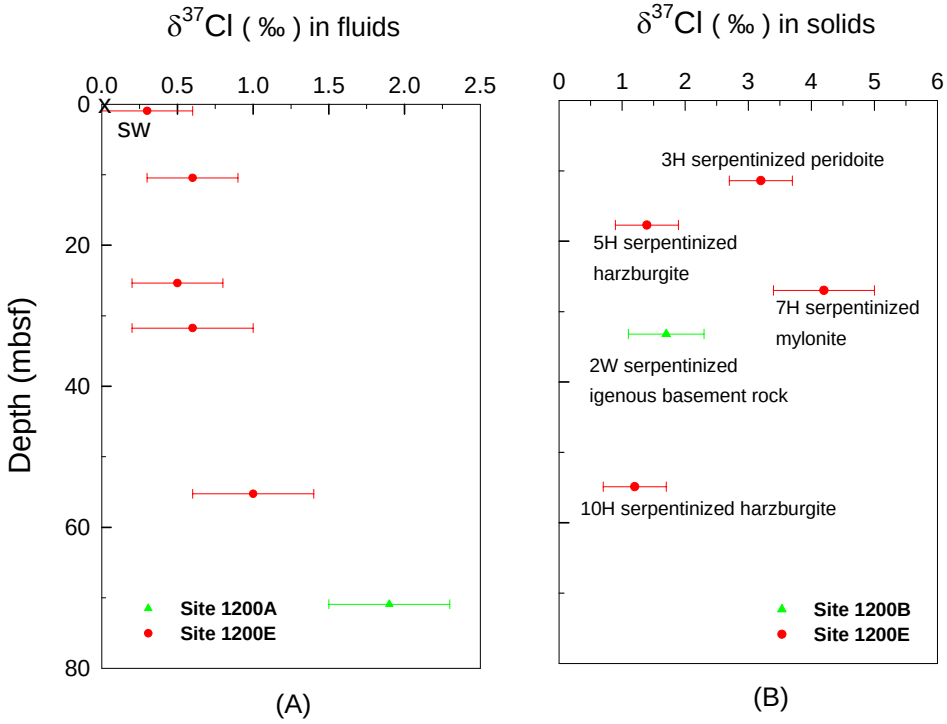

Figure 2.6.1 (A) $\delta^{37}Cl$ (‰)-depth profile in pore fluids at the Mariana subduction zone, South Chamorro seamount ODP Site 1200.
(B) $\delta^{37}Cl$ (‰)-depth profile of serpentines from the Mariana subduction zone, South Chamorro seamount ODP Site 1200. The error bars represent external errors.

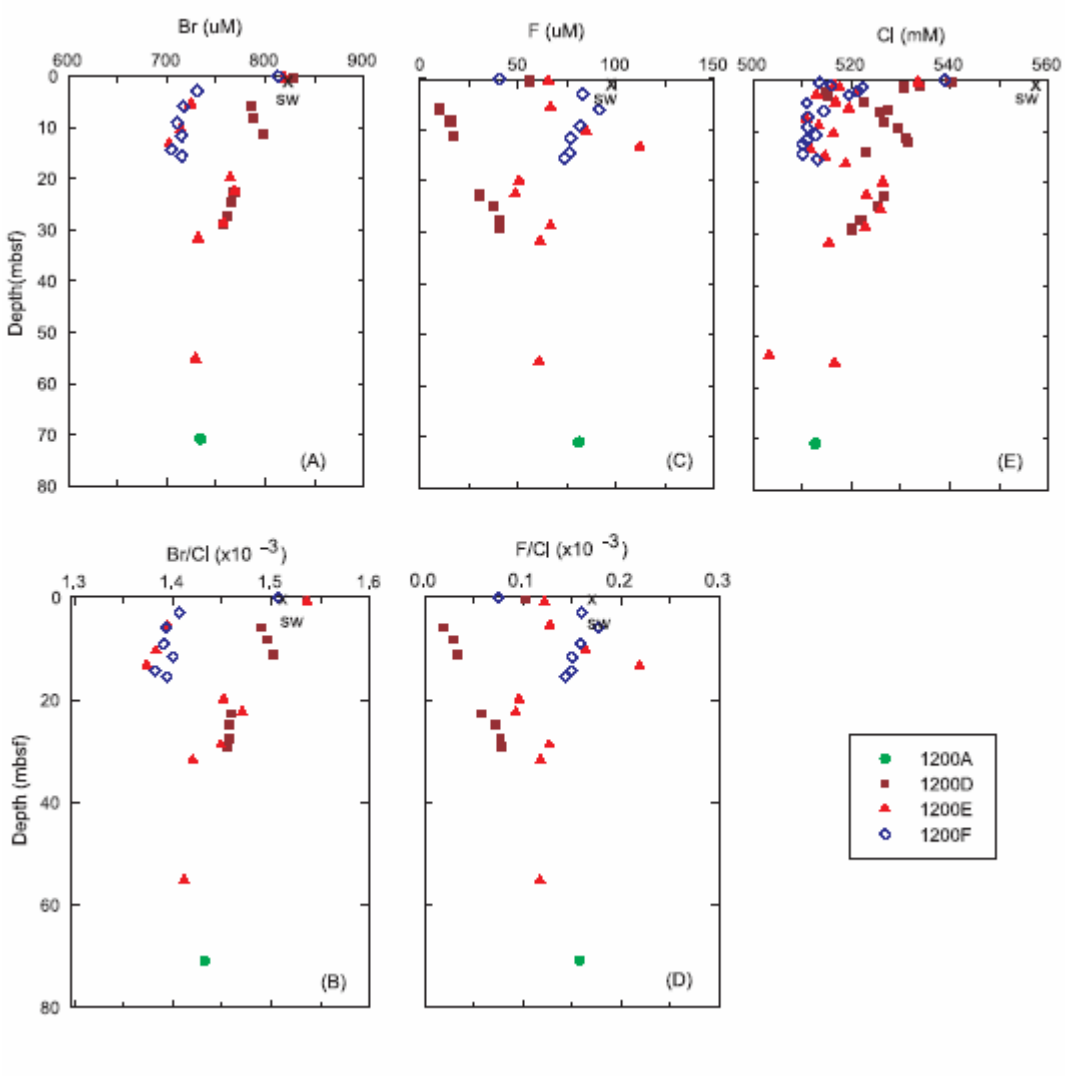

Figure 2.6.2 (A) Br concentration (B) F concentration (C) Br/Cl ratios (D) F/Cl ratios of pore fluids at Site 1200, Mariana subduction zone.

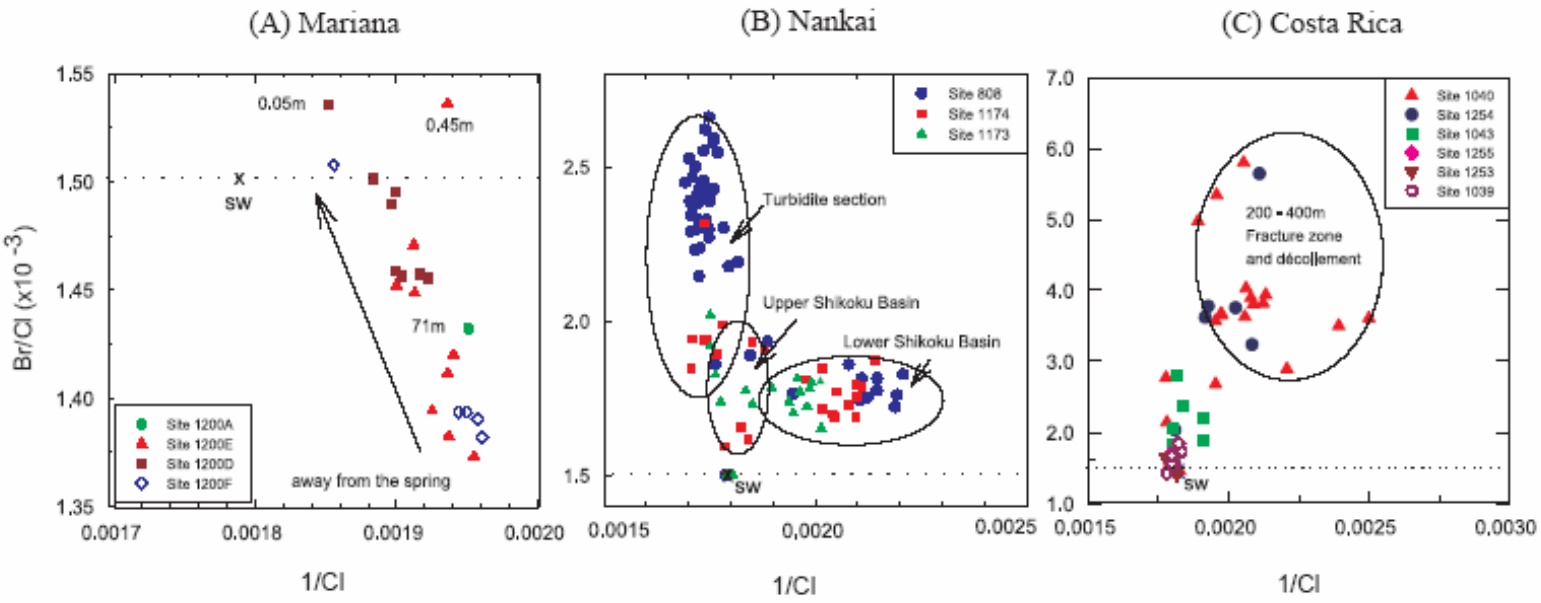

Figure 2.6.3 Br/Cl vs 1/Cl plots of pore fluids at (A) Mariana, (B) Nankai, and (C) Costa Rica subduction zones. In (A), the arrow demonstrates the direction away from the spring. The closer to the spring (Hole F, E, and A), the lower the Br/Cl ratios is. Hole D is the furthest away from the spring and the Br/Cl ratios are approaching the seawater value. The dotted horizontal line indicates the seawater Br/Cl value and the symbol "×" indicates seawater value for both Br/Cl and 1/Cl. Note that at Mariana, most data points are below the seawater line whereas at Nankai and Costa Rica, the data points are above the seawater line.

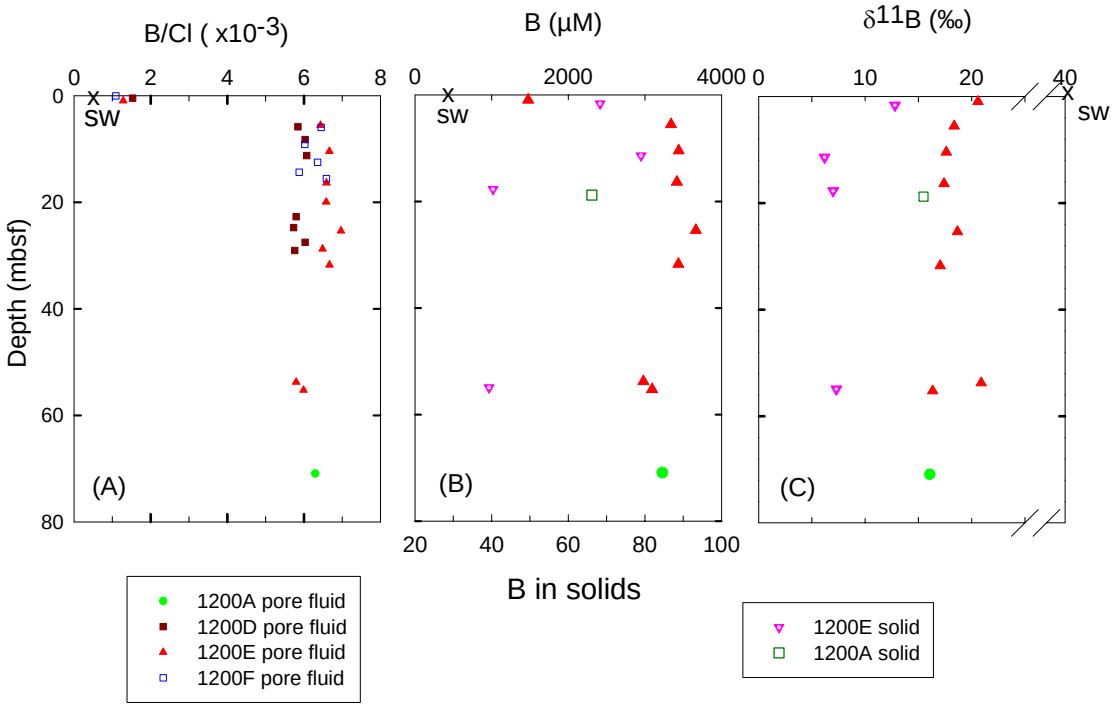

Figure 2.6.4 (A) B/Cl concentration ratio-depth profiles in pore fluids of all the holes at Site 1200, (B) B concentrations-depth profiles in both pore fluids and solids, and (C) $\delta^{11}B$ in both pore fluids and solids at Site 1200, Holes A and E, ODP Leg 195.

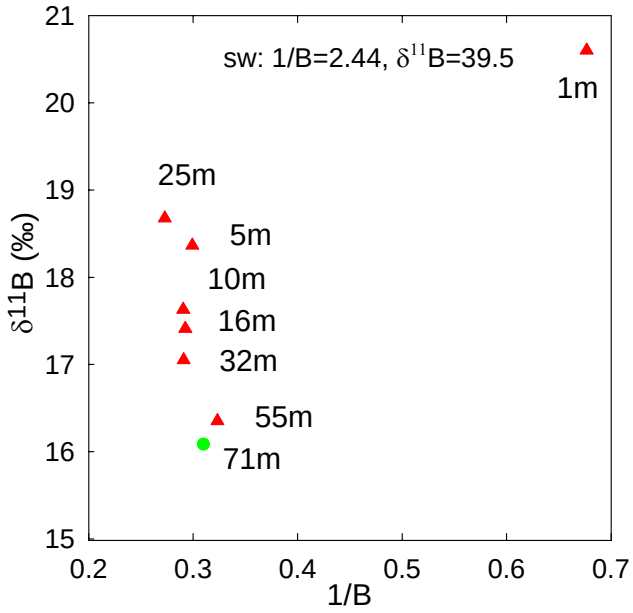

Figure 2.6.5 $\delta^{11}B$ vs 1/B in pore fluids at Site 1200, Site 1200 Hole A and E, ODP Leg 195.

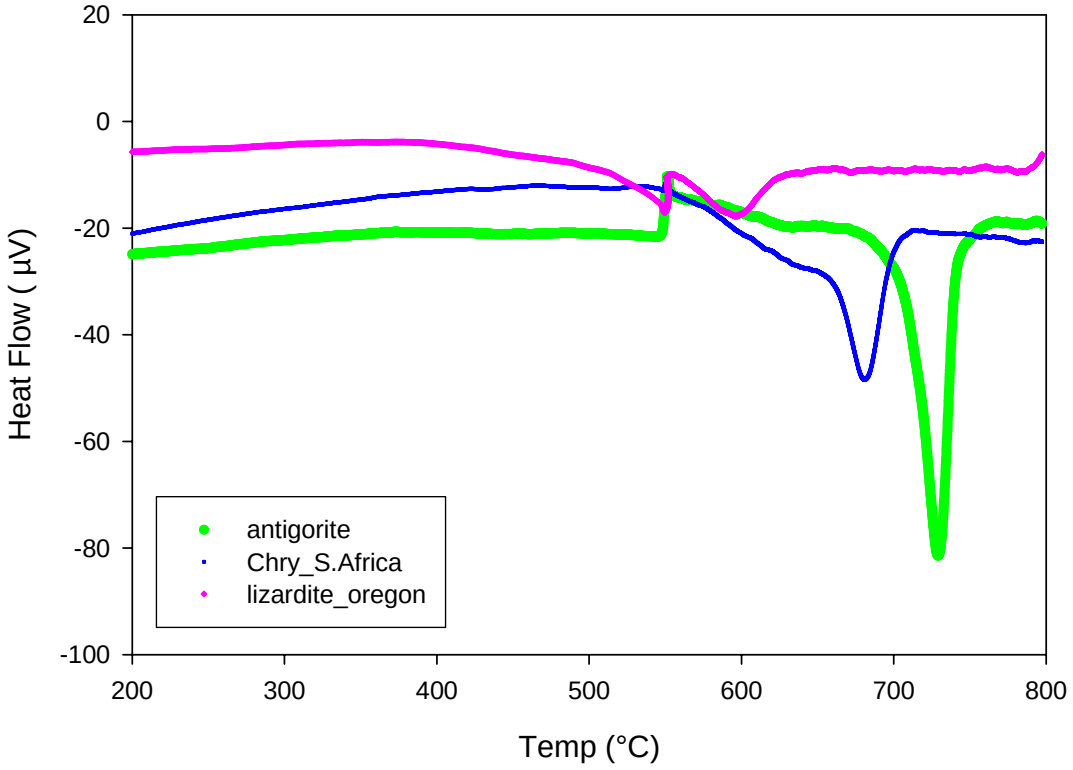

Figure 2.6.6 TG-DSC results for three different forms of serpentines. Antigorite gives an endothermic peak at about 730 °C, the peak for chrysotile occurs at 640-690°C; lizardite peaks at 600-630°C, with another associated peak at 550°C. Because different amounts of samples were used in the analyses, the endothermic peak intensities do not reflect differences in the amount of water in these serpentine samples.

2.7 Implications of Cl isotope cycle on Earth

2.7.1 The Importance of Serpentinization In the Oceanic Chlorine and Water Cycles

Serpentine is estimated to compose 10-20 % of oceanic crust (Carlson, 2001). In the slow-spreading Mid-Atlantic Ridge system, serpentinization occurs in association with fracture zones, at transform-ridge intersections; hydrothermal circulation of seawater is serpentinizing shallow peridotites (Miyashiro et al., 1969; Aumento et al., 1971; Christensen, 1972). Serpentinization also occurs at the outer rise of subduction zones, where faulting associated with lithosphere bending provides deep conduits for seawater to react with lithospheric mantle when entering the subduction zone (Peacock, 2001; Ruepke et al., 2002; Hyndman et al., 2003). The recent discovery of serpentine mud volcanoes in the Mariana subduction zone (Fryer et al., 1990; Fryer et al., 1992; Fryer et al., 2000) suggests that serpentine also forms in the forearc, resulting from the slab derived fluids rehydrating the upper mantle wedge.

Serpentines contain ~13 wt% H_2O and hundreds to thousands of ppm of Cl (e.g. (Seno, 2001; Ruepke et al., 2002; Carlson et al., 2003) and references therein), hence, they are the most important Cl and H_2O solid phase reservoir in the subducting plate and the mantle wedge. During subduction, Cl and water in serpentines are carried into subduction zones with the down-going plate and are subsequently released by dehydration/dechlorination reactions at depth, providing a particularly fertile water and Cl source, enriched in ^{37}Cl for magma generated in subduction-related arc volcanoes (Thompson, 1992; Scambelluri et al., 1995; Ulmer et al., 1995; Ruepke et

al., 2002). The $\delta^{37}Cl$ value of +1.7 ‰ of the 747°C gas condensate recently collected from Nicaragua Momotombo volcano (Shaw et al., 2003) reported in Table 2 probably reflects such a Cl recycling process. The resulting overpressure from mineral dehydration reactions may be partly responsible for subduction zone earthquakes (e.g. (Kerrick, 2002; Ruepke et al., 2002; Hyndman et al., 2003) and references therein).

Philippot et al. and Scambelluri et al.(Philippot et al., 1991; Philippot et al., 1998; Scambelluri et al., 2001) and references therein) suggested that the Cl released during the breakdown of serpentine may be responsible for the hypersaline fluid inclusions in eclogites which have little or no interaction with an external fluid source. O'Hanley (O'Hanley, 1996) and Scambelluri *et al.* (Scambelluri et al., 1997) suggested that Cl is expelled mostly from the fibrous serpentine forms, chrysotile and lizardite, when they transform to the more massive antigorite structure. The Cl concentrations in different serpentine forms, analyzed in this study and reported in Table 3, support this suggestion; in chrysotile, the Cl concentration is 415 ppm and only 140 ppm in the analyzed antigorite.

In serpentinite, Cl may occur in three different modes: (1) as a substitute for structural OH^- in the hydrous silicate (Sanford, 1981); (2) situated structurally between the basal layers perpendicular to the c-axis (Miura et al., 1981); and (3) as finely-disseminated NaCl along grain boundaries (Sharp et al., 2004). The first mode involves distinct chlorine isotope fractionations (Schauble et al., 2003) and the latter two will show no isotopic fractionation as they simply represent disseminated NaCl crystals deposited in interstices and the Cl is not involved in a chemical reaction (Kaufmann et al., 1984). In order to distinguish between these modes of occurrence

analytically, four individual serpentine bulk samples from Hess Deep were divided and each was prepared in the following two distinct ways and analyzed separately: (1) one piece was washed and sonicated without crushing, up to 10 times until no chloride was detected in the washing solution, followed by routine pyrohydrolysis for Cl extraction. This extracted Cl consists of the structural Cl in the serpentine and also possibly of trapped pore fluid Cl that may be present as finely-disseminated NaCl along grain boundaries, as suggested by Sharp and Barnes (Sharp et al., 2004). (2) The second piece of each of the serpentine samples was crushed and powdered, sonicated, and washed thoroughly, up to 10 times, until no chloride was detected in the washing solution, followed by routine pyrohydrolysis for Cl extraction. The residual powdered serpentine should only contain structurally bound Cl. Sharp and Barnes (Sharp et al., 2004) followed an overall similar sample preparation protocol, except that in their procedure, samples were washed only four times and no Cl checking procedure of the washing solution was used.

In the washing solutions, Cl content is ~0.09 to 0.11 wt% of the bulk samples (n=4) prepared by procedure (1), and ~0.28 to 0.45 wt% in the powdered samples (n=2) prepared by procedure (2). The $\delta^{37}Cl$ is 0 ± 0.5 ‰ in the washing solutions prepared by both procedures, which indicates that the water-soluble fraction of Cl in serpentines has the seawater $\delta^{37}Cl$ value. After washing by procedure (1), $\delta^{37}Cl$ values of the pyrohydrolyzed uncrushed samples range from -0.1 to +1.8 ‰ and Cl content is 447-745 ppm (Table 2.6.1). After the washing by procedure (2), $\delta^{37}Cl$ value of the crushed sample, is ~ +6.0 ‰ and Cl content is 290 ppm, indicating structurally

controlled chlorine isotope fractionation. Thus, the lower δ^{37}Cl values of -0.1 to +1.8 ‰ in the uncrushed serpentines, compared with structural δ^{37}Cl of ~ +6.0 ‰, suggests that the uncrushed sample values represent a mixture of soluble NaCl and from structurally bound Cl (insoluble Cl). Based on the results from the above procedures (1) and (2), the high Cl concentration of ~0.2 wt% and δ^{37}Cl value of ~0.5‰ in the water-soluble fraction of Cl, reported by Sharp and Barnes (Sharp et al., 2004), most likely represent a mixture of soluble Cl with seawater δ^{37}Cl and of structural Cl with higher positive δ^{37}Cl values.

Using their data on Cl concentrations and δ^{37}Cl in serpentines, Sharp and Barnes (Sharp et al., 2004) have estimated that serpentines carry 12×10^{12} g/yr of Cl into subduction zones, undoubtedly contributing an important Cl flux in this tectonic environment. They also suggested that the δ^{37}Cl of the ocean has increased with time, assuming a δ^{37}Cl value +4.7‰ for MORB and a δ^{37}Cl serpentinite equal to the seawater value (0 ‰). Their estimates, however, did not include: the subduction zone pore fluid refluxes into the ocean with negative δ^{37}Cl values (-7.8 to -5.5‰), as observed at Nankai and Costa Rica; the positive δ^{37}Cl of hydrothermal fluids (+2.4 to +4.1 ‰); the efficient recycling of dehydrated slab fluids (+1.8 ‰); and that serpentines have positive δ^{37}Cl values (+1.4 to +6.0 ‰), which imply that serpentines could be an important ^{37}Cl sink. With these newly acquired data in this study, reported in Table 2.7.1, the Cl and Cl stable isotope cycle in the ocean is re-examined below.

2.7.2 The Cl and Cl Isotope Cycle in the Ocean

The chlorine cycle in subduction zones may be largely responsible for the observed seawater/mantle Cl isotope fractionation. The negative $\delta^{37}Cl$ values of the pore fluids observed in both Nankai and Costa Rica subduction zones, fractionated by hydrous mineral reactions with pore fluids described above, suggest that the cycling of seawater through subduction zones should have a significant impact on the $\delta^{37}Cl$ of seawater and the earth's mantle. The limited $\delta^{37}Cl$ data recently acquired from hydrothermal fluids and gas condensates constitute compensating fluxes, that transfer enriched ^{37}Cl from the mantle via mid-ocean ridges, hotspots and/or island arc volcanism to the ocean (Table 2.7.1). For hydrothermal fluids, the published $\delta^{37}Cl$ data are, however, conflicting (Table 2.7.1). Bach et al. (Bach et al., 2002) reported end-members $\delta^{37}Cl$ values of +4.6‰ at MAR and +6.5 to +7.1‰ at the EPR; these samples were analyzed by Secondary Ion Mass Spectrometry (SIMS). Using a gas source dual-inlet isotope ratio mass spectrometer, Bonifacie et al. (Bonifacie et al., 2005) reported $\delta^{37}Cl$ values of -0.03 ± 0.06 ‰ for hydrothermal fluids collected from the same locations with chlorinities ranging from 251 to 821 mmol/kg. It is not yet clear whether this discrepancy is caused by the different analytical methods or by the nature of the samples obtained (Bonifacie et al., 2005). In this study, $\delta^{37}Cl$ of hydrothermal fluids collected from EPR (9°N) were analyzed by TIMS, following the method used for the pore fluid samples. Based on the compositions of the fluids, such as Mg concentration, the 359 °C fluid from EPR 9°N (P vent, Seyfried et al., personal

communications) is a mixture of 97% hydrothermal fluid and 3% seawater; its $\delta^{37}Cl$ value is +3.8 ± 0.4‰. The 313-343°C fluids (n=3) from EPR 9°N (Tica and Q-vents), that consists of a mixture of ~17% hydrothermal fluids and ~83% seawater, have $\delta^{37}Cl$ of +0.4 to +0.7 ‰ (Table 2.7.1). Based on the Cl and Cl isotope ratios of these two types of hydrothermal mixed with seawater fluids, the calculated end-member hydrothermal fluid carries a $\delta^{37}Cl$ signal up to +4.1‰, which is close to the unaltered mid-ocean ridge basalt of +4.7 ‰ (Magenheim et al., 1995).

The efficient recycling of Cl, with positive $\delta^{37}Cl$ of +1.8 ‰, released from slab dehydration as observed in the Mariana subduction zone serpentine seamount vents, is another compensating source of enriched in ^{37}Cl fluid into the ocean. An estimate of the $\delta^{37}Cl$ budget for the ocean thus involves the following three main input fluxes: (1) hydrothermal vents of 1.7×10^{13} mol/yr (global water flux through hydrothermal vents (Elderfield et al., 1996) times the average seawater Cl concentration (Elderfield, personal communication), with end-member $\delta^{37}Cl$ values up to +4.1‰; (2) the recycling of Cl associated with the upwelling fluid from slab dehydration. The Cl flux used is 3.6×10^{10} mol/yr (average Cl concentration 510 mM × 7.0×10^{10} kg/yr (Wei, 2005)) with $\delta^{37}Cl$ values of +1.8 ‰. It is noteworthy that this fluid flux is a conservative flux estimate through serpentine mud volcanoes, so far only nine active ones were identified at Mariana, thus representing a minimum value in the global flux calculation; (3) assuming that the Cl concentration and isotope ratios at Nankai and Costa Rica are representative of global subduction zones (Kastner et al., 1991; Spivack et al., 2002), and the entire volume of the ocean is recycled through

subduction zones in 200 Ma, it gives a global water flux of 7.0×10^{12} kg/yr (Kastner et al., 1991). The Cl reflux to the ocean with negative δ^{37}Cl of -5.5 to -7.8 ‰ is thus 3.2×10^{12} mol/yr. Although these three input fluxes are considered neither sources nor sinks for the Cl concentration cycle in the ocean, they constitute important Cl isotope sources. Rivers are an important Cl source; however, they play a negligible role in the δ^{37}Cl oceanic cycle. In rivers average Cl concentration is ~ 0.07 mM (Holland, 1978) and the δ^{37}Cl is 0 ± 0.1 ‰. Gas condensates from island arcs are as well not considered in the overall oceanic Cl isotope budge calculation because the estimated Cl flux is only 0.4% of the total flux (Schilling et al., 1978). The database for the above input fluxes is listed in Table 2.7.1.

Serpentines and evaporites are the main Cl sinks from seawater. What are their contributions to the Cl isotope budget? Based on this study, serpentines have an average structural Cl content of ~400 ppm and δ^{37}Cl value of +1.2 to +6.0 ‰ (Table 2). With a crustal production rate of 5.6×10^{16} g/yr (Hart et al., 1982) with ~15% being serpentinized (Peacock, 1990; Carlson et al., 2003), the Cl flux into the serpentines is 1.9×10^{11} mol/yr. Rapidly accumulating massive evaporites could also impact oceanic chlorinity. The estimate based on the total volume of evaporites for the past 200 Ma of 2.2×10^{5} km^3 (Table 2.7.1, (Warren, 2006)) suggests that the average Cl flux into evaporites is 2.0×10^{11} mol/yr. The total Cl sink is, however, much less than the total Cl source fluxes (Table 4). The δ^{37}Cl value of evaporites is within ±0.5 ‰ over the past 200 Ma (Eggenkamp, 1995), thus does not influence the seawater δ^{37}Cl.

Combine all the important input and output fluxes,

$$(\delta^{37}Cl)_{input} = f_1(\delta^{37}Cl)_1 + f_2(\delta^{37}Cl)_2 + f_3(\delta^{37}Cl)_3 \quad (2.8)$$

$$(\delta^{37}Cl)_{output} = f_4(\delta^{37}Cl)_4 + f_5(\delta^{37}Cl)_5 \quad (2.9)$$

in which f denotes the fraction of the total input or output flux ($f_1+f_2+f_3=1$ and $f_4+f_5=1$); subscripts 1, 2, and 3 correspond to the three major input fluxes: hydrothermal vents, serpentine mud volcanoes, and recycled subduction zone fluids, respectively. Subscripts 4 and 5 correspond to the two sinks for Cl isotope cycle in the ocean, serpentines and evaporites, respectively. At steady state, $f_1(\delta^{37}Cl)_1 + f_2(\delta^{37}Cl)_2 + f_3(\delta^{37}Cl)_3 = f_4(\delta^{37}Cl)_4 + f_5(\delta^{37}Cl)_5$, or $(\delta^{37}Cl)_{input} - (\delta^{37}Cl)_{output} = 0$. Using instead the data in Table 4, the calculations suggest that depending on maximum and minimum fluxes, $(\delta^{37}Cl)_{input}-(\delta^{37}Cl)_{output}$ = -0.9 ‰ to +0.4 ‰, respectively. Based on the marine evaporite $\delta^{37}Cl$ data of 0 ± 0.5‰ (Eggenkamp, 1995), +0.4 ‰ is within the error of ±0.5 ‰, whereas the difference between the input and output $\delta^{37}Cl$ of -0.9 ‰ suggests that the ocean $\delta^{37}Cl$ has probably decreased by at most 0.4‰ (0.9-0.5‰) over the past 200 Ma.

Table 2.7.1 Data-base for the marine $\delta^{37}Cl$ cycle

Cl sources and sinks	Water or rock mass	Cl	Cl flux	$\delta^{37}Cl$ range (‰)		$\delta^{37}Cl$ contribution of each source or sink to the ocean (‰)	
	kg/yr	mol/kg	mol/yr	min	max	min	max
Cl sources							
Hydrothermal vents	3.0×10^{13} [a]	0.56[g]	1.7×10^{13}	2.4	4.1	1.75	2.98
Subduction zones	7.0×10^{12} [b]	0.45	3.2×10^{12}	-7.8	-5.5	-1.06	-0.75
Serpentine mud volcanoes	7.1×10^{10} [c]	0.51	3.6×10^{10}	0.1	1.8	0.00	0.00
Rivers	3.7×10^{16} [d]	7×10^{-5} [h]	2.6×10^{12}	-0.1	0.1	0.00	0.00
Island arc volcanoes	5.0×10^{12} [e]	1.69×10^{-2}	8.5×10^{10}	-0.6	1.7	-0.01	0.02
Input total			2.3×10^{13}			0.7	2.3
Cl sinks							
Serpentines	5.6×10^{16}[f]	1.13×10^{-2}	1.9×10^{11}	1.2	6.0	0.01	0.06
Evaporites	1.2×10^{10}[i]	17.2	2.0×10^{11}	-0.5	0.5	0.00	0.00
Output total			3.9×10^{11}			0.3	3.2
$\delta^{37}Cl$(input)-$\delta^{37}Cl$(output)						0.4	-0.9

[a] (Elderfield et al., 1996)
[b] (Kastner et al., 1991; Spivack et al., 2002)
[c] (Wei, 2005). Notice that this is a minimum value for Cl flux through serpentine mud volcanoes, for as yet they have only been identified at the Mariana subduction zone.
[d](Palmer et al., 1989)
[e](Schilling et al., 1978)
[f] (Hart et al., 1982)
[g] The average Cl concentration at hydrothermal vents is taken as seawater value, based on the assumption that MOR hydrothermal activity is neither a source nor a sink for Cl (Elderfield, personal communication)
[h] (Holland, 1978)
[i] (Warren, 2006)

Chapter 2, in part, has been submitted for publication as it appears in *ODP Leg 195 Scientific Results*. Wei Wei, Miriam Kastner, Annette Deyhle, Arthur J. Spivack (2005). Geochemical cycling of halogens and boron and its implications for fluid-rock reactions in the non-accretionary Mariana supra-subduction zone. 23 pages. The dissertation author is the primary investigator and author of the paper.

Chapter 2, in part, will be submitted to Earth and Planetary Science Letters, Wei Wei, Miriam Kastner, Arthur J. Spivack. Chlorine stable isotopes and halogen concentrations in convergent margins with implications for Cl isotope cycling. The dissertation author is the primary investigator and author of the paper.

CHAPTER 3

HYDROTHERMAL EXPERIMENTS

3.1 Introduction

Chemical fluxes into and out of seawater are significant at mid-ocean ridge hydrothermal systems (Edmond et al., 1979; Von Damm, 1988; Von Damm, 1990). At ridge flanks chemical exchange between seawater and Mid-Ocean Ridge Basalt (MORB) is also important and the sediment cover impacts the exchange reactions and the fluxes into and out of the ocean (Kastner et al., 2004). When the sediments and altered oceanic crust enter subduction zones, the temperature and pressure increase with depth, promoting extensive diagenetic and metamorphic reactions (e.g. (Peacock, 1990)) and significant element re-mobilizations. Depending on the volume of the return flux of pore fluid into the ocean, subduction zone processes may also impact the global geochemical mass balances.

Laboratory experiments can provide constraints on understanding hydrothermal reactions in natural systems. Early hydrothermal experiments (Bischoff et al., 1975; Seyfried et al., 1977; Seyfried et al., 1979) focused on reproducing the observations at Mid Ocean Ridge (MOR) hydrothermal vents. Seawater was reacted with MORB under specific temperatures (70, 150, 200 and 300°C) and at 500 bars pressure for approximately two months, with water/rock (w/r) ratio of ~10. Similar to seafloor hydrothermal systems, seawater was modified in these experiments, Mg and SO_4 concentrations decreased and the concentrations of Ca, SiO_2, H_2S, CO_2, K, Fe, Mn, Ba, and Al increased. MORB was altered to smectite, similar to that found in

altered oceanic ophiolites. Seyfried *et al.* (Seyfried et al., 1998) also examined alkali metal mobility and Li isotope exchange in seafloor weathered basalt in an experiment at 350^{o}C, 500 bars. These experiments were, however, conducted at a constant temperature and pressure. The experiments by You et al. (You et al., 1996; You et al., 2001) on interaction between synthetic NaCl-$CaCl_2$ fluid and clay-rich hemi-pelagic sediments were conducted between 25 and 350 °C with 25 or 50 °C intervals, at 800 bars, with a w/r of ~3; the equilibration time for each temperature increment was 3-7 days. These experiments, which better mimic the natural condition in subduction zones, demonstrated that the fluid chemistry changed significantly: Na, Mg, and SO_4 concentrations decreased sharply and NH_4, SiO_2, K, B and Li concentrations increased with temperature. The sediment composition showed minor modifications: only B, Li, As, Br and Pb were significantly depleted, and adsorbed B ($\delta^{11}B$= ~15 ‰) was completely leached below 150°C (You et al., 1996; You et al., 2001). James *et al.* (James et al., 2003) conducted experiments between 51 and 350 °C at 400 bars for 30 days, with w/r of ~ 4 (20 days of heating and 10 days of cooling episodes) to study the nature and temperature control of basalt-seawater and sediment- seawater reactions at the Juan de Fuca Ridge (JFR) flank. It was shown that K and Si were leached from basalt, and U was taken up between 150 and 350 °C. The mobilities of Ca, Li, Rb, Cs, and Sr were different in the basalt and sediment experiments. Li and Sr isotopes suggested the formation of secondary minerals in both basalt and sediment experiments.

In order to better characterize the partition behavior of the major (Mg, Ca) and alkali elements (Li, K, Rb, and Cs) in different types of solids, as well as to study Li and Sr isotope exchanges from 35 to 350°C at 25 or 50 °C increments, we chose basaltic ash and smectite to mimic the fluid-rock reactions at hydrothermal vents, ridge flanks, and subduction zones; the experiments were conducted at a w/r mass ratio of ~5 (Table 3.3.1). The temperature increments in this study were smaller than in all previous experiments, hence, detailed profiles of element behaviors were obtained, especially at low temperatures (35-150°C). The experiments lasted two to eight months, longer than the previous experiments, to ensure that steady state had been reached at each temperature.

The focus of the experiments was on alkali metal (Li, K, Rb, and Cs) concentration variation with increasing temperature, on the exchanges of Li and Sr isotope ratios between the fluids and solids, and the reactivities of the solids. The data provide new information on the flux of alkali metals through hydrothermal vents and the approximate temperature at the reaction sites, as well as new insights on the nature of the alteration of the solid phases, thus, on the involvement of sediments in arc volcanism (Hart, 1969; Hart et al., 1982; Palmer et al., 1989; You et al., 1996; Seyfried et al., 1998). The Li isotopes were emphasized because of the large relative mass difference of 14.4% between ^{6}Li and ^{7}Li and the affinity of Li for the fluid phase. In contrast, the relative mass difference of ^{87}Sr and ^{86}Sr is only 1.1%, therefore, Sr isotopes provide critical information on the nature of source materials involved in the reactions.

3.2 METHODS

3.2.1 Experimental Apparatus

Dickson-type rocking autoclaves were employed for the experiments at USGS, Menlo Park, CA. An inert reaction environment was provided by collapsible reaction cells fabricated from gold (up to 300 cm^3). The reaction cells were housed in a pressure vessel secured to a rotating furnace, which serve the purpose of better mixing the reactants and minimizing potential temperature gradient. Pure water acted as the pressure fluid in the annular space surrounding the cell. This system allowed reactions to take place under controlled pressure and temperature conditions (Bischoff et al., 1975; Rosenbauer et al., 1993). It also permitted fluid samples to be withdrawn at constant pressure and each temperature on-line, avoiding quenching reactions and allowing reaction progress to be monitored as a function of time.

3.2.2 Materials and Procedures

Two types of solids were chosen as starting materials: (1) basaltic ash from Lau Basin (ODP Leg 135, 836 A-3H-4, 10-51 cm) which consists mostly of volcanic ash, with some calcite, cristobalite and traces of clay minerals; thus it is slightly altered and has somewhat higher than end-member MORB Li concentration, as shown in Table 3.3.2; (2) smectite from Barbados (ODP Leg 110, 110-671B-51 X), a typical detrital smectite in continental margins, that consists of ~90% clay minerals (mostly

smectite), 0-3% quartz, 0-2% feldspar and 0-2% opaque, as well as up to 30% ± 20% of the volcanic glass (ODP Leg 110 initial reports). The two starting fluid were: (1) filtered seawater (sw) taken from Scripps Pier at La Jolla, CA; and (2) artificial seawater (asw) with a composition of: 29.52 g NaCl, 11.01 g $MgCl_2 \cdot 6H_2O$, 1.14 g $CaCl_2$, 0.69 g KCl, 0.03 g H_3BO_3, 0.06 g $SrCl_2 \cdot 6H_2O$ in 1000 ml H_2O. The asw was sulfate-free to avoid complication associated with anhydrite precipitation (Table 3.2.1). Seven different types of experiments were conducted: basalt with sw (001), smectite with sw (002), basalt and smectite mixture (2:1) with asw (003), basalt with asw (004 and 017), and smectite with asw (005 and 016). Experiments 017 and 016 were duplicates of experiments 004 and 005, respectively, to examine experimental reproducibility. The details are summarized in Table 3.2.1.

The solids were homogenized prior to use to achieve reproducibility. In the experiments, solids were placed in flexible gold bags filled with filtered or artificial seawater in Dixon rocking autoclaves (Rosenbauer et al., 1993), at the water/rock (w/r) ratios listed in Table 3.2.1. The w/r ratios chosen are similar to those in the experiments by You *et al*., 1996 (You et al., 1996). The solid-seawater mixtures were equilibrated at room temperature for several hours prior to placement in the reaction vessel. Constant pressure of 600 bars was maintained during sampling. Except near the critical point, temperature but not pressure, is the dominant variable controlling reaction kinetics, and to a great extent, the equilibrium mineral assemblage. At a pressure of 600 bars, our system was supercritical and single phase. During the experiments, about 1.0-2.0 ml of solution was extracted between 35 and 350°C at

intervals of 25 or 50°C, over the course of 3-8 months.

Reaction duration at each temperature lasted until an apparent steady-state was reached, as determined by monitoring the fluid chemistry. At the end of each experiment, the w/r ratio was ~2-3.

3.2.3 Analytical Methods

Concentrations of major elements (Mg, Ca, K, and SO_4) and some minor elements (Ba, Sr, and Li) in the fluids were analyzed by ICP-OES (analytical error < 3%); Cl concentration was determined by titration with $AgNO_3$ (error < 0.1%); Si by spectrophotometry using the silicomolybdate complex (error < 3%); Rb and Cs by ICP-MS (ThermoQuest/Finnigan Element2) (analytical error < 3%); Li isotope ratios by TIMS (external error < 1‰) (You et al., 1996); and Sr isotope ratios by TIMS (internal error < 5.5×10^{-6} and external error < 0.002‰).

The solids were characterized for mineralogy by XRD before and after the reactions. The concentrations were also analyzed by ICP-OES for major elements and by ICP-MS for trace elements. For these analyses each solid was dissolved in HNO_3 and HF acid, and diluted 2000 fold by weight with 2.5% optima nitric acid solution.

Table 3.2.1 Starting reactants

Exp ID	Solid	Fluid	W/R mass ratio	Temp. range (ºC)	Duration (days)
Basalt experiments[1]					
001	Basaltic ash 26.5 g	Filtered sea water 138 ml	5.3	35-353	107
004*	Basaltic ash 27.1 g	Artificial sea water 140 ml	5.2	35-300	260
017	Basaltic ash 17.5 g	Artificial sea water 121 ml	6.9	35-352	179
Smectite experiments[2]					
002	Smectite 27.0 g	Filtered sea water 169 ml	6.4	35-350	107
005*	Smectite 27.1 g	Artificial sea water 164 ml	6.1	35-150	85
016*	Smectite 21.4 g	Artificial sea water 167 ml	7.8	35-226	97
Basalt and Smectite mixture experiment					
003	Basaltic ash 20.0 g Smectite 10.0 g	Artificial sea water 220ml	7.5	35-350	192

Note: * Experiment terminated early due to the suspicion of leakage

[1]The basaltic ash is from Lau Basin (ODP Leg 135, 836 A-3H-4, 10-51 cm). It contains mostly volcanic ash, with some calcite, cristobalite, and traces of clay minerals.

[2]The smectite is from offshore Barbados (ODP Leg 110, 110-671B-51 X) with 0-3% quartz, 0-2% feldspar, 0-2% opaques. The two starting fluids are: filtered seawater taken from Scripps Pier, and artificial seawater composition: 29.52 g NaCl, 11.01 g $MgCl_2.6H_2O$, 1.14 g $CaCl_2$, 0.69 g KCl, 0.03 g H_3BO_3, 0.06 g $SrCl_2.6H_2O$ in 1000 ml H_2O, and without sulfate to avoid complication of anhydrite precipitation.

3.3 RESULTS AND DISCUSSIONS

3.3.1 Fluid Chemistry

In the basalt or smectite hydrothermal experiments seawater was considerably modified; the overall chemical trends with increasing temperature are rather similar in both sw and asw experiments, and are compared with submarine hydrothermal vents chemistry. The experimental fluid and solid data are presented in Table 3.3.2 and 3.3.3, respectively, and Fig. 3.3.1-3.3.7.

Cl concentrations

The continuous decrease in Cl concentration (~3-8 %), especially in the basalt-sw experiment, shown in Table 3.3.2, was unexpected because hydration of basalt to form smectite should consume water. Phase separation is ruled out at the experimental conditions of 600 bars and ≤ 350 °C (Oosting et al., 1996). A small but significant Cl decrease at T ≥ 200 °C was also observed (up to 3% at 350 °C) in You *et al*'s experiment (You et al., 2001), and was suggested to derived from organic matter decomposition and/or clay mineral dehydration. In our experiments smectite dehydration could account for at most 3% decrease in Cl concentration based on ~15 wt% interlayer water in smectite. Formation of a Fe/Mg hydroxy chloride phase (e.g. $Fe_2(OH)_3Cl$) has been suggested to explain chlorinity variations in submarine hydrothermal vent fluids (Edmond et al., 1979; Campbell et al., 1988). The Fe/Mg hydroxy chloride phase contains a theoretical ~18wt% Cl. If it is assumed that if present, it comprises a maximum of 2-3% in the solid, as it was not detected by XRD.

The mass balance calculation suggests that 2-3 % Fe/Mg hydroxy chloride phase could account for ~6-7% of Cl decrease in the fluid. The most likely explanation of some leakage of pure water from the pressure fluid into the reaction cell was also suspected but could not be proven at the end of the experiments. Therefore, in the following discussion and in Figs 3.3.1-3.3.7, the elemental concentrations are normalized to Cl.

Si concentrations

Dissolved silica concentration is an established geothermometer ((Fournier, 1981; Von Damm et al., 1991) and references therein). In this study, Si concentrations in both basalt and smectite experiments are compared to the quartz solubility in seawater experiment from 35 to 350 °C (Von Damm et al., 1991). As indicated in Fig. 3.3.1, the experimental Si concentrations from 35 to 300 °C are within 2-3 mM to the empirical values. At 350 °C, however, the analyzed Si is ~8-10 mM lower than the empirical value. The discrepancy was most probably caused by Si polymerization when the 350 °C fluid was cooled to room temperature prior to analysis, as the analytical method only detects the Si monomer (Fournier, 1981).

Mg and Ca

In the ***basalt experiments***, Mg/Cl decreases rapidly to near zero from 35 °C to ~200-250 °C and remains at ~zero concentration from 250 and 350 °C in both sw and asw fluids (Fig. 3.3.2 and Table 3.3.1), suggesting that Mg-fixation by Mg-smectites starts already at ~50 °C (Seyfried et al., 1979) and is complete at ~250°C. The close

match of the two duplicate asw experiments (Exp 004 and 017) confirm the reproducibility of the analytical procedure. Previous studies used synthetic NaCl-$CaCl_2$ fluid without Mg as reacting fluid (You et al., 1996; You et al., 2001; James et al., 2003), and it has been shown by Seyfried *et al.*(Bischoff et al., 1975; Seyfried et al., 1977; Seyfried et al., 1979) that Mg removal from the fluid at 70, 150, and 260°C is important for creating charge balance, i.e. replacing it with other cations, such as Ca, Na, K, and trace metals. The Ca/Cl gradually increases between 35 and 100 °C then steeply increases between 100 and 150 °C (Fig. 3.3.2-b). This is consistent with the observation in the axial high-temperature hydrothermal fluids (Edmond et al., 1979; Elderfield et al., 1999). From 175 to 350 °C, the differences in the observed Ca/Cl ratios between sw and asw experiments stems from $CaSO_4$ precipitation, which is also indicated by the SO_4 concentrations (Table 3.3.1)**.**

In the ***smectite experiment***, Mg/Cl ratios gradually decrease from 35°C to zero at 350 °C, and the rate of decrease is continuous throughout the experiment (Fig. 3.3.2-c), similar to at hydrothermal vents, where Mg decrease uniformly and reaches zero at ~350 °C (Edmond et al., 1979). The results also agree with the observations that at ridge flanks at the sediment-basement interface, ≤ 25°C the loss of Mg is small (< 10%) from the circulating seawater, whereas all sites with basement temperatures ≥ 45°C show a large (> 80%) Mg loss (Mottl et al., 1994). Ca/Cl ratio increases from 0.02 in the starting fluid to ~0.04 between 35°C and 150 °C and drops to ~0.01 between 150 and 350 °C in the sw experiment (Fig. 3.3.2-d), while it remains constant at ~0.03 from 50 to 225 °C in the asw experiment (the experiment was terminated at 225 °C). The difference is mainly caused by anhydrite precipitation.

In Fig. 3.3.2, the profiles of ***basalt-smectite (2/1) mixture-asw experiment*** are compared with those of the pure basalt and smectite experiments, respectively. The data indicate that basalt is dominating the reactions in the mixture experiment.

The Alkali Metals

Each of the alkali elements shows a unique concentration profile versus temperature (Fig. 3.3.3 and 3.3.4**)**. In the ***basalt-sw experiments***, fluid K/Cl molar ratio increases slightly from 35 to 65°C, and decreases to a minimum of 1.10×10^{-2} at 275°C. Beyond 275°C the ratio sharply increases to 6.53×10^{-2} at 350°C (Fig. 3.3.3-a). In contrast, Li/Cl, Rb/Cl and Cs/Cl ratios increased with temperature from 35 to 350°C. Each of the ratios shows a distinct profile as a function of temperature. The Li/Cl ratio increases gradually between 35 and 250 °C, then increases sharply to 350°C (Fig. 3.3.3-b). Rb/Cl ratio has a higher inflection temperature, at ~300°C, and a steeper slope between 300 and 350°C (Fig. 3.3.3-c). Cs/Cl ratio exhibits a unique trend: at <100°C, the ratio barely increases and stays below 1.2×10^{-8}; it increases ten-fold from 100°C to 350°C to 1.7×10^{-7} (Fig. 3.3.3-d).

In the ***smectite-sw experiments***, each alkali element concentration normalized to Cl also demonstrates distinct temperature-dependant profile. These profiles, however, differ from those obtained in the basalt-sw experiments, demonstrating the strong influence by solid on the partition profiles of the alkali elements. At 35 °C, K/Cl ratio decreases to 1.5×10^{-3} from the starting sw value 1.9×10^{-3}, possibly due to adsorption by clay minerals (James et al., 2000). From 35°C to 150°C, it again increases to the value of 1.9×10^{-3}, during which process K is possibly taken up by

illite and released from the bulk solid simultaneously. From 150 °C to 250 °C, K/Cl ratio steadily and steeply increases, followed by a lower increase rate from 250°C to 350°C (Fig. 2II-a), indicating that K is released from the solid at higher than 150 °C temperatures. Li/Cl ratio shows a trend similar to that observed in the basalt-sw experiment, but the ratio is ~3 times higher and the threshold is at 275 °C (Fig. 3.3.4 - b). Rb/Cl ratio remains at sw value between 35 and 125°C. It gradually increases to 2.4×10^{-5} at 350°C (Fig. 3.3.4 -c), only 0.2×10^{-5} lower than the Rb/Cl ratio at 350°C in the basalt experiment. Thus the enrichment factor for Rb in the fluid is ~10 in both experiments although Rb concentration in the smectite is 8 times higher than in the basalt. This suggests that Rb concentration in the fluid is controlled mostly by temperature. Cs/Cl ratio remains constant until 200°C (100 °C higher than in the basalt experiment), and increases to 9×10^{-7} at 350°C (5 times higher than in the basalt) (Fig. 3.3.3 and 3.3.4). The higher maximum value and threshold temperature in the smectite experiment compared to the basalt experiment suggest that Cs mobility is determined by both source solid and temperature.

In summary, the loss of Ca, Si, and alkali elements from the solids and the gain of Mg during solid alteration in the basalt and smectite experiments agree well with exchanges of these elements observed in submarine hydrothermal systems (Edmond et al., 1979; Elderfield et al., 1996). The data at the lower temperatures (35-300°C) in both basalt and smectite experiments are especially important in providing new insights on alkali element mobilities at ridge flanks and diagenetic environments. For example, Cs is steadily leached from basalt already at low temperature of 100 °C, which implies that ridge flanks most probably are significant contribution to the Cs

oceanic budget. The relative alkali metal contributions to the ocean from fluid-sediment versus fluid-oceanic basement reactions may also be derived from the alkali metal-temperature profiles (Fig. 3.3.3 and 3.3.4). For instance, the enrichment factors (defined as alkali concentrations at 350 °C ÷ alkali concentrations at 25 °C) of Li/Cl and Cs/Cl ratios in the smectite experiments are 70 and 155, respectively, considerably higher than in the basalt experiments with corresponding enrichment factors of 20 and 30.

The mobility pattern with temperature of each alkali element is as well significantly different in the two experiments. In the basalt experiment, Li/K and Cs/Rb exhibit sharp maxima of 35 $\times 10^{-3}$ at 275°C and 0.42 $\times 10^{-3}$ at 250°C, respectively (Table 3.3.1). In comparison, in the smectite experiment, Li/K reaches the maximum of 123 $\times 10^{-3}$ at 350 °C, and Cs/Rb has a distinct minimum value of 10 $\times 10^{-3}$ at 200°C (Table 3.3.1). Assuming no retrograde reactions, these results suggest that alkali elements may be used to indicate the approximate temperature at the source of fluid-rock reactions, as discussed in the Implications section.

Ba

Because as yet no solid work was performed only the observations with no interpretations are provided. In the ***basalt experiments***, with or without SO_4, Ba/Cl gradually increases from seawater value (8×10^{-8}) at 35 ºC to 2×10^{-5} at 175 ºC, and decreases to the starting seawater value at 300 ºC (Fig. 3.3.5). From 300 to 350 ºC, Ba/Cl ratio increases rapidly to 0.06×10^{-4} in the seawater experiment and 0.12×10^{-4}

in the asw experiment at 350 ºC. The Ba profile suggests that with increasing temperature, Ba is released from the basalt into the fluid phase in the temperature range of 35- 175 and 300-350 ºC but is incorporated into an as yet unidentified solid phase in the temperature range of 175-300 ºC. The fact that the experiments with and without SO4 behave the same suggest that it is not barite. In the 350 ºC fluid Ba concentration is ~32 μM, similar to the observation in the natural hydrothermal fluid, of >8 μM or >42 μM (Elderfield et al., 1996).

In the ***smectite-sw experiment***, Ba/Cl increases slowly from 0 (asw) to 8×10^{-8} (sw) in the starting fluid to 9×10^{-6} at 200 ºC; from 200 to 250 ºC, it increases more rapidly and reaches ~3×10^{-5} at 250 ºC and remains close to this value between 250-350 ºC (Fig.3.3.5). The profile suggests that Ba is leached from the smectite to the fluid from 35 to 250 ºC; a similar Ba mobility profile from 35 to 350 ºC was also obtained by James et al., (2003) (James et al., 2003), in the experiments between hemipelagic sediment (ODP Leg 169, 1037B 6H-03, comprises 29% quartz, 24% feldspar, 34% lithic fragments with abundant volcanic component) and artificial seawater without SO_4. The comparison of Ba profile in the basalt/smectite (2:1) mixture-asw experiments with the basalt experiments and smectite experiments (Fig.3.3.5) suggests that basalt is the dominant solid in the fluid-solid reaction for Ba.

U and F

In the hydrothermal fluids from 21 °N, East Pacific Rise and Guayamas Basin, Gulf of California, U was reported quantitatively removed from seawater and

deposited into the oceanic crust during the hydrothermal circulation (Chen et al., 1986). It has also been shown that U was undetectable in the 60°C fluid at Baby Bare springs (Wheat et al., 2002) and completely removed from the fluid into basalt at 150 °C in the hydrothermal experiment by James et al (James et al., 2003). Thermodynamic modeling of U mobility (25-300 °C, 500 bars) between seawater and the redox assemblage, hematite-magnetite-pyrite, indicated that the removal of U from seawater during basalt alteration is more controlled by shifting to reducing conditions than by temperature effect (Dunk et al., 2002). This is because U forms the soluble uranyl-carbonate species in oxidizing aqueous conditions, such as those found in most seawater. In anoxic or suboxic conditions, such as below or at seafloor (Teichert et al., 2003), U is reduced from its hexavalent to its tetravalent state and becomes insoluble.

In the basalt-sw experiments, U concentration of the fluid was below the detection limit thus is not shown. In the smectite-sw experiments, U decreased from seawater value (13 nM) from 35 to 150 °C, and was completely removed from the fluid at 150 °C. Only between ~275 and 350 °C, it gradually increased to 4.7 nM (Fig. 3.3.6 a). The trend of U being removed from seawater from 35 to 150 °C agrees with that observed in hydrothermal fluids and previous experiments (James et al., 2003). From 275 to 350°C, the U increase could not be explained by forming soluble uranyl-carbonate species in the anoxic or suboxic condition of the hydrothermal experiments, but possibly by the behavior of fluoride in the fluid: F concentration decreases from 111 μM at 50°C to 85 μM at 200 °C, remains at ~80-85 μM till 300 °C, then increases to 121 μM at 350 °C (Fig. 3.3.6 b). Similar fluoride behavior was observed by

Seyfried and Ding (1995) (Seyfried et al., 1995). The F decrease in the fluid from 25 to 250 °C was explained by F precipitation with magnesite and magnesium-hydroxide-sulfate-hydrate (MHSH). At temperature greater than 250°C, F-rich minerals dissolve and F is released to the fluid (Seyfried and Ding, 1995). The U-F cross plot demonstrates the relationship between U and F: they both remain lower than seawater value from ~200 to 300°C in the fluid but their mobilities increase above 300 °C. (Fig. 3.3.7).

Enrichments of uranium ^{238}U over ^{230}Th have been found in historic lavas from the Southern Volcanic Zone of Chile (33-42°S) (Sigmarsson et al., 1990) and central American arc lava (Patino et al., 2000), and are attributed to preferential partitioning of U into a fluid phase during dehydration of the recently subducted sediments. High F concentration has also been detected in the deep-sourced fluids at the Costa Rica subduction zones (Chapter 2). Uranium concentration data of the deep-sourced fluid at the Costa Rica subduction zone, however, are as yet not available. Based on the limited data to date, it is still preliminary to suggest that a complex is formed between U and F in the fluid phase, such as $U(F)_6^{2-}$, in order to explain the enrichment of U in the fluid phase in anoxic or suboxic conditions at subduction zones and should be pursued in the future research.

3.3.2 Li and Sr Isotope Ratios, with Implications for Solid Reactivities

Li isotope exchange between the fluid and solid

In order to answer the following questions: have the solids been extensively altered by the fluids in the hydrothermal experiments conducted in a close system with water/rock mass ratio of ~5; Are the experimental results representative of fluid-rock reactions at submarine hydrothermal systems; and what controls the reactivity of the source solid? A water-rock interaction model by Magenheim et al. (Magenheim et al., 1995) is used, to monitor reactivity of the solids for Li concentration and the Li isotope exchange between the fluids and solids, that can also be applied to an open system:

$$\text{Reactivity}(R) = -K^{-1} \times \ln[(Xr\text{-}KX\}/(Xr\text{-}KX_o)] \quad (3.1)$$

$$\text{Reactivity}(R) = -(\alpha K)^{-1} \times \ln[(Yr\text{-}\alpha KY\}/(Yr\text{-}\alpha KY_o)] \quad (3.2)$$

in which

α : fractionation factor for Li isotopes (^{6}Li and ^{7}Li). The empirical equation is $\alpha = 1.0192 - 8.0505\times10^{-5}T + 1.0625\times10^{-7}\ T^2$ (James et al., 1999).

K: distribution coefficient of Li element between the altered phase and the solution. The empirical equation is $K=2.4757e^{(-0.0075\times T)}$ (James et al., 1999).

X and Y: concentrations of ^{6}Li and ^{7}Li isotopes in the reacted fluid;

X_r and Y_r: the initial concentrations of the two isotopes in the solid;

X_o and $Y_{o:}$ the initial concentrations of the two isotopes in the starting fluid.

Equation (1) is applied for ^{6}Li and equation (2) is for ^{7}Li. In the model, the Li concentration and isotopic composition of the hydrothermal fluid are controlled by the Li concentrations and isotopic compositions of the reacting rock and fluid, the distribution coefficient (K) of Li between the altered phase and the fluid, as well as the Li isotopic fractionation factor (α) between these two phases; the latter two factors (K and α) are temperature dependent. The distribution coefficient (K) for Li also varies among different mineral phases. For example, at 50 °C, K is 1.7 for chlorites, 2.3 for smectites, and 33 for zeolites; at 260 °C, 0.35 for chlorites, 1.9 for smectites, and 3.5 for zeolites (Berger et al., 1988). The estimated K based on the above empirical equation is similar to Berger's experimental results for chlorite (Berger et al., 1988) and is used for modeling the basalt experiment. In the smectite experiment, a higher K (33) has to be assumed due to the different mineral alteration phases and different Li concentration and isotope ratio data of the fluid.

The measured Li concentration and isotope values of the starting ash and seawater ($X_{0,}$ $Y_{0,}$ Xr and Yr), and of the reacted fluids at 50, 100, 150, 200, 300, 350°C are known (Table 3.3.1). In equations (1) and (2), reactivity values were chosen to generate Li concentration and isotopic values to fit the measured values in the reacted fluids. The results show that at T<150 °C the reactivity is low, suggesting that rocks are not extensively reacted; at T ≥ 150 °C, more rock begins to react with the fluid, more Li is leached out; reactivity increased sharply from 200 to 350 °C (Table 3.3.3 and Fig. 3.3.8). The results for both basalt and smectite experiments are

remarkably similar, implying that the reactivity for Li is mostly temperature controlled.

The calculated δ^7Li from equations (1) and (2) and the measured δ^7Li values are plotted on Fig. 3.3.9. In the smectite experiment, between 100 and 200°C, the analyzed δ^7Li in the fluid is higher than the calculated ones, possibly as a result of isotope exchange during the dissolution of the starting solid and partition of Li between secondary minerals and the fluid.

In the basalt experiment, the ^{7}Li/^{6}Li isotopic fractionation between the 350°C fluid and the final solid is ~3 ‰ (Table 3.3.1 and 3.3.2), which is rather close to the empirical value from natural hydrothermal fluids (Chan et al., 1994), implying that the experiments do mimic the natural hydrothermal reactions. The good agreement between the calculated and experimental data for both Li concentration and isotopes from 35 to 350 °C, presented in Table 3.3.3 and Fig. 3.3.9, and the similar reactivity profiles for both basalt and smectite experiments, indicate that it is a system where rock is dissolved and new minerals precipitate, and the partitioning of Li between the newly formed minerals and fluid is governed by the temperature.

Sr and Sr Isotope Exchanges

As shown in Fig. 3.3.10, in ***the basalt-asw experiment*** between 35 and 150 ºC, Sr/Cl ratio slightly increases from 0.25 $\times 10^{-3}$ to 0.35 $\times 10^{-3}$, then drops to ~0.10 $\times 10^{-3}$ at 300 ºC and returns to the sweater value at 350 ºC. In the smectite-asw experiment, the ratios are similar to the basalt experiment data. When SO_4 was present in the

starting fluid, Sr/Cl ratio drops from ~0.3 $\times 10^{-3}$ at 150 ºC to ~0.10 $\times 10^{-3}$ at 200 ºC and remains at ~0.10 $\times 10^{-3}$ to 350 ºC, most likely due to co-precipitation of Sr with $CaSO_4$. The observed narrow range of Sr concentration from 35 to 350 ºC is consistent with that of the natural hydrothermal vent fluids (Edmond et al., 1979; Elderfield et al., 1996), suggesting that without phase separation, the oceanic crust is overall neither a sink nor a source for Sr, as some Sr is extracted from basalt by hydrothermal fluids, a similar amount of Sr is removed by mineral precipitation (Davis et al., 2003).

The $^{87}Sr/^{86}Sr$ ratios of the fluids are significantly affected, showing less radiogenic values than the starting seawater value ($^{87}Sr/^{86}Sr$ = 0.709221) throughout the course of ***basalt-sw experiment*** (Fig. 3.3.11). At 150 ºC, $^{87}Sr/^{86}Sr$ is 0.708480 and at 350ºC, $^{87}Sr/^{86}Sr$ decreases to 0.705770, reflecting Sr isotopic exchange between the fluid and the basalt ($^{87}Sr/^{86}Sr$ = 0.703610). The percentage of isotope exchange is calculated using the equation (Davis et al., 2003):

percentage exchange =

$$(^{87}Sr/^{86}Sr_{sw} - {}^{87}Sr/^{86}Sr_{reacted\ fluid})/(^{87}Sr/^{86}Sr_{sw} - {}^{87}Sr/^{86}Sr_{starting\ solid}) \times 100 \qquad (3.3)$$

In the natural hydrothermal vent fluids, Sr isotope exchange is ~100% as indicated by the average $^{87}Sr/^{86}Sr$ of 0.7037 (Davis et al., 2003). In the 350 ºC experimental fluid, the Sr isotope exchange is ~52% based on the final fluid $^{87}Sr/^{86}Sr$ ratio of 0.705770. A similar exchange ratio of ~60% was obtained in the hydrothermal experiments by James et al., 2003 (James et al., 2003). The lower $^{87}Sr/^{86}Sr$ exchange in the experimental results relative to the natural ridge crest fluids is probably caused by the considerably lower affinity of Sr for the fluid, unlike Li, which shows ~100%

reactivity of the solid; thus even after 8 months, the reactivity of the solid for Sr has not reached 100%.

In the ***smectite-sw experiment***, $^{87}Sr/^{86}Sr$ is 0.70817 at 50 ºC, 0.708138 at 150 ºC, and 0.708140 at 200 ºC. These are considerably less radiogenic ratios than both of the starting sw (0.709221) and the smectite (0.712390) values, suggesting that a reactive non-radiogenic phase is as well present, such as volcanic ash, and Sr isotope exchange preferentially occurs between the volcanic ash and fluid from 50 to 200 ºC. At higher temperature, however, $^{87}Sr/^{86}Sr$ of the fluid increases from 0.708693 at 200 ºC to 0.708693 at 250 ºC, and 0.709189 at 350 ºC, approaching the smectite value (Table 3.3.1c and Fig. 3.3.11).

The Sr isotope ratio in the experiment suggests that Sr exchange is not confined to high-temperature reactions, but begins to occur at a temperature as low as 50 ºC. Considering the large fluid fluxes inferred for ridge flank hydrothermal systems (Elderfield et al., 1999), even a small degree of exchange at ridge flank temperature could make a significant contribution to the oceanic Sr isotopic budget (Davis et al., 2003). Sr mass balance calculations have shown that for a very low Δ Sr concentration value of 10 μ mol kg^{-1} in pore fluids overlying young (~ 5 m.y.) oceanic basement and a $^{87}Sr/^{86}Sr$ value of 0.7070, with 5 cm yr^{-1} fluid advection from basement, the Sr ridge flank flux is more significant than the axial hydrothermal flux, thus, may help to resolve the apparent Sr imbalance in the ocean (Elderfield et al., 1999; Butterfield et al., 2001; Davis et al., 2003).

3.3.3 The Alteration of the Solids

X-ray diffraction (XRD) analyses of the starting and ending solids (basalt and smectite) show significant mineralogical changes. In the bulk ending solids, in addition to the minerals produced at 350 ºC, retrograde products, which are the lower temperature "overprints" from the quenching procedure from 350 ºC to 25 ºC in 24 hours (Seyfried et al., 1979), may also be present.

Based on the XRD results, the reactions at 350 ºC could be summarized as:

- **basaltic ash + sw/asw reaction:**

basaltic glass + calcite + traces of smectite + Mg^{2+} →

recrystallized smectite + mordenite + analcime + albite + Ca^{2+} + Na^{+} + K^{+} + Li^{+} + Rb^{+} + Cs^{+} + H_4SiO_4

Ca^{2+} (Sr^{2+}) + SO_4^{2-} → anhydrite forms in the sw experiments

- **smectite + sw/asw reaction:**

smectite + chlorite + traces of illite + traces of volcanic ash + quartz + Mg^{2+} →

recrystallized smectite + illite-smectite + quartz + traces of albite + Ca^{2+} +Na^{+} +K^{+} + Li^{+} + Rb^{+} + Cs^{+} + H_4SiO_4

Ca^{2+} (Sr^{2+}) + SO_4^{2-} → anhydrite forms in the sw experiments

Two smectite experiments (005 and 016) were terminated at 150 °C and 226 ºC, respectively, due to suspicion of leakage. Hence, the solid products at these two temperatures were obtained. The progressive mineral change is clearly demonstrated by XRD results: relative intensity of the chlorite peak is decreasing with increasing temperature until it is no more present at 350°C whereas the intensity of the illite-smectite peaks increase. The relative intensity of illite peak reaches its maximum at 150 °C. A poorly crystallized mixed layer chlorite-smectite may form at 350 °C but was not detected by XRD (Seyfried et al., 1998).

The chemical changes in the solids are listed in Table 3.3.2. The main results are: Mg concentration increases while Ca, Na, K, Li, Rb concentrations decrease. No significant change of Cs concentration is detected in the solids, because the Cs leached from the solid into the fluid is < 3% of the total Cs in the solid, within the analytical error. Overall the elemental concentration changes in the solids correspond to these in the fluids (Fig. 3.3.3 and 3.3.4).

Table 3.3.1. Major and trace element concentrations in the reacting fluids from 35 to 350 °C in different experiments: (a) basalt + sw; (b) basalt + asw; (c) smectite + sw; (d) smectite+ asw; (e) basalt/smectite (2/1)+ asw.

(a)- part 1. major and trace element concentration data in basalt + sw exp (001).

Sample ID	temp °C	time day	Cl mM	SO_4 mM	Mg mM	Ca mM	Sr µM	K mM	Li µM	Rb µM	Cs µM
sw	20	0	536	28.6	52.1	10.4	83	9.5	33	1.4	0.003
001-1	37	1	534	28.4	51.9	17.4	122	8.7	41		
001-4	50	10	539	27.4	49.5	18.4	116	8.9	43	0.9	0.003
001-6	75	28	531	26.9	48.4	18.0	114	8.6	39	1.4	0.006
001-7	94	29	518	26.2	45.1	17.9	154	8.7	59		
001-9	100	51	500	26.0	41.9	21.8	111	9.5	62	1.5	0.002
001-10	150	52	501	25.2	30.3	29.9	130	9.0	74	2.0	0.013
001-12	148	62	496	12.6	18.0	33.5	112	9.5	84	2.1	0.011
001-13	200	62	486	4.1	5.8	30.8	106	9.1	98	2.2	0.017
001-18	253	82	470	0.6	0.2	25.9	89	6.0	155	2.1	0.041
001-22	303	94	466	0.7	0.2	26.3	41	6.1	251	3.4	0.053
001-26	353	107	459	0.6	0.1	32.6	68	23.3	458	11.7	0.075
quench	20	107	439	4.8	0.8	47.5	99	15.0	495	4.8	0.032

(a)-part 2. Li and Sr isotopic ratio data.

Sample ID	temp °C	time day	δ^7Li ‰	$^{87}Sr/^{86}Sr$
sw	20	0	30.95	0.709189
001-1	37	1		
001-4	50	10	20.95	0.709184
001-6	75	28	22.90	
001-7	94	29	19.66	
001-9	100	51	21.02	
001-10	150	52	17.41	0.708480
001-12	148	62		
001-13	200	62	14.40	0.707694
001-18	253	82		
001-22	303	94	9.53	0.706235
001-26	353	107	7.33	0.705770
quench	20	107	8.31	

Table 3.3.1. (continued)
(b) major and trace element concentration data in basalt-artificial sw experiment (017)

Sample ID	temp °C	time day	Cl mM	SO_4 mM	Mg mM	Ca mM	Sr µM	K mM	Li µM	Rb µM	Cs µM
asw	35	0.0	630	0.2	51.4	8.9	159	8.9	36	0.7	0.005
017-1	35	7	648	0.3	51.4	16.2		9.0		0.6	0.001
017-2	52	14	637	0.3	49.9	16.5	173	8.7	41	0.6	0.002
017-3	52	21	634	0.4	50.8	17.2	176	9.3	46	0.8	0.008
017-4	77	28	624	0.4	48.7	17.0	175	9.3	49	0.8	0.023
017-5	77	35	608	0.4	46.3	18.2	180	10.1	74	1.1	0.014
017-6	102	43	617	0.4	45.9	18.5	182	10.0	61	1.0	0.007
017-7	102	50	610	0.5	41.5	21.8	182	10.7	70		
017-8	124	56	601	0.4	39.0	22.3	176	9.7	69	1.3	0.007
017-9	128	62	609	0.6	32.1	28.5	187	9.8	77	1.5	0.012
017-10	150	68	601	0.7	28.3	31.7	192	9.8	80	1.5	0.012
017-11	150	76	603	1.0	12.3	45.9	209	9.5	93	1.7	0.017
017-12	176	83	600	1.1	6.0	49.7	210	8.7	93	1.6	0.013
017-13	200	89	596	1.7	3.0	51.5	203	8.8	103	1.8	0.022
017-14	224	97	584	0.0	0.8	48.8	185	8.6	106	1.8	0.036
017-15	250	104	585	0.0	0.4	47.4	172	7.6	107	1.9	0.043
017-16	275	111	582	0.0	0.4	44.1	152	6.3	141	1.9	0.059
017-17	301	121	579	0.2	0.3	41.5	97	5.9	206	2.3	0.061
017-18	323	133	596	0.0	0.2	55.1	89	21.3	468	9.1	0.074
017-19	352	179	593	0.0	0.2	52.7	113	28.8	664	11.6	0.071
017-20	35	0.0	590	0.0	0.1	39.2	151	35.3	706	15.8	0.094

Table 3.3.1. (continued)
(c)-part 1. major and trace element concentration data Smectite- sw experiment (002)

Sample ID	temp °C	time day	Cl mM	SO_4 mM	Mg mM	Ca mM	Sr µM	K mM	Li µM	Rb µM	Cs µM
sw	20	0	536	27.6	51.6	10.3	83	10.3	25	1.4	0.003
002-1	35	1	567	29.0	48.1	18.7	119	8.7	65		
002-4	50	10	542	26.5	41.5	20.2	126	8.5	55	0.5	0.011
002-5	50	28	539	28.5	43.6	21.3	125	8.9	75	0.5	0.010
002-7	94	29	551	27.2	41.5	20.5	129	9.8	125	0.5	0.011
002-9	92	51	512	25.1	37.5	19.9	126	9.5	181		
002-12	150	62	535	27.0	36.4	21.8	125	11.8	222	0.9	0.015
002-13	200	62	542	9.6	32.0	9.4	64	14.1	293	2.1	0.023
002-18	251	82	530	3.4	20.3	6.7	53	16.4	400	4.5	0.100
002-22	295	94	527	1.8	15.3	6.4	42	17.0	844	7.5	0.160
002-26	350	107	535	1.2	7.8	6.6	48	17.6	1,929	12.7	0.466
quench	25	107	473	10.8	13.2	13.2	65	13.2	1,626	14.2	0.120

(c)-part 2. Li and Sr isotopic ratio data in smectite- sw experiment (002)

Sample ID	temp °C	time day	δ^7Li ‰	$^{87}Sr/^{86}Sr$
sw	20	0	30.95	0.709189
002-1	35	1		
002-4	50	10	13.68	0.708167
002-5	50	28		
002-7	94	29	15.80	
002-9	92	51	14.71	
002-12	150	62	11.91	0.708138
002-13	200	62	11.34	0.708139
002-18	251	82		0.708693
002-22	295	94	5.65	0.709016
002-26	350	107	6.15	0.709189
quench	25	107	5.97	

Table 3.3.1. (continued)
(d) major and trace element concentration data in smectite-artificial sw experiment (016)

Sample ID	temp °C	time day	Cl mM	SO_4 mM	Mg mM	Ca mM	Sr µM	K mM	Li µM	Rb µM	Cs µM
asw	20		630	0.2	51.6	9.0	159	10.0	61	0.7	0.005
016-1	35	0	657	0.5	47.9	16.3		8.9			
016-2	35	7	642	0.7	43.6	19.1	186	8.3	51	1.5	0.017
016-3	50	14	522	0.8	34.2	15.5	150	7.0	67		
016-4	50	21	550	0.6	33.4	15.4	162	6.9	63	0.3	0.010
016-5	75	28	584	0.7	37.7	18.1	170	8.9	91		
016-6	74	35	585	0.7	37.7	18.2	173	8.0	95	0.4	0.008
016-7	104	43	609	0.7	37.6	19.0	173	9.6	127		
016-8	102	50	610	0.8	37.9	19.3	172	9.3	138	0.5	0.011
016-9	125	56	610	0.8	36.7	19.1	170	10.3	176		
016-10	125	62	610	0.7	35.7	19.2	173	10.8	188	0.7	0.014
016-11	150	68	608	0.8	33.4	19.0	169	11.8	224		
016-12	150	76	604	0.8	32.5	18.8	169	11.9	228	0.9	0.014
016-13	175	83	594	0.8	29.2	18.2	164	13.2	260	1.6	0.013
016-14	202	89	574	0.7	24.5	17.5	162	15.2	329	2.1	0.015
016-15	226	97	509	0.8	17.8	14.7	135	16.0	351	3.1	0.077

Table 3.3.1. (continued)
(e) Basalt/smectite(2/1)-artificial sw experiment (003)

Sample ID	temp °C	time day	Cl mM	SO_4 mM	Mg mM	Ca mM	Sr µM	K mM	Li µM
asw	20	0	633	0.2	51.5	9.8	151	9.5	39
003-1	40	0	652	0.6	49.2	15.6	170	9.5	31
003-3	47	9	645	0.6	49.7	17.4	176	10.2	22
003-4	50	25	649	0.6	49.0	17.1	178	10.4	48
003-5	76	26	646	0.6	48.9	17.9		11.7	58
003-7	74	47	621	1.1	43.1	18.6	178	10.6	58
003-9	98	48	594	0.7	40.6	18.9		10.9	58
003-11	100	68	609	0.7	37.2	23.7	173	10.7	81
003-13	117	69	609	1.0	34.6	26.2	182	11.1	85
003-15	133	90	608	1.0	19.6	39.5	183	10.7	104
003-16	150	91	600	1.0	17.4	39.3	190	10.6	110
003-18	154	112	602	1.0	6.7	47.1	183	9.6	115
003-19	171	113	606	1.2	4.5	51.5	198	10.4	130
003-21	171	131	605	1.3	2.5	50.3	208	9.0	150
003-22	197	131	593	1.2	1.8	50.0		9.3	
003-25	199	143	588	1.4	1.3	49.4	187	8.4	143
003-27	225	150	586	0.9	1.2	47.1		7.4	
003-30	243	161	585	1.3	1.1	48.5	174	7.4	231
003-33	271	169	589	2.0	1.2	63.7	163	9.0	254
003-36	298	180	605	1.4	1.4	64.4	90	9.4	721
003-38	320	182	587	2.2	0.6	62.5	86	11.7	919
003-41	355	192	591	1.6	0.9	65.1	83	16.6	989
quench	25	192	608	2.6	4.8	75.5	120	9.0	966

Table 3.3.2. Major and trace element compositions in the Starting and Ending Solids at 350 ºC

	Basaltic ash ODP 836A-3H4 10-51cm		Smectite ODP Leg110-671B-51x	
Element	Starting solid (ppm)	Ending Solid (ppm)	Starting solid (ppm)	Ending Solid (ppm)
Mg	20357	24739	19989	25386
Ca	53289	47569	8990	7752
Na	15283	13729	6875	3557
K	2189	2189	7308	7050
Li	15	2.3	88.1	3.0
Sr	156	184	99	103
Ba	71	84	207	180
Rb	7	6	58	55
Cs	1	1	4	4
δ^7Li	7.04	2.30	4.41	7.60
$^{87}Sr/^{86}Sr$	0.702520		0.712386	

Table 3.3.3. Estimated reactivity, distribution coefficient (K) and fractionation factor (α), Li concentration and δ^7Li (calculated and measured values) with temperature in basalt-sw and smectite-sw reactions.

temp (˚C) Basalt Experiment	reactivity R	K	α	δ^7Li (‰) calculated values	Li (μm/kg) calculated values	δ^7Li (‰) measured values	Li (μm/kg) measured values
50	0.010	1.7	0.985	21.48	55	20.95	43
75	0.010	1.41	0.986	21.44	55	22.90	39
100	0.013	1.17	0.988	21.40	55	21.02	62
100	0.013	1.17	0.988	19.73	62	19.66	59
150	0.020	0.8	0.991	17.27	77	17.41	74
200	0.033	0.55	0.993	14.43	105	14.40	98
300	0.100	0.26	0.995	10.14	250	9.53	251
350	0.200	0.18	0.997	8.71	464	7.58	458
Smectite Experiment							
50	0.005	33	0.985	14.58	87	13.68	55
100	0.005	9.5	0.989	13.64	94	15.80	125
100	0.007	9.5	0.989	12.08	113	14.71	181
150	0.020	8.5	0.991	8.05	262	11.91	222
200	0.025	4	0.993	7.16	332	11.34	293
300	0.071	3	0.995	5.78	843	5.65	844
350	0.222	3	0.996	5.83	2076	6.15	1,929

Note: the calculated Li concentration and δ^7Li are derived from the fluid-rock interaction model (equation 1 and 2), and compared with the measured values.

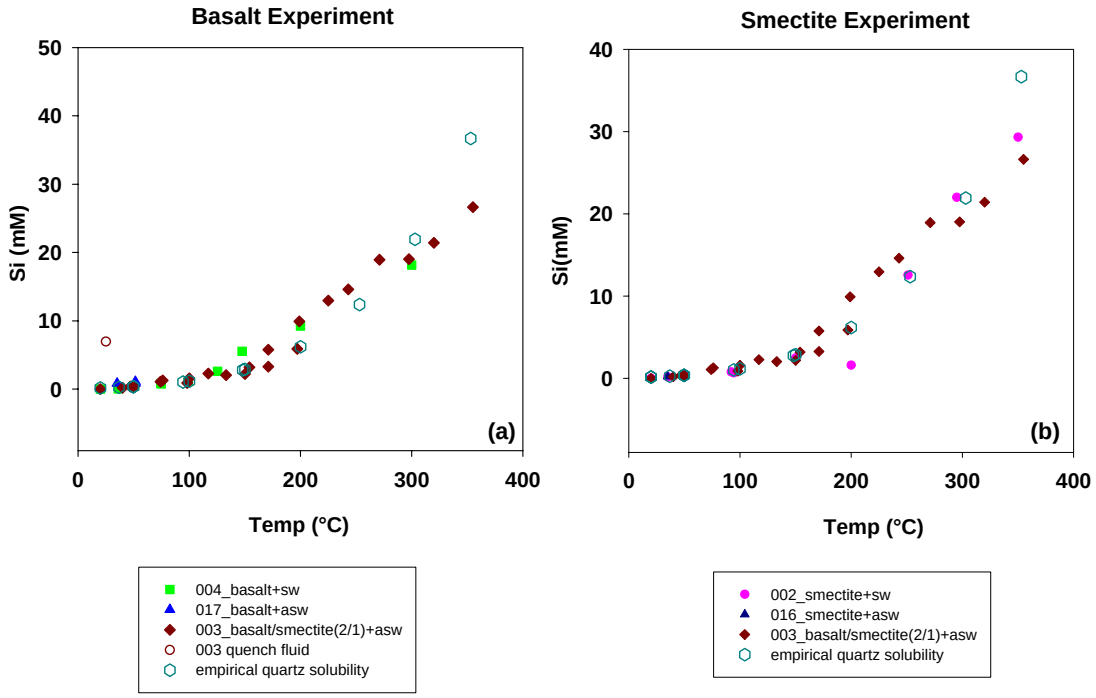

Figure 3.3.1 Silica concentration versus temperature in (a) basalt and (b) smectite experiments. Both analyzed concentrations and theoretical values, using quartz solubility in seawater (Von Damm et al., 1991), from 35 to 350 °C, are shown.

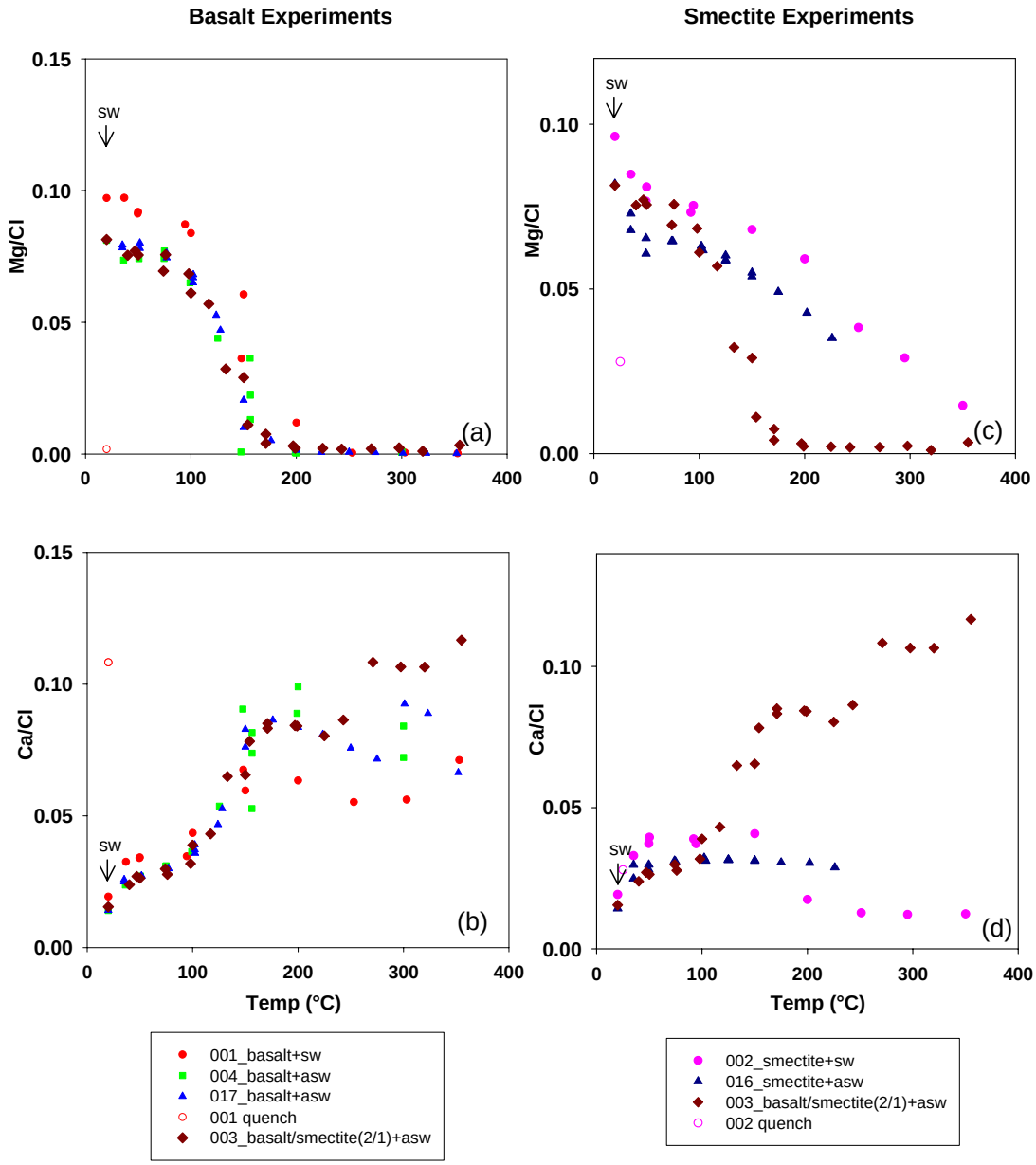

Figure 3.3.2 Normalized to Cl Major element concentrations versus temperature in hydrothermal experimental fluids: (a) Mg/Cl in basalt experiment; (b) Mg/Cl in smectite experiment; (c) Ca/Cl in basalt experiment; (d) Ca/Cl in smectite experiment.

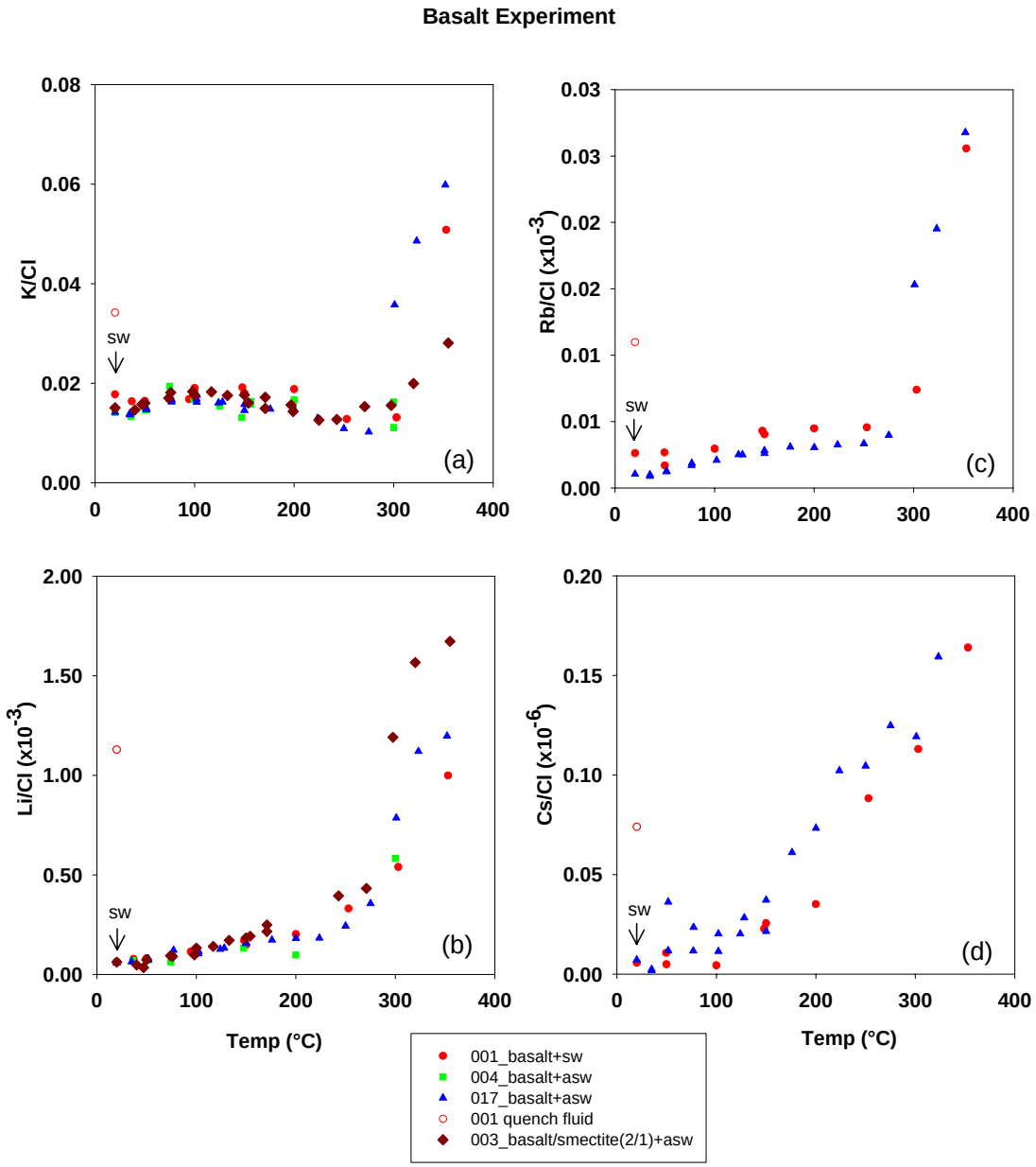

Figure 3.3.3 Alkali metal concentrations normalized to Cl (μM/mM) versus temperature in reacting fluids in basalt experiment: (a) K/Cl; (b) Li/Cl; (c) Rb/Cl; (d) Cs/Cl.

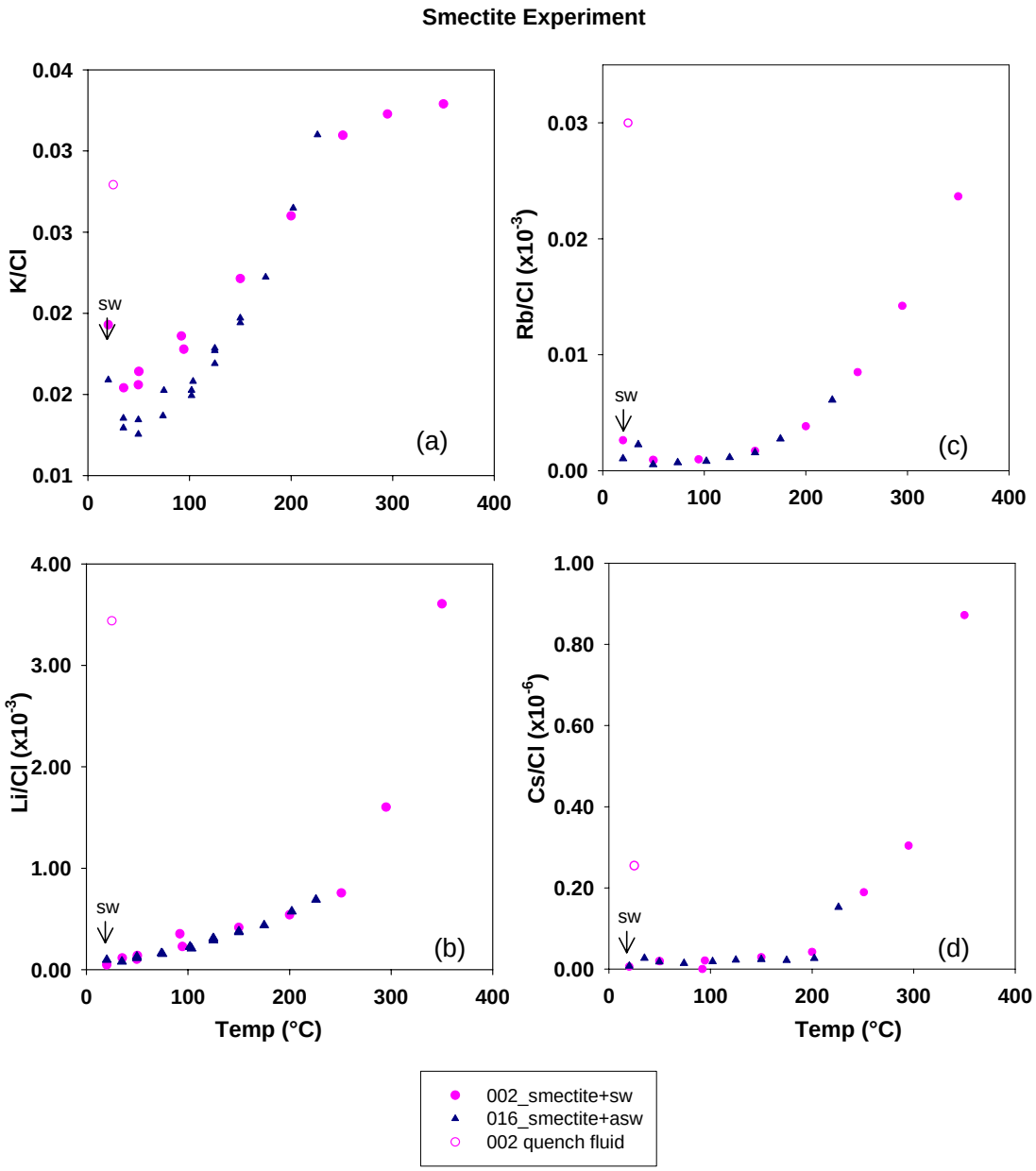

Figure 3.3.4 Alkali metal concentrations normalized to Cl (µM/mM) versus temperature in reacting fluids in smectite experiment: (a) K/Cl; (b) Li/Cl; (c) Rb/Cl; (d) Cs/Cl.

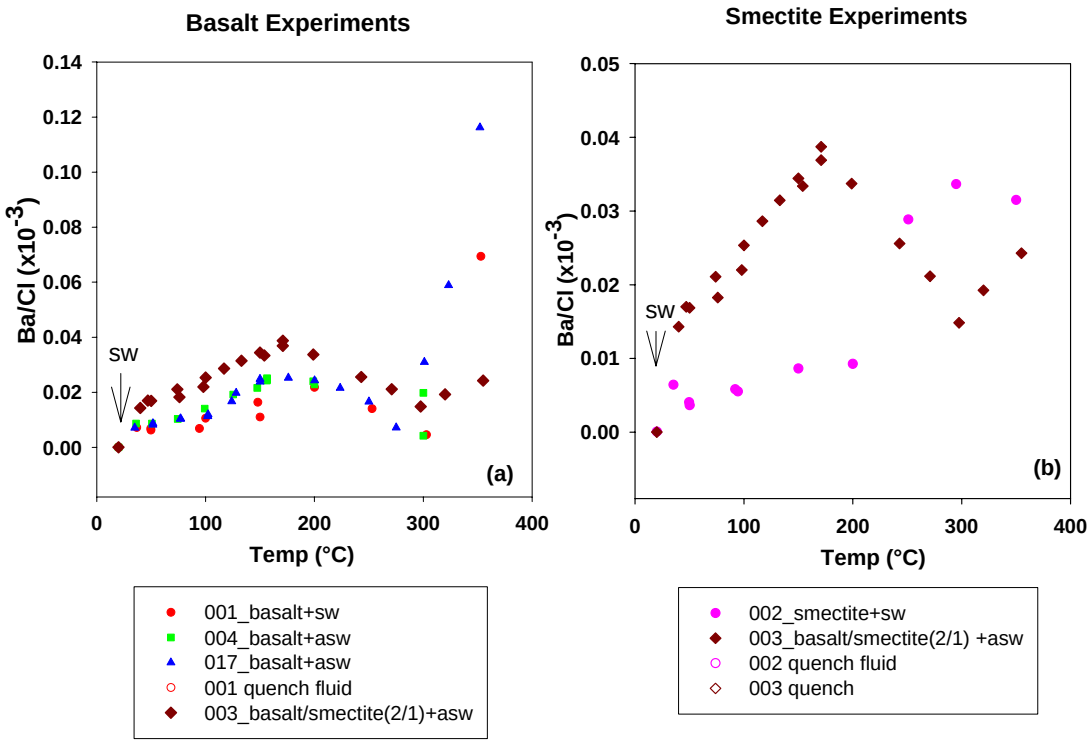

Figure 3.3.5 Ba/Cl versus temperature in hydrothermal experimental fluids: (a) Ba/Cl versus temperature in basalt experiment; (b) Ba/Cl versus temperature in smectite experiment.

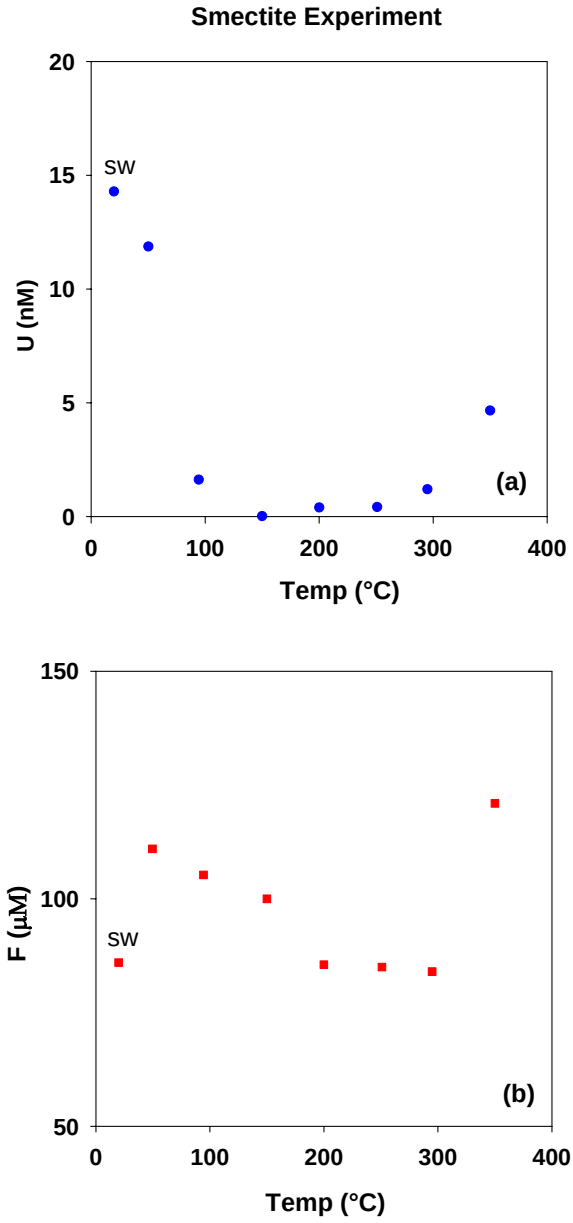

Figure 3.3.6. (a) U concentration and (b) F concentration versus temperature in hydrothermal experimental fluids of smectite experiment.

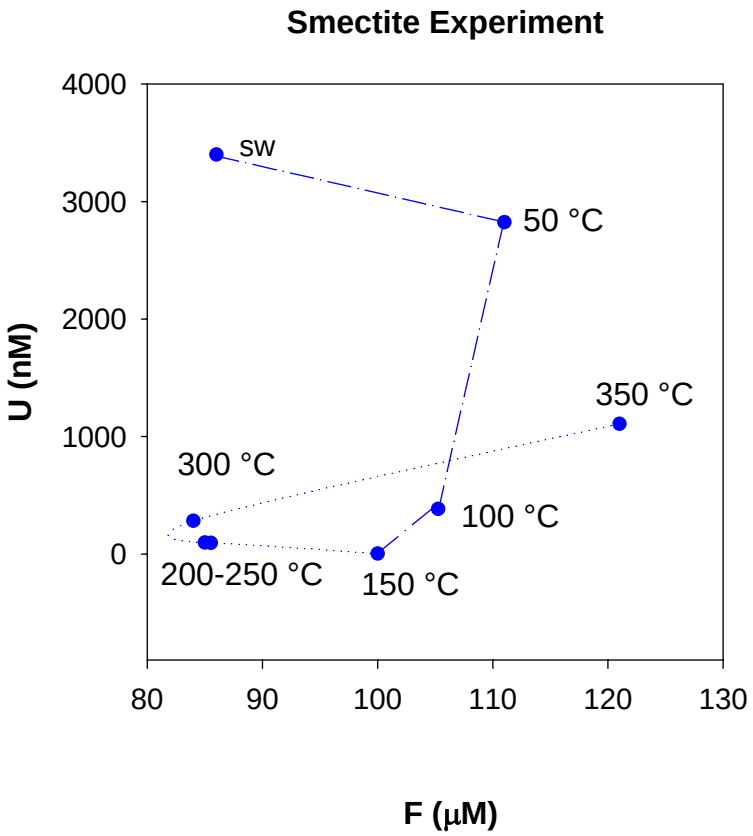

Figure 3.3.7. U concentration and F concentration cross plot in the smectite-sw experiment from 35 to 350°C.

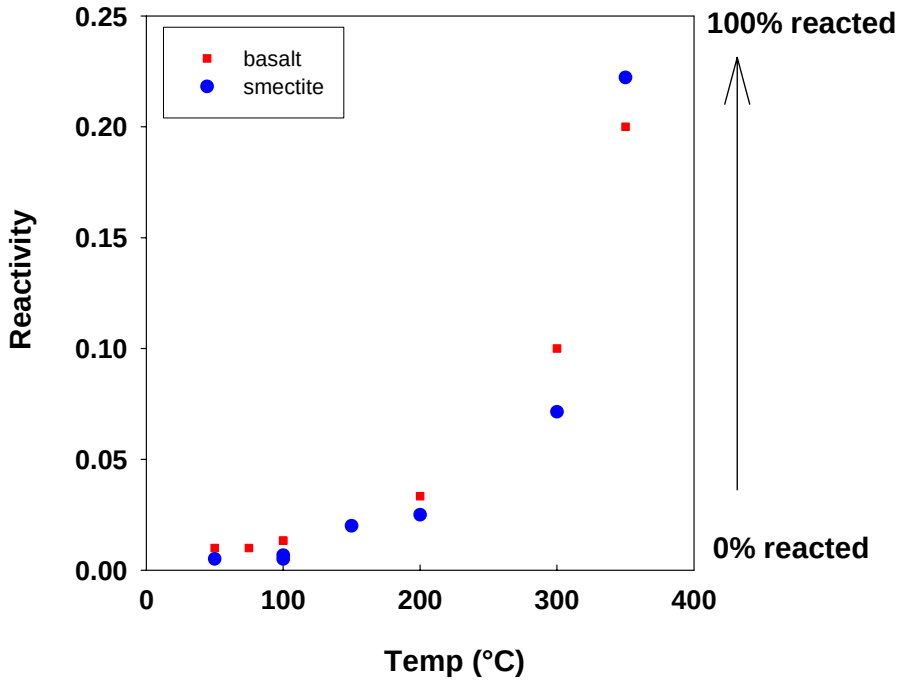

Figure 3.3.8. The reactivity of the solid for Li versus temperature in both basalt and smectite experiments. The reactivity was estimated based on equation (1) and (2) (Magenheim et al., 1995).

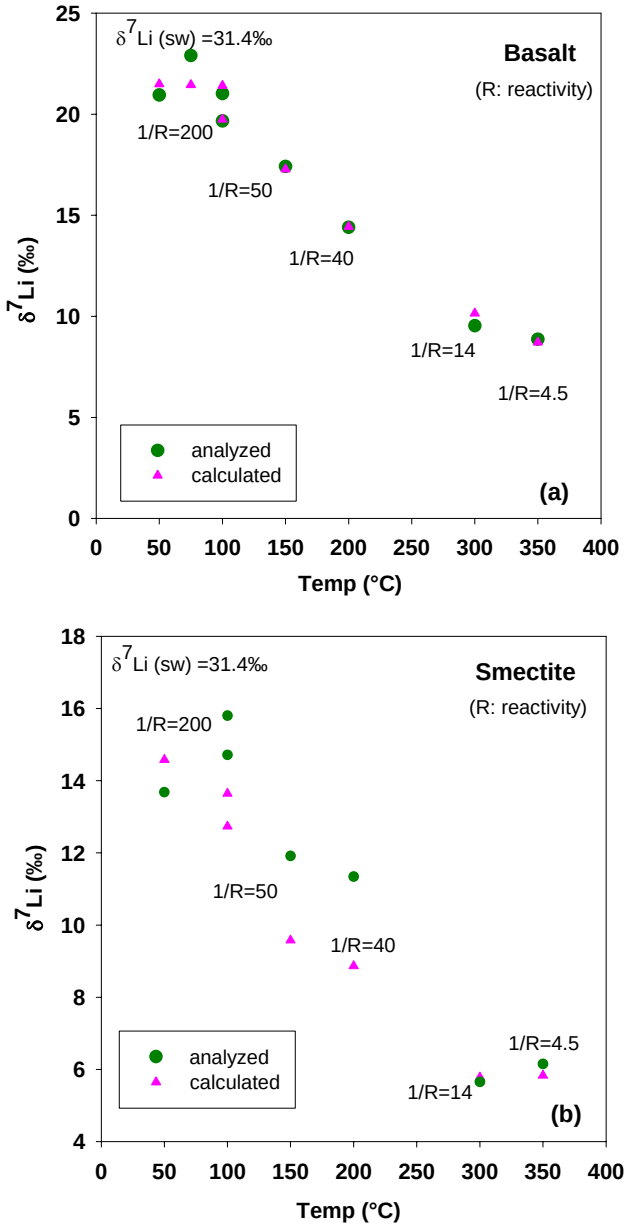

Figure 3.3.9. Analyzed and calculated Li isotope ratio versus temperature in (a) basalt + sw experiment; and (b) smectite + sw experiment.

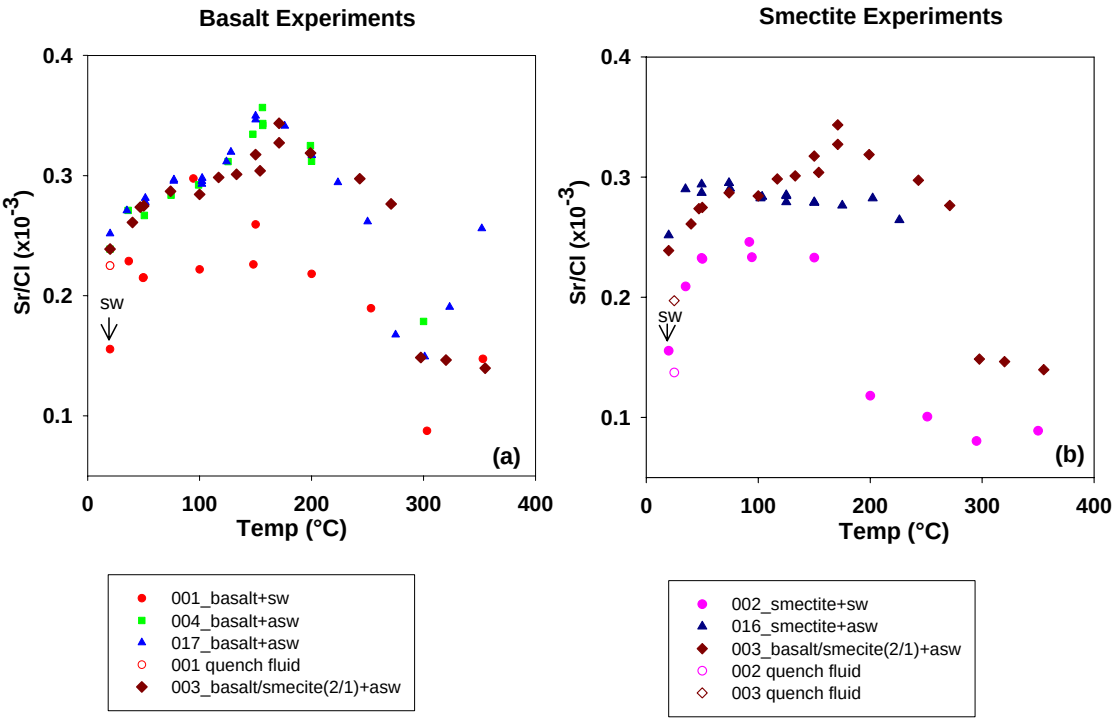

Figure 3.3.10. Sr/Cl (μM/mM) versus temperature in (a) basalt; and (b) smectite experiments.

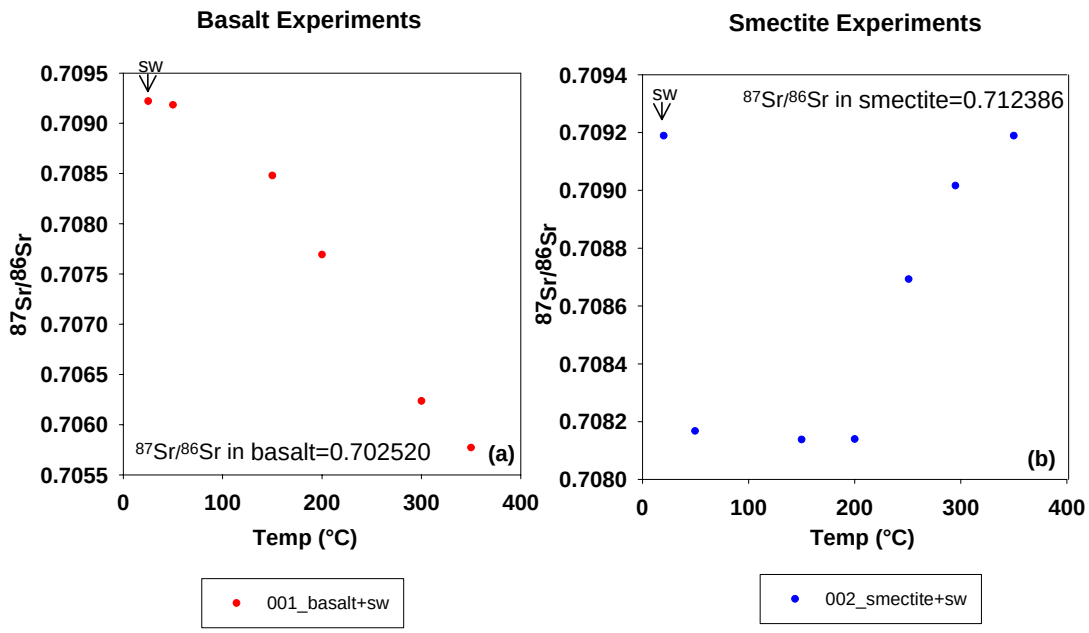

Figure 3.3.11. $^{87}Sr/^{86}Sr$ versus temperature in (a) basalt-sw experiment; and (b) smectite-sw experiment.

3.4 Implications

3.4.1 Oceanic Cycles of Alkali Metals and Li isotopes

Previous studies have shown estimates of oceanic crust alteration control on K, Rb, and Cs in seawater (Hart, 1969; Hart et al., 1982), and of Li and Li isotope cycling in the ocean (*e.g.* (Edmond et al., 1979; Holland, 1984; Huh et al., 1998; Zhang et al., 1998)). Important questions are how alkali elements recycle in the ocean, what the important sources and sinks are, and whether the steady state in the ocean is maintained. The hydrothermal experimental data acquired in this study, especially at the low temperature range (50 to 300°C), provide new insights on mass balance calculations for the four alkali elements (Li, K, Rb, and Cs).

The suggested ultimate sinks of alkali elements in the ocean are altered oceanic crust and sediments (Holland, 1984). Alkali elements are conservative in the ocean, hence, if in steady state, the total input fluxes (F) from hydrothermal (ht) and river should equal the total output fluxes removed by altered oceanic crust and newly formed sediments:

$$F_{ht} + F_{river} = F_{altered\ basalt} + F_{sed} \qquad (3.4)$$

Estimate of F_{ht} + F_{river} : despite the fact that the ash sample used in this experiment has somewhat higher Li concentration and δ^7Li value compared to average MORB, which has generally Li of ~5ppm and δ^7Li value between 3 and 5‰ (Chan et

al., 1992), all the alkali concentrations in the fluids in the basalt-sw experiment are within the range of the corresponding values in natural hydrothermal fluids (Elderfield et al., 1996), and the δ^7Li value 7.3 ‰ is close to the average value of 7 ‰ in hydrothermal fluids at ridge crests (Chan et al., 1992; Bray, 2001; Bray, 2001; Foustoukos et al., 2004), as shown in Table 3.4.1. Therefore, the alkali elements at 350°C in the experiments are used to represent the average concentration in natural hydrothermal fluids. Using the hydrothermal water flux of 3 to 6 $\times 10^{13}$ kg/yr (Elderfield et al., 1996), the range of F_{ht} (Input 2) is estimated and shown with F_{river} (Input 1) in Table 3.4.2. For Li, the river input is updated by Huh *et al.* (Huh et al., 1998).

Estimate of $F_{altered\ basalt}$ + F_{sed}: the alkali metal fluxes into altered oceanic crust have been estimated by Hart and Holland and are listed in Table 3.4.2 (Hart et al., 1982); (Holland, 1984). Flux into sediments is a major sink for alkali metals and only the Li flux has been calculated to be 1- 4×10^{11} g/yr (Holland, 1984). Given that clay minerals represent ~60% of the detrital fraction in sediments (Griffin et al., 1968), and the Li/Al ratio of 0.88×10^{-3} in the detrital smectite from Barbados is within the range of 0.77-0.95 $\times10^{-3}$ in sediments suggested by Holland (Holland, 1984), it is suggested that the smectite used in our experiments represents average altered sediment. Using the Li concentration in the smectite, Li flux to sediment is calculated to be ~3×10^{11} g/yr, within the range obtained by Holland (1984) (Holland, 1984). Fluxes of K, Rb, and Cs were also obtained, following a similar calculation, and are listed in Table 3.4.2.

In Table 3.4.2, the total output fluxes for K, Li and Rb are on the same magnitude of the total input fluxes, implying that K, Li, and Rb are in steady-state in the ocean. For Cs, however, the sink into the sediments is about one order of magnitude higher than the input fluxes from high temperature hydrothermal fluids (350°C) and rivers. As shown in Fig. 3.3.3, Cs release from basalt to the fluid is already significant at 100°C. Based on these experimental results, it is suggested that ridge flank circulation is probably responsible for a significant input flux to the Cs cycle in the ocean.

The Li isotopic data obtained from the hydrothermal experiments also help to resolve the imbalance of the oceanic Li isotope cycle. Under steady state conditions (Chan et al., 1992; Huh et al., 1998):

$$(\delta^7Li)_{input} = f_{river}\,(\delta^7Li)_{river} + f_{ht}\,(\delta^7Li)_{ht} \qquad (3.5)$$

$$\alpha = (^6Li/^7Li)_{input}/(^6Li/^7Li)_{ocean} = (^6Li/^7Li)_{output}/(^6Li/^7Li)_{ocean} \qquad (3.6)$$

where f_{river} and f_{ht} are fractions of the total flux due to river and hydrothermal inputs to the ocean, respectively; α is Li isotope fractionation factor. For $(^6Li/^7Li)_{output}/(^6Li/^7Li)_{ocean,}$ the empirical α was obtained based on low temperature weathering of seafloor basalt of 0.019 (Chan et al., 1992).

Based on Li flux data summarized in Table 6, the average $(\delta^7Li)_{river}$ value of 19-23 ‰ (Huh et al., 1998), and the update average $(\delta^7Li)_{ht}$ value of 7 ‰ (Foustoukos

et al., 2004), α is 1.019 to 1.012, slightly lower than the pervious estimate of 1.023 (Chan et al., 1992; Huh et al., 1998). These Li fluxes, however, did not include the input from subduction zones. If the Li flux at subduction zones (sz) is considered as well in the mass balance calculation, with the value of δ^7Li_{sz} of 22‰ (Chan et al., 2000) and Li flux of 0.2-1.4 $\times 10^9$ mol/yr based on the data from Costa Rica and Peru convergent margins (Kastner et al., 1991; Martin et al., 1991), α is only changed slightly to the range of 1.019 to 1.021.

Another important unknown in the Li isotope cycle is the ridge flank flux. As shown in the hydrothermal experiments, Li concentration and isotope ratios of the reacted fluid have been significantly modified already at temperature as low as 50 °C (Fig. 3.3.9), with the lighter isotope ^{6}Li preferentially leached from the solid into the fluid. Equation (4) is thus modified to include the inputs from ridge flank and subduction zones:

$$(\delta^7Li)_{input} = f_{river}\,(\delta^7Li)_{river} + f_{ht}\,(\delta^7Li)_{ht} + f_{sz}\,(\delta^7Li)_{sz} + f_{\text{ridge flank}}\,(\delta^7Li)_{\text{ridge flank}} \qquad (3.7)$$

If Li input flux through ridge flank is taken as the total output flux (4.1×10^{10} mol/yr) minus the total input flux (2.9×10^{10} mol/yr) shown in Table 6, and $(\delta^7Li)_{\text{ridge flank}}$ value is between ~20‰ at 50°C to 10 ‰ at 200°C, based on the Li isotope data from the hydrothermal experiments (Fig. 3.3.9), the range of α is significantly greater, from 1.017 to 1.021. The calculation suggests that the ridge flank must play an

important role in the δ^7Li input to the ocean, thus also contributes to the Li isotopic mass balance problem in the ocean.

3.4.2 Geothermometry

Several chemical and isotopic reactions have been used as geothermometers to estimate reservoir temperatures (Fournier, 1981). The best known ones are silica concentration (Von Damm et al., 1991), Mg/Li ratio (Kharaka et al., 1989), Na/Li ratio (Fouillac et al., 1981) and Na-K-Ca (Fournier et al., 1979). The results from these experiments (Fig. 3.3.4 and 3.3.5) demonstrate that the mobility of each alkali metal between the fluid and solid is distinct, *i.e.* each has a characteristic behavior in terms of temperature-dependent fluid phase partitioning, which gives rise to the observed fractionation among the alkali metals at all temperatures from 25 to 350°C. Accordingly, alkali elements may be used as geothermometers to constrain the temperature of the deep fluid at the source.

At the Costa Rica subduction zone, the upper 160m of the subducted hemipelagic sediments consist of mainly volcanic ash and clays (ODP Leg 170 Initial Reports). The detrital smectite used in the hydrothermal experiments is considered as a proxy for the subducted clays in Costa Rica, as its chemical composition (Table 3.3.2) is close to the average detrital smectite chemistry (Perry et al., 1970). The K concentration and Li/K profiles with depth at ODP Sites 1040 and 1254 from Costa Rica subduction zone are shown in Fig. 6-I. The K concentration-depth profile (Fig. 3.4.1) shows minima at the décollement and fault zone (200 mbsf) while Li

concentrations show maxima at the same depths (Chan et al., 2000). Based on a calculation that the fluid at the décollement consists of ~70-100% of the deep sourced fluid (discussed in chapter 2), the Li/K ratios of the deep sourced fluids is 80 $\times 10^{-3}$ to 115 $\times 10^{-3}$, which are up to twice as high as the experimentally observed value at 275°C in the basalt-sw experiment, but are similar to those observed in the basalt/smectite (2/1) mixture -asw experiment (Fig. 3.4.2). Assuming no retrograde reactions (You et al., 2001), the K concentration together with the Li/K ratio constrain the temperature range of the deep-sourced fluid at 100 - 275°C and suggest the involvement of sediments similar in composition to the hemipelagic sediments at the reaction site.

Alkali concentration- temperature profiles may as well be used to identify sediment recycling at subduction zones, using the alkali metal enrichments in the sediments relative to the basalt. During plate subduction, with increasing temperature with depth, fluids are released by compaction or hydrous mineral dehydration, together with volatiles and elements having strong affinity for the fluid, such as alkali metals. When the fluids enter the zone of magma generation and trigger melting of the mantle wedge, arc magmas may reflect their enrichments. For example, it was suggested that in Central American arc volcanoes, based on comparison of input and output fluxes of the arc, the alkali elements are efficiently recycled and transferred from the subducted slab to the mantle wedge (Chan et al., 1999; Patino et al., 2000; Chan et al., 2002).

Table 3.4.1. Alkali metal concentrations and δ^7Li values at 350 ºC in the basalt+sw experiments (001 and 007) and in natural hydrothermal fluids

Exp #	Conc. at 350 ºC in Exp 001 mol/kg	017 mol/kg	Conc. in submarine hydrothermal fluids mol/kg
Li	474 µ	664 µ	411-1322 µ (Elderfield et al., 1996)
K	23 m	35.5m	17-32.9 m (Elderfield et al., 1996)
Rb	11.73 µ	15.8 µ	10-33 µ (Elderfield et al., 1996)
Cs	75 n	98 n	100-202 n (Elderfield et al., 1996)
δ^7Li	7.3‰		7.2 - 8.9‰; average 7‰ (Bray, 2001; Foustoukos et al., 2004)

Table 3.4.2. Alkali metal budgets in the ocean

	OUTPUT 1 through sediments			
	Conc.in sed. ppm	Conc in ignenous rock ppm	Total flux into sed * $\times 10^{10}$ g/yr	Total flux into sed $\times 10^{10}$ mol/yr
K	7308[a]	2189[a]	2600	65
Li	88[b]	30[b]	29	4.2
Rb	58[a]	6[a]	26	0.3
Cs	4[a]	1[a]	1.5	0.011

	OUTPUT 2 through oceanic basement				
	Conc in altered basement ppm	Conc in unaltered basement ppm	Total flux into basement ** $\times 10^{10}$ g/yr	Total flux into basement $\times 10^{10}$ mol/yr	Total output $\times 10^{10}$ mol/yr
K	3990[c]	1064[c]	1500	40	105
Li	16[f]	6[d]	5.8	0.84	4.9
Rb	9[c]	1[c]	4.2	0.05	0.354
Cs	0.2[c]	0.01[c]	0.088	0.00066	0.012

	INPUT 1 through river	INPUT 2 Hydrothermal		Total Input		Total Input average
		min	max	min	max	
	$\times 10^{10}$ mol/yr	$\times 10^{10}$ mol/yr	$\times 10^{10}$ mol/yr	$\times 10^{10}$ mol/yr	$\times 10^{10}$ mol/yr	$\times 10^{10}$ mol/yr
K	190[b]	23[a]	69[a]	210	260	236
Li	0.8[e]	1.4[a]	2.7[a]	2.2	3.5	2.9
Rb	0.04[b]	0.03[a]	0.10[a]	0.0063	0.13	0.10
Cs	0.0005[b]	0.0003[a]	0.0006[a]	0.00077	0.0011	0.001

[a] this study
[b] Holland 1984
[c] Hart and Staudigel, 1982
[d] Chan et al., 1992
[e] Huh et al., 1998
[f] Chan et al., 1992; Bouman et al., 2004; Kelley et al., 2003
* based on the study in Holland (1984), rate of transport of sediments to the oceans=2×10^{16} g/yr with 25% being the weathering products of igneous rocks and high-grade metamorphic rocks
** based on the study in Hart and Staudigel (1982), the crustal production rate =5.3 $\times 10^{15}$ g/yr

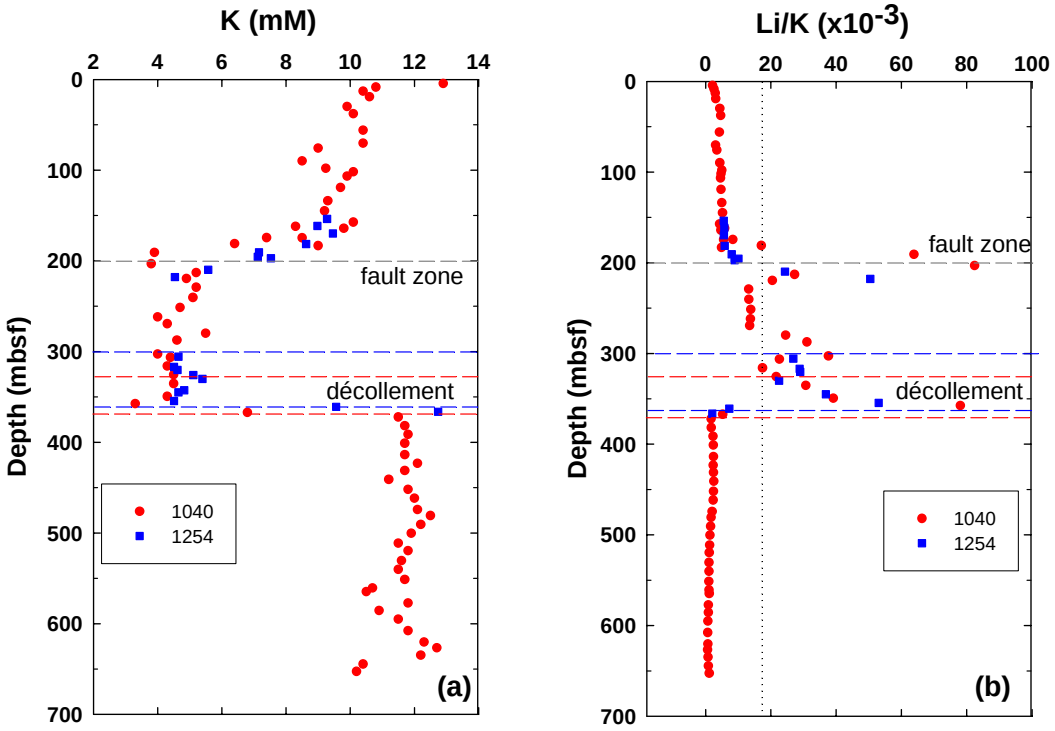

Figure 3.4.1. Depth profiles of (a) K concentration and (b) Li/K offshore Costa Rica (ODP Sites 1040 and 1254)**.** The sharp decrease in K and increase in Li/K at 200 mbsf and at the décollement signify fluid flow from greater depths. The data are from ODP Leg 170 Initial Reports (Kimura, 1997).

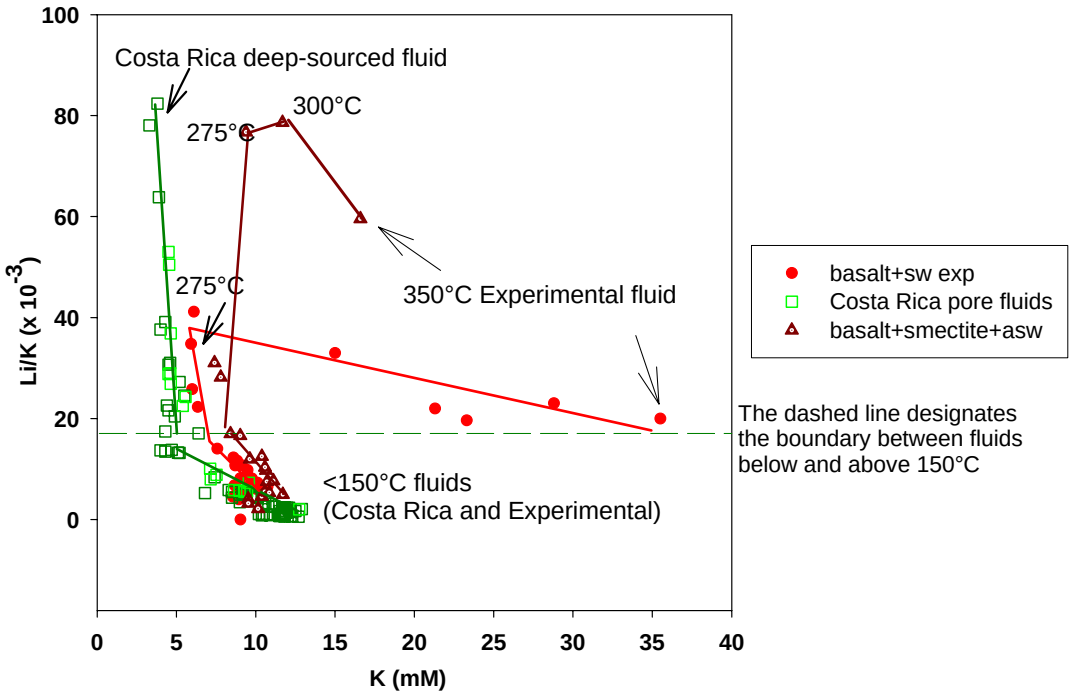

Figure 3.4.2. Li/K (μM/mM) versus K concentration. The data above the green dashed line are for the temperatures above 150 ºC. The composition of the Costa Rica pore fluid data at the fault (at 200 mbsf), and at décollement (at 350 mbsf), overlap with the hydrothermal experimental data at ~ 275 ºC in the basaltic and smectite mixture experiment (003).

Chapter 3, in part, will be submitted to Earth and Planetary Science Letters, Wei Wei, Lui H. Chan, Miriam Kastner, Robert Rosenbauer, Yishai Weinstein. Alkali elements mobility, Li and Sr isotope exchanges in hydrothermal experiments: implications for reaction temperatures and fluxes at ridge crests and subduction zones. The dissertation author is the primary investigator and author of the paper.

CHPATER 4

SUMMARY AND PROSPECTIVES

4.1 Summary

4.1.1 Halogen concentrations and Cl isotope at convergent margins

This study has surveyed three subduction zones, the Nankai Trough (Ocean Drilling Program Legs 131 and 190), the Middle America Trench Offshore Costa Rica (ODP Legs 170 and 205), and the Mariana Forearc (ODP Leg 195), for chlorine stable isotope ratios ($\delta^{37}Cl$) and halogen concentrations (F, Br and Cl) in pore fluid and solid samples. The focus on solids is on the hydrous silicate serpentine from Mariana mud volcanoes. The F, Br and Cl concentrations and $\delta^{37}Cl$ data were used to interpret the fluid sources, paths, and fluid-rock reactions, to calculate fluid mixing between the *in situ* and the deep-sourced fluids, and to estimate the $\delta^{37}Cl$ cyclings in the ocean.

Along the Nankai Muroto transect, the high resolution $\delta^{37}Cl$-depth profiles show that the $\delta^{37}Cl$ minimum value, situated below the décollement, evolves laterally from -7.8‰ at the most arcward Site 808 (3.4 km from the trech), to -7.1‰ at Site 1174 (~2 km seaward from Site 808), and to -5.8‰ at the reference Site 1173 (Chapter 2.4.1). Along the Costa Rica transect, the $\delta^{37}Cl$ minimum value evolves similarly along the décollement from -5.5‰ at the most arcward Site 1040/1254 (1.6km from the trench), to -3.2‰ at Site 1043/1255 (~1km seaward from Site 1040/1254), and to 0‰ at the reference Site 1039/1253 (Chapter 2.5.1). At both subduction zones, the

Br/Cl ratios are higher than seawater value (1.5×10^{-3}) and also show seaward evolutions from the most arcward site to the reference site along the transects.

In contrast, the $\delta^{37}Cl$ values in the pore fluids at the Mariana mud volcanoes are higher than the seawater value, ranging from +0.3‰ to +1.8‰. The Br/Cl ratios are lower than the seawater ratio. The positive $\delta^{37}Cl$ values in the pore fluid and the high content of Cl (hundreds of ppm) with positive $\delta^{37}Cl$ values (+1.2 to +4.2 ‰) in the serpentines, support the suggestion that hydrous minerals have relatively high concentrations of Cl and become enriched in $^{37}Cl/^{35}Cl$ upon formation by fluid-rock reactions (Schauble et al., 2003). The evolved residual fluids thus become depleted in Cl and $^{37}Cl/^{35}Cl$, as shown in the pore fluids at Nankai and Costa Rica. In contrast, the upwelling pore fluid at the Mariana serpentine mud volcanoes originates from dehydration of the subducting slab (Fryer et al., 1999; Mottl, 2003), thus is enriched in $^{37}Cl/^{35}Cl$ and Cl/Br ratios (chapter 2.6.1).

4.1.2 Implications for fluid flow and fluid mixing

The $\delta^{37}Cl$ data of the pore fluids acquired are used to interpret the fluid origins at the three subduction zones. At the Nankai subduction zone, due to the high geothermal gradient (~110°C/km), *in situ* smectite dehydration could account at most for ~13% dilution of Cl concentration in the pore fluid, whereas 19% of Cl dilution was observed. In addition, smectite dehydration alone does not explain the observed negative $\delta^{37}Cl$ signature because dilution does not fractionate the Cl stable isotopes or

Br/Cl ratios. Mass balance calculations show that the *in situ* clay mineral reaction can only decrease the pore fluid $\delta^{37}Cl$ from the seawater value to -0.1‰, compared to the $\delta^{37}Cl$ value of -7.8‰ observed. Hence, the very negative $\delta^{37}Cl$ observed in the lower Shikoku Basin requires mixing with a fluid having a negative $\delta^{37}Cl$ signature of ≤ -7.8‰, that originated from greater depths where higher temperature (Sharp et al., 2004) hydrous mineral formation, such as serpentine, uptake Cl, preferentially with ^{37}Cl, and exclude Br (Chapter 2.4.1).

At the Costa Rica subduction zone, the geothermal gradient is low (~10°C/km) thus the smectite-illite transition does not contribute to the *in situ* Cl freshening at the fracture zone and décollement at Site 1043/1255 and 1040/1254. The fresher than seawater pore fluid along the décollement and fracture zone represents a mixed fluid involving a fluid advected from the underthrust sediments where Cl concentration is close to the seawater value, and a deeply sourced fluid flowing along the décollement (Saffer et al., 2003). On the basis of transient advection-diffusion modeling in one dimension for the underthrust section (Desaulniers et al., 1986) (Crank, 1975), with the ratio of diffusivities of Cl (D_{37Cl}/D_{35Cl}=0.99857), the $\delta^{37}Cl$ value of the *in situ* fluid should be ~-1‰ at both Sites 1040/1254 and 1043/1255. The lower than ~-1‰ $\delta^{37}Cl$ values of -3.2 to -5.5 ‰ observed along the Costa Rica décollement, thus, suggest that a deep-sourced fluid along the décollement has Cl concentration of ≤ 480mM and $\delta^{37}Cl$ of ≤ -5.5 ‰ (Chapter 2.5.1).

By combining the mass balance equations (in Chapter 2.4.2) for Cl concentration and Cl stable isotope ratios, the pore fluid sample at the Cl

concentration minimum depth in the lower Shikoku Basin at Nankai is estimated to consists of ~50% *in situ* fluid and ~50% deep-sourced fluid at Site 808 and a ~55% and 45% mixture, respectively at Site 1174. Accordingly, the Cl concentration of the deep sourced fluid is ~410 mM and δ^{37}Cl is ~-16.9‰. At the Costa Rica décollement at ODP Site 1040, the sampled pore fluid is estimated to have Cl concentration of ~480-450 mM and δ^{37}Cl of -5.5 to -7.9 ‰. Hence, ~0-30 % of the *in situ* measured fluid is from advection/diffusion from the underthrust section, and ~100-70% consists of the deep sourced fluid at Site 1040; at Site 1043, the calculated fluid mixing is 40-55% and 60-45%, respectively (Chapter 2.5.2).

4.1.3 Cl and Cl isotope cyclings in the ocean

Serpentines are estimated to compose 10-20 % of oceanic crust (Carlson, 2001) and contain ~13 wt% H_2O and hundreds to thousands of ppm of Cl. They are the most important Cl and H_2O solid phase reservoir in the subducting plate and the mantle wedge, thus may impact Cl and δ^{37}Cl cyclings in the ocean. Therefore, in addition to Mariana, serpentines collected from Hess Deep and various other locations also have high Cl concentration (up to ~600 ppm) and positive δ^{37}Cl (~+1.2 to +6.0 ‰). Using TG-DSC, three different forms of serpentine, chrysotile, lizardite, and antigorite, can be identified, thus may explain the various Cl concentrations in serpentines (Chapter 2.6.2 and 2.7.1).

In summary, three fluid sources carrying distinct $\delta^{37}Cl$ signals into the ocean have been identified. They are (1) pore fluid refluxes with negative $\delta^{37}Cl$ values (-7.8‰ to -5.5‰) observed at the Nankai and Costa Rica subduction zones. The deep sourced fluid is originated from hydrous minerals formation; (2) the recycling of Cl associated with the upwelling fluid from slab dehydration with higher than seawater $\delta^{37}Cl$ values of +1.8 ‰; and (3) fluids through hydrothermal vents with end-member $\delta^{37}Cl$ values of +2.4 to 4.1‰. Serpentines and evaporites constitute the sink for Cl and ^{37}Cl. The oceanic $\delta^{37}Cl$ mass balance calculation indicates that when the minimum $\delta^{37}Cl$ value of each input and output flux is used, the ocean $\delta^{37}Cl$ is at steady state, whereas if the maximum values are used, the ocean $\delta^{37}Cl$ decreased by at most ~0.4‰ over the past 200 Ma (Chapter 2.7.2).

4.1.4 Hydrothermal Experiments

Although the $\delta^{37}Cl$ and Br/Cl data are powerful tools to trace the type of fluid-rock reactions, they can only be used to differentiate low temperature diagenesis from higher temperature hydrous mineral formation, or dehydration. Therefore, a different approach was taken to better constrain the fluid-rock reaction temperatures by conducting hydrothermal experiments. Two types of solids, basaltic ash from Lau Basin and smectite from Barbados, and two types of fluids, filtered seawater (sw) or sulfate-free artificial seawater (asw), were used as the starting materials. The

water/rock mass ratio was ~5-8, and the temperature is from 35 to 350°C at 25°C to 50°C increments, at 600 bar pressure (Chapter 3).

The mobilities of major (Ca and Mg), trace elements (Sr, Ba, and U), and especially of alkali metals (Li, K, Rb, Cs) were studied in detail. In general, the loss of Ca, Si and alkali elements from the solids and the loss of Mg from the fluid in the basalt and smectite experiments agree well with the behaviors of these elements in natural submarine hydrothermal systems (Edmond et al., 1979; Elderfield et al., 1996). In both basalt and smectite experiments, all four alkali metals show different release patterns as a function of temperature, implying that alkali elements fractionate during hydrothermal reactions and may be used as approximate geothermometers, to derive fluid source temperature at subduction zones. An example discussed in Chapter 3 is using K concentration and Li/K ratio of the pore fluids to constrain the temperature range at the deep fluid source along the décollement between 100 - 275˚C at the Costa Rica subduction zone.

The hydrothermal experiment data also show that Cs and Li concentrations, and Li and Sr isotope ratios in the reacted fluids have already been significantly modified at temperature as low as 50 °C. This observation suggests that their exchanges between the solids and fluids are not confined to the high-temperature hydrothermal ridge crest environment, but also occurs to a lesser extent at lower temperatures (50-200°C). Hence, Cs, Li and $^{87}Sr/^{86}Sr$ fluxes at ridge flanks most probably contribute significantly to their oceanic budgets. The newly obtained data for

alkali metals, especially for Cs, and Li and Sr isotopes in the hydrothermal experiments may partially resolve their apparent imbalances in the ocean.

4.2 Prospective

4.2.1 Cl isotopes of hydrothermal fluids

The hydrothermal flux may exert an important influence on Cl isotope cycling in the ocean due to its large fraction in the total Cl fluxes (Chapter 2.7.2). In this study, the newly acquired $\delta^{37}Cl$ values for the hydrothermal fluids from EPR (9°N) obtained by Seyfried are used to estimate the $\delta^{37}Cl$ input from hydrothermal vents. The available data of hydrothermal fluids from EPR (9°N), however, may not represent the average $\delta^{37}Cl$ value of global hydrothermal fluids. In addition, the published $\delta^{37}Cl$ data of hydrothermal fluids to date are rather variable and different methodologies were used. For sites at EPR (9°N), the data range from +7.1 to +6.5 ‰, analyzed by Secondary Ion Mass Spectrometry (SIMS) (Bach et al., 2002), and +2.4 to 4.1 ‰, analyzed by TIMS in this study. For Logatchev site (Mid-Atlantic Ridge), the data range from +4.6‰ analyzed by SIMS (Bach et al., 2002), to -0.03 ‰ analyzed by Isotope Ratio Mass Spectrometer (IRMS) (Bonifacie et al., 2005). Thus, for better average $\delta^{37}Cl$ value of natural hydrothermal ridge crest fluid, it would be necessary to conduct a global survey and have an inter-laboratory calibration of Cl stable isotope analysis for different methods.

4.2.2 Br element and Br stable isotope ratio

Although bromine is two orders of magnitude less abundant than chlorine, it accounts for approximately one-third of halogen-catalysed ozone depletion. It has been suggested that local ozone depletion and small ozone "holes" may occur in the vicinity of active volcanoes, and that the amount of bromine emitted from volcanoes might be sufficiently large to play a role in both stratosphere and troposphere chemistry (Bobrowski, 2003). Therefore, future research on Br concentration in volcanoes is especially important for environmental concerns.

Based on the relative mass difference of the two Br stable isotopes (^{79}Br and ^{81}Br) and observed Cl stable isotope variations, the expected range for the natural environment Br isotopes is at least 5-6 ‰. The combination of the Cl and Br systems could provide unique constraints on fluid/mineral reactions and temperatures.

4.2.3 Geothermometry

Alkali metals have been shown to be potential approximate geothermometers that may be used to estimate temperatures at greater depths where the deep-sourced fluid originates in subduction zones (Chapter 3.4). The current estimated temperature based on alkali concentrations is based on curve fitting. Similar to existing cation geothermometers, such as Li-Mg, Na-Li, Na-K-Ca (Martin, 1993), the empirical equation is yet to be derived in order to better constrain the temperature calculations of

fluids originated in various geologic settings. To achieve this goal, it is essential to conduct a series of fluid-rock hydrothermal experiments with different type of minerals and reach fluid-mineral equilibria, thus determine the controlling mineral(s) during the fluid-rock reactions at given temperature and pressure.

REFERENCES

Al-Niami, A. N. S. and Rushton, K. R., 1977. Analysis of flow against dispersion in porous media. *J. Hydrol.* 33: 87-97.

Anderson, A. T., 1974. Chlorine, Sulfur, and Water in Magmas and Oceans. *Geological Society of America Bulletin* 85(9): 1485-1492.

Aumento, F. and Loubat, H., 1971. The Mid-Atlantic ridge near 45 degrees N; XVI, Serpentinized ultramafic intrusions. *Canadian Journal of Earth Sciences* 8(6): 631-663.

Bach, W., Layne, G. L., Von Damm, K. L. and Anonymous, 2002. delta (super 37) Cl of mid-ocean ridge vent fluids determined by a new SIMS method for stable chlorine isotope ratio measurements. Eos, Transactions, AGU.

Baker, P. A., Gieskes, J. M. and Elderfield, H., 1982. Diagenesis of carbonates in deep-sea sediments; evidence from Sr/Ca ratios and interstitial dissolved Sr (2+) data. *Journal of Sedimentary Petrology* 52(1): 71-82.

Benton, L. D., 1997. Origin and evolution of serpentine seamount fluids, Mariana and Izu-Bonin forearcs; implications for the recycling of subducted material. Thesis, University of Tulsa, Tulsa, OK, United States (USA): 209 pp.

Benton, L. D., Ryan, J. G. and Tera, F., 2001. Boron isotope systematics of slab fluids as inferred from a serpentine seamount, Mariana Forearc. *Earth and Planetary Science Letters* 187(3-4): 273-282.

Berger, G., Schott, J. and Guy, C., 1988. Behavior of Li, Rb and Cs during basalt glass and olivine dissolution and chlorite, smectite and zeolite precipitation from seawater; experimental investigations and modelization between 50 degrees and 300 degrees C. *Chemical Geology* 71(4): 297-312.

Bischoff, J. L. and Dickson, F. W., 1975. Seawater-basalt interaction at 200 degrees C and 500 bars; implications for origin of sea-floor heavy-metal deposits and regulation of seawater chemistry. *Earth and Planetary Science Letters* 25(3): 385-397.

Bobrowski, N. H., G.; Galle, B.; Platt, U., 2003. Detection of bromine monoxide in a volcanic plume. *Nature* 423: 273-276.

Bonifacie, M., Charlou, J. L., Jendrzejewski, N., Agrinier, P. and Donval, J. P., 2005. Chlorine isotopic compositions of high temperature hydrothermal vent fluids over ridge axes. *Chemical Geology* 221(3-4): 279-288.

Boudreau, A. E., Stewart, M. A. and Spivack, A. J., 1997. Stable Cl isotopes and origin of high-Cl magmas of the Stillwater Complex, Montana. *Geology* 25(9): 791-794.

Bray, A. M., 2001. The Geochemistyr of boron and lithium in mid-ocean rige hydrothermal vent fluids. *Ph.D. thesis, University of New Hampshire*: 125pp.

Bray, A. M., Chan, L. H. and Von Damm, K. L., 2001. Constancy of the Li-isotope signature in mid-ocean hydrothermal fluids; evidence for equilibrium control. *EOS, Trans. Amer. Geophysical Union* 82(47): Abstract V12E-09.

Butterfield, D. A., Nelson, B. K., Wheat, C. G., Mottl, M. J. and Roe, K. K., 2001. Evidence for basaltic Sr in midocean ridge-flank hydrothermal systems and implications for the global oceanic Sr isotope balance. *Geochimica et Cosmochimica Acta* 65(22): 4141-4153.

Campbell, A. C., Palmer, M. R., Klinkhammer, G. P., Bowers, T. S., Edmond, J. M., Lawrence, J. R., Casey, J. F., Thompson, G., Humphris, S., Rona, P. A. and Karson, J. A., 1988. Chemistry of hot springs on the Mid-Atlantic Ridge. *Nature* 335(6190): 514-519.

Carlson, R. L., 2001. The abundance of ultramafic rocks in Atlantic Ocean crust. *Geophysical Journal International* 144(1): 37-48.

Carlson, R. L. and Miller, D. J., 2003. Mantle wedge water contents estimated from seismic velocities in partially serpentinized peridotites. *Geophysical Research Letters* 30: no.5, 4.

Carson, B., Suess, E. and Strasser, J. C., 1990. Fluid flow and mass flux determinations at vent sites on the Cascadia margin accretionary prism. *Journal of Geophysical Research, B, Solid Earth and Planets* 95(6): 8891-8897.

Chan, L.-H., Gieskes, J. M., You, C.-F. and Edmond, J. M., 1994. Lithium isotope geochemistry of sediments and hydrothermal fluids of the Guaymas Basin, Gulf of California. *Geochimica et Cosmochimica Acta* 58(20): 4443-4454.

Chan, L.-H. and Kastner, M., 2000. Lithium isotopic compositions of pore fluids and sediments in the Costa Rica subduction zone: implications for fluid processes and sediment contribution to the arc volcanoes. *Earth and Planetary Science Letters* 183(1-2): 275-290.

Chan, L. H., Edmond, J. M., Thompson, G. and Gillis, K., 1992. Lithium isotopic composition of submarine basalts: implications for the lithium cycle in the oceans. *Earth and Planetary Science Letters* 108(1-3): 151-160.

Chan, L. H., Leeman, W. P. and You, C.-F., 1999. Lithium isotopic composition of Central American Volcanic Arc lavas: implications for modification of subarc mantle by slab-derived fluids. *Chemical Geology* 160(4): 255-280.

Chan, L. H., Leeman, W. P. and You, C.-F., 2002. Lithium isotopic composition of Central American volcanic arc lavas: implications for modification of subarc mantle by slab-derived fluids: correction. *Chemical Geology* 182(2-4): 293-300.

Christensen, N. I., 1972. The abundance of serpentinites in the oceanic crust. *Journal of Geology* 80(6): 709-719.

Chung, C.-H., You, C.-F., Huang, W.-R. and Hsieh, Y.-T., 2002. The systematics of strontium and chlorine isotopes in hot springs and mud volcano fluids in Taiwan accretionary wedge. *Eos, Transactions, American Geophysical Union* 83(47, Suppl.): 1422.

Crank, J., 1975. *The mathematics of diffusion*, Oxford University press.

Davis, A. C., Bickle, M. J. and Teagle, D. A. H., 2003. Imbalance in the oceanic strontium budget. *Earth and Planetary Science Letters* 211(1-2): 173-187.

Deer, W. A., Howie, R.A., and Zussman, J., 1978. Rock-forming minerals.

Deruelle, B., Dreibus, G. and Jambon, A., 1992. Iodine abundances in oceanic basalts; implications for Earth dynamics. *Earth and Planetary Science Letters* 108(4): 217-227.

Desaulniers, D. E., Kaufmann, R. S., Cherry, J. A. and Bentley, H. W., 1986. (super 37 Cl- (super 35 Cl variations in a diffusion-controlled groundwater system. *Geochimica et Cosmochimica Acta* 50(8): 1757-1764.

Deyhle, A., 2001. Improvements of boron isotope analysis by positive thermal ionization mass spectrometry using static multicollection of Cs2BO2+ ions. *International Journal of Mass Spectrometry* 206(1-2): 79-89.

Driebus, G. S., B., Wanke, H., 1979. *Origin and distribution of the elements : proceedings of the second symposium, Paris, May 1977*. Oxford; New York, Pergamon Press.

Dunk, R. M., Mills, R. A., Jenkins, W. J., Mottl, M. J., Wheat, G., Devey, C. W. and Anonymous, 2002. The behaviour of uranium in a ridge flank setting. *Eos, Transactions, American Geophysical Union* 83(47, Suppl.): 1421.

Edmond, J. M., Measures, C., McDuff, R. E., Chan, L. H., Collier, R. and Grant, B., 1979. Ridge crest hydrothermal activity and the balances of the major and minor elements in the ocean; the Galapagos data. *Earth and Planetary Science Letters* 46(1): 1-18.

Eggenkamp, H. G. M., and Coleman, M.L., 1995. δ^{37}Cl variations in selected minerals: a possible tool for exploration. *J Geoch Exploration* 55: 249-255.

Eggenkamp, H. G. M., Middelburg, J. J. and Kreulen, R., 1994. Preferential diffusion of 35Cl relative to 37Cl in sediments of Kau Bay, Halmahera, Indonesia. *Chemical Geology* 116(3-4): 317-325.

Elderfield, H. and Schultz, A., 1996. Mid-ocean ridge hydrothermal fluxes and the chemical composition of the ocean. *Annual Review of Earth and Planetary Sciences* 24: 191-224.

Elderfield, H., Wheat, C. G., Mottl, M. J., Monnin, C. and Spiro, B., 1999. Fluid and geochemical transport through oceanic crust: a transect across the eastern flank of the Juan de Fuca Ridge. *Earth and Planetary Science Letters* 172(1-2): 151-165.

Fouillac, C. and Michard, G., 1981. Sodium/lithium ratio in water applied to geothermometry of geothermal reservoirs. *Geothermics* 10(1): 55-70.

Fournier, R. O., 1981. *Geothermal systems : principles and case histories*. New York, Wiley.

Fournier, R. O. and Potter, R. W., II, 1979. Magnesium correction to the Na-K-Ca chemical geothermometer. *Geochimica et Cosmochimica Acta* 43(9): 1543-1550.

Foustoukos, D. I., James, R. H., Berndt, M. E. and Seyfried, W. E., Jr., 2004. Lithium isotopic systematics of hydrothermal vent fluids at the Main Endeavour Field, northern Juan de Fuca Ridge. *Chemical Geology* 212(1-2): 17-26.

Froelich, P. N., Mortlock, R. A., Mefferd, M. and Powers, J., 1991. Interstitial water chemistry: abyssal South Atlantic and East Georgia Basins, Islas Orcadas and Meteor Rises. *Proc. ODP, Scientific Results* 114: 719-731.

Fryer, P., Ambos, E. L. and Hussong, D. M., 1985. Origin and emplacement of Mariana forearc seamounts. *Geology* 13(11): 774-777.

Fryer, P., Lockwood, J. P., Becker, N., Phipps, S. and Todd, C. S., 2000. Significance of serpentine mud volcanism in convergent margins. *Special Paper - Geological Society of America* 349: 35-51.

Fryer, P., Mottl, M., Johnson, L., Haggerty, J., Phipps, S. and Maekawa, H., 1995. Serpentine bodies in the forearcs of western Pacific convergent margins; origin and associated fluids. *Geophysical Monograph* 88: 239-279.

Fryer, P., Mottl, M. J., Pearce, J. A., Stokking, L. B., Ali, J. R. and al, e., 1992. Lithology, mineralogy, and origin of serpentine muds recovered from Conical and Torishima forearc seamounts; results of Leg 125 drilling. *Proceedings of the Ocean Drilling Program, Scientific Results* 125: 343-362.

Fryer, P., Pearce, J. A., Stokking, L. B. and Anonymous, 1990. Results of ODP Leg 125 drilling in the Mariana/Izu-Bonin forearcs. *AAPG Bulletin* 74(6): 973.

Fryer, P., Wheat, C. G. and Mottl, M. J., 1999. Mariana blueschist mud volcanism; implications for conditions within the subduction zone. *Geology* 27(2): 103-106.

Gieskes, J. M., Mahn, C., and Schnetzger, B., 2000. Data report: Trace element geochemistry of I-, Br-, F-, HPO42-, Ba2+, and Mn2+ in pore waters of Escanaba Trough, Sites 1037 and 1038. . *In Zierenberg, R.A., Fouquet, Y., Miller, D.J., and Normark, W.R. (Eds.), Proc. ODP, Sci. Results* 169.

Gieskes, J. M., Simoneit, B. R. T., Goodfellow, W. D., Baker, P. A. and Mahn, C., 2002. Hydrothermal geochemistry of sediments and pore waters in Escanaba Trough--ODP Leg 169. *Applied Geochemistry* 17(11): 1435-1456.

Godon, A., Jendrzejewski, N., Eggenkamp, H. G. M., Banks, D. A., Ader, M., Coleman, M. L. and Pineau, F., 2004. A cross-calibration of chlorine isotopic measurements and suitability of seawater as the international reference material. *Chemical Geology* 207(1-2): 1-12.

Griffin, J. J., Windom, H. and Goldberg, E. D., 1968. The distribution of clay minerals in the world ocean. *Deep-Sea Research and Oceanographic Abstracts* 15(4): 433-459.

Hart, S. R., 1969. K, Rb, Cs contents and K/Rb, K/Cs ratios of fresh and altered submarine basalts. *Earth and Planetary Science Letters* 6(4): 295-303.

Hart, S. R. and Staudigel, H., 1982. The control of alkalies and uranium in seawater by ocean crust alteration. *Earth and Planetary Science Letters* 58(2): 202-212.

Henry, P. and Bourlange, S., 2004. Smectite and fluid budget at Nankai ODP sites derived from cation exchange capacity. *Earth and Planetary Science Letters* 219(1-2): 129-145.

Hodell, D. A., Mead, G. A. and Mueller, P. A., 1990. Variation in the strontium isotopic composition of seawater (8 Ma to present) : Implications for chemical weathering rates and dissolved fluxes to the oceans. *Chemical Geology: Isotope Geoscience section* 80(4): 291-307.

Holland, H. D., 1978. *The chemistry of the atmosphere and oceans*. New York, Wiley.

Holland, H. D., 1984. The chemical evolution of the atmosphere and oceans. Princeton series in geochemistry. Princeton, N.J. :, Princeton University Press,.

Hubbert, M. K. and Rubey, W. W., 1959. Mechanics of fluid-filled porous solids and its application to overthrust faulting, [Part] 1 of Role of fluid pressure in mechanics of overthrust faulting. *Geological Society of America Bulletin* 70(2): 115-166.

Huh, Y., Chan, L.-H., Zhang, L. and Edmond, J. M., 1998. Lithium and its isotopes in major world rivers; implications for weathering and the oceanic budget. *Geochimica et Cosmochimica Acta* 62(12): 2039-2051.

Hurwitz, S., Mariner, R. H., Fehn, U. and Snyder, G. T., 2005. Systematics of halogen elements and their radioisotopes in thermal springs of the Cascade Range, Central Oregon, Western USA. *Earth and Planetary Science Letters* 235(3-4): 700-714.

Hyndman, R. D. and Peacock, S. M., 2003. Serpentinization of the forearc mantle. *Earth and Planetary Science Letters* 212(3-4): 417-432.

Hyndman, R. D. and Wang, K., 1993. Thermal constraints on the zone of major thrust earthquake failure; the Cascadia subduction zone. *Journal of Geophysical Research, B, Solid Earth and Planets* 98(2): 2039-2060.

Jackson, M. L., 1973. Soil chemical analysis-advanced course 2nd edition, 8th printing. Dept. Soil Science, University of Wisconsin, Madison.

Jambon, A., 1994. Earth degassing and large-scale geochemical cycling of volatile elements. *Reviews in Mineralogy* 30: 479-517.

James, R. H., Allen, D. E. and Seyfried, W. E., Jr., 2003. An experimental study of alteration of oceanic crust and terrigenous sediments at moderate temperatures (51 to 350 degrees C); insights as to chemical processes in near-shore ridge-flank hydrothermal systems. *Geochimica et Cosmochimica Acta* 67(4): 681-691.

James, R. H. and Palmer, M. R., 2000. Marine geochemical cycles of the alkali elements and boron; the role of sediments. *Geochimica et Cosmochimica Acta* 64(18): 3111-3122.

James, R. H., Rudnicki, M. D. and Palmer, M. R., 1999. The alkali element and boron geochemistry of the Escanaba Trough sediment-hosted hydrothermal system. *Earth and Planetary Science Letters* 171(1): 157-169.

Kastner, M., Elderfield, H., Jenkins, W. J., Gieskes, J. M. and Gamo, T., 1993. Geochemical and isotopic evidence for fluid flow in the western Nankai subduction zone, Japan. *Proceedings of the Ocean Drilling Program, Scientific Results* 131: 397-413.

Kastner, M., Elderfield, H. and Martin, J. B., 1991. Fluids in convergent margins; what do we know about their composition, origin, role in diagenesis and importance for oceanic chemical fluxes? *Philosophical Transactions of the Royal Society of London, Series A: Mathematical and Physical Sciences* 335(1638): 243-259.

Kastner, M. and Rudnicki, M. D., 2004. *Hydrogeology of the ocean lithosphere*. New York :, Cambridge,.

Kastner, M., Solomon, E., Wei, W., Chan, L.-H., and Saether, O.M., 2006. Data report: Chemical and isotopic compositions of pore fluids and sediments from across the Middle America Trench, offshore Costa Rica. *In Morris, J.D., Villinger, H.W., and Klaus, A. (Eds.), Proc. ODP, Sci. Results* 205.

Kaufmann, R., Long, A., Bentley, H. and Davis, S., 1984. Natural chlorine isotope variations. *Nature* 309(5966): 338-340.

Kerrick, D., 2002. Serpentinite seduction. *Science* 298(5597): 1344-1345.

Kharaka, Y. K. and Mariner, R. H., 1989. Chemical geothermometers and their application to formation waters from sedimentary basins.

Kimura, G., Silver, E., Blum, P., *et al.*, 1997. *Proc. ODP, Init. Repts.* 170: College Station, TX (Ocean Drilling Program).

Lemarchand, D., Gaillardet, J., Lewin, E. and Allegre, C. J., 2000. The influence of rivers on marine boron isotopes and implications for reconstructing past ocean pH. *Nature* 408(6815): 951-954.

Long, A., Eastoe, C. J., Kaufmann, R. S., Martin, J. G., Wirt, L. and Finley, J. B., 1993. High-precision measurement of chlorine stable isotope ratios. *Geochimica et Cosmochimica Acta* 57(12): 2907-2912.

Magenheim, A. J., Spivack, A. J., Alt, J. C., Bayhurst, G., Chan, L. H. and al, e., 1995. Borehole fluid chemistry in Hole 504B, Leg 137; formation water or in-situ reaction. *Proceedings of the Ocean Drilling Program, Scientific Results* 137/140: 141-152.

Magenheim, A. J., Spivack, A. J., Michael, P. J. and Gieskes, J. M., 1995. Chlorine stable isotope composition of the oceanic crust; implications for Earth's distribution of chlorine. *Earth and Planetary Science Letters* 131(3-4): 427-432.

Magenheim, A. J., Spivack, A. J., Volpe, C. and Ransom, B., 1994. Precise determination of stable chlorine isotopic ratios in low-concentration natural samples. *Geochimica et Cosmochimica Acta* 58(14): 3117-3121.

Martin, J. B., 1993. Origins and compositions of fluids at convergent margins, University of California at San Diego. Ph.D. thesis: 181 pages.

Martin, J. B., Kastner, M. and Elderfield, H., 1991. Lithium; sources in pore fluids of Peru slope sediments and implications for oceanic fluxes. *Marine Geology* 102(1-4): 281-292.

Miura, Y., Rucklidge, J. and Nord, G. L., 1981. The occurrence of chlorine in serpentine minerals. *Contributions to Mineralogy and Petrology* 76(1): 17-23.

Miyashiro, A., Shido, F. and Ewing, M., 1969. Composition and origin of serpentinites from the mid-atlantic ridge near 24deg and 30deg north latitude. *Contributions to Mineralogy and Petrology* 23(2): 117-127.

Moore, G. F., Shipley, T. H., Stoffa, P. L., Karig, D. E., Taira, A., Kuramoto, S., Tokuyama, H. and Suyehiro, K., 1990. Structure of the Nankai Trough accretionary zone from multichannel seismic reflection data. *Journal of Geophysical Research, B, Solid Earth and Planets* 95(6): 8753-8765.

Moore, G. F., Taira, A. and Bangs, N. L., 2001. *Proc. ODP Init. Repts.* 190:College Station, TX (Ocean Drilling Program).

Moore, J. C. and Vrolijk, P., 1992. Fluids in accretionary prisms. *Reviews of Geophysics* 30(2): 113-135.

Morris, J. D., Villinger, H.W., Klaus, A., *et al.*, 2003. *Proc. ODP Init. Repts.* 205: College Station, TX (Ocean Drilling Program).

Mottl, M. J., Fryer, P., Pearce, J. A., Stokking, L. B., Ali, J. R. and al, e., 1992. Pore waters from serpentinite seamounts in the Mariana and Izu-Bonin forearcs, Leg 125; evidence for volatiles from the subducting slab. *Proceedings of the Ocean Drilling Program, Scientific Results* 125: 373-385.

Mottl, M. J., S. C. Komor, P. Fryer, C. L. Moyer, 2003. Deep-slab fluids fuel extremophilic Archaea on a Mariana forearc serpentinite mud volcano: Ocean Drilling Program Leg 195. *Geochem. Geophys. Geosyst.* 4(11): doi:10.1029/2003GC000588.

Mottl, M. J. and Wheat, C. G., 1994. Hydrothermal circulation through mid-ocean ridge flanks: Fluxes of heat and magnesium. *Geochimica et Cosmochimica Acta* 58(10): 2225-2237.

Musashi, M. and Eggenkamp, H. G. M., 2000. Cl isotope compositions of fumarolic gas from a Japanese volcanic island. *Goldschmidt* 5(2): 733.

Numata, M., Nakamura, N. and Gamo, T., 2001. Precise measurement of chlorine stable isotopic ratios by thermal ionization mass spectrometry. *Geochemical Journal* 35(2): 89-100.

O'Hanley, D. S., 1996. *Serpentinites : records of tectonic and petrological history*.

Oosting, S. E. and Von Damm, K. L., 1996. Bromide/chloride fractionation in seafloor hydrothermal fluids from 9-10 degrees N East Pacific Rise. *Earth and Planetary Science Letters* 144(1-2): 133-145.

Page, N. J. and Coleman, R. G., 1967. Serpentine-mineral analyses and physical properties. *Geological Survey Research*(U.S. Geol. Survey Prof. Paper 575B): B103-107.

Palmer, M. R. and Edmond, J. M., 1989. Cesium and rubidium in submarine hydrothermal fluids; evidence for recycling of alkali elements. *Earth and Planetary Science Letters* 95(1-2): 8-14.

Palmer, M. R. and Edmond, J. M., 1989. The strontium isotope budget of the modern ocean. *Earth and Planetary Science Letters* 92(1): 11-26.

Patino, L. C., Carr, M. J. and Feigenson, M. D., 2000. Local and regional variations in Central American arc lavas controlled by variations in subducted sediment input. *Contributions to Mineralogy and Petrology* 138(3): 265-283.

Peacock, S. M., 1990. Fluid processes in subduction zones. *Science* 248(4953): 329-337.

Peacock, S. M., 2001. Are the lower planes of double seismic zones caused by serpentine dehydration in subducting oceanic mantle? *Geology* 29(4): 299-302.

Peacock, S. M. and Hervig, R. L., 1999. Boron isotopic composition of subduction-zone metamorphic rocks. *Chemical Geology* 160(4): 281-290.

Perry, E. and Hower, J., 1970. Burial diagenesis in Gulf Coast pelitic sediments. *Clays and Clay Minerals* 18(3): 165-177.

Philippot, P., Agrinier, P. and Scambelluri, M., 1998. Chlorine cycling during subduction of altered oceanic crust. *Earth and Planetary Science Letters* 161(1-4): 33-44.

Philippot, P. and Selverstone, J., 1991. Trace-element-rich brines in eclogitic veins; implications for fluid composition and transport during subduction. *Contributions to Mineralogy and Petrology* 106(4): 417-430.

Price, N. B. and Calvert, S. E., 1977. The contrasting geochemical behaviours of iodine and bromine in recent sediments from the Namibian shelf. *Geochimica et Cosmochimica Acta* 41(12): 1769-1775.

Ransom, B., Spivack, A. J. and Kastner, M., 1995. Stable Cl isotopes in subduction-zone pore waters; implications for fluid-rock reactions and the cycling of chlorine. *Geology* 23(8): 715-718.

Richter, F. M., Mendybaev, R. A., Christensen, J. N., Hutcheon, I. D., Williams, R. W., Sturchio, N. C. and Beloso, J. A. D., 2006. Kinetic isotopic fractionation during diffusion of ionic species in water. *Geochimica et Cosmochimica Acta* 70(2): 277-289.

Rosenbauer, R. J., Bischoff, J. L. and Potter, J. M., 1993. A flexible Au-Ir cell with quick assembly for hydrothermal experiments. *American Mineralogist* 78(11-12): 1286-1289.

Rubey, W. W., 1951. Geologic history of sea water. *Geological Society of America Bulletin* 62(9): 1111-1147.

Ruepke, L. H., Morgan, J. P., Hort, M. and Anonymous, 2002. Does slab serpentinization and deserpentinization create the primary HIMU mantle component? *Geochimica et Cosmochimica Acta* 66(15A): 656.

Saffer, D. M. and Bekins, B. A., 1998. Episodic fluid flow in the Nankai accretionary complex; timescale, geochemistry, flow rates, and fluid budget. *Journal of Geophysical Research* 103(B12): 30,351-30,370.

Saffer, D. M. and Screaton, E. J., 2003. Fluid flow at the toe of convergent margins; interpretation of sharp pore-water geochemical gradients. *Earth and Planetary Science Letters* 213(3-4): 261-270.

Salisbury, M. H., Shinohara, M., Richter, C., *et al.* , 2002. *Proc. ODP Init. Repts.* 195: College Station, TX (Ocean Drilling Program).

Sanford, R. F., 1981. Mineralogical and chemical effects of hydration reactions and applications to serpentinization. *American Mineralogist* 66(3-4): 290-297.

Scambelluri, M., Muentener, O., Hermann, J., Piccardo, G. B. and Trommsdorff, V., 1995. Subduction of water into the mantle; history of an Alpine peridotite. *Geology* 23(5): 459-462.

Scambelluri, M. and Philippot, P., 2001. Deep fluids in subduction zones. *Lithos* 55(1-4): 213-227.

Scambelluri, M., Piccardo, G. B., Philippot, P., Robbiano, A. and Negretti, L., 1997. High salinity fluid inclusions formed from recycled seawater in deeply subducted Alpine serpentinite. *Earth and Planetary Science Letters* 148(3-4): 485-499.

Schauble, E. A., Rossman, G. R. and Taylor, J., H. P., 2003. Theoretical estimates of equilibrium chlorine-isotope fractionations. *Geochimica et Cosmochimica Acta* 67(17): 3267-3281.

Schilling, J. G., Bergeron, M. B., Evans, R., Bailey, D. K., Tarney, J. and Dunham, K., 1980. Halogens in the mantle beneath the North Atlantic. *Philosophical Transactions of the Royal Society of London, Series A: Mathematical and Physical Sciences* 297(1431): 147-178.

Schilling, J. G., Unni, C. K. and Bender, M. L., 1978. Origin of chlorine and bromine in the oceans. *Nature* 273(5664): 631-636.

Seno, T. D. Z., Y.Kobayashi, and M.Nakamura, 2001. Dehydration of serpentinized mantle: Seismic evidence from southwest Japan. *Earth Planets Space* 53: 861-871.

Seyfried, W. and Bischoff, J. L., 1977. Hydrothermal transport of heavy metals by seawater; the role of seawater/basalt ratio. *Earth and Planetary Science Letters* 34(1): 71-77.

Seyfried, W. E., Jr. and Bischoff, J. L., 1979. Low temperature basalt alteration by seawater; an experimental study at 70 degrees C and 150 degrees C. *Geochimica et Cosmochimica Acta* 43(12): 1937-1948.

Seyfried, W. E., Jr., Chen, X. and Chan, L.-H., 1998. Trace element mobility and lithium exchange during hydrothermal alteration of seafloor weathered basalt; an experimental study at 350 degrees C, 500 bars. *Geochimica et Cosmochimica Acta* 62(6): 949-960.

Seyfried, W. E., Jr. and Ding, K., 1995. The hydrothermal chemistry of fluoride in seawater. *Geochimica et Cosmochimica Acta* 59(6): 1063-1071.

Seyfried, W. E., Jr., Janecky, D. R. and Mottl, M. J., 1984. Alteration of the oceanic crust; implications for geochemical cycles of lithium and boron. *Geochimica et Cosmochimica Acta* 48(3): 557-569.

Sharp, Z. D. and Barnes, J. D., 2004. Water-soluble chlorides in massive sea-floor serpentinites; a source of chloride in subduction zones. *Earth and Planetary Science Letters* 226(1-2): 243-254.

Shaw, A. M., Hilton, D. R., Fischer, T. P., Walker, J. A. and Alvarado, G. E., 2003. Contrasting He-C relationships in Nicaragua and Costa Rica: insights into C cycling through subduction zones. *Earth and Planetary Science Letters* 214(3-4): 499-513.

Sigmarsson, O., Condomines, M., Morris, J. D. and Harmon, R. S., 1990. Uranium and (super 10) Be enrichments by fluids in Andean arc magmas. *Nature* 346(6280): 163-165.

Silver, E., Kastner, M., Fisher, A., Morris, J., McIntosh, K. and Saffer, D., 2000. Fluid flow paths in the Middle America Trench and Costa Rica margin. *Geology* 28(8): 679-682.

Smith, H. J., Spivack, A. J., Staudigel, H. and Hart, S. R., 1995. The boron isotopic composition of altered oceanic crust. *Chemical Geology* 126(2): 119-135.

Spivack, A. J. and Edmond, J. M., 1987. Boron isotope exchange between seawater and the oceanic crust. *Geochimica et Cosmochimica Acta* 51(5): 1033-1043.

Spivack, A. J., Kastner, M. and Ransom, B., 2002. Elemental and isotopic chloride geochemistry and fluid flow in the Nankai Trough. *Geophysical Research Letters* 29(14).

Spivack, A. J., You, C.-F. and Smith, H. J., 1993. Foraminiferal boron isotope ratios as a proxy for surface ocean pH over the past 21 Myr. *Nature* 363(6425): 149-151.

Stewart, M. A., Klein, E. M., Spivack, A. J., Langmuir, C. H., Karsten, J. L., Bender, J. F., Magenheim, A. J. and Anonymous, 1997. Stable Cl isotope compositions of N- and E-MORB glasses. *Eos, Transactions, American Geophysical Union* 78(17, Suppl.): 323.

Taylor, J. W. and Grimsrud, E. P., 1969. Chlorine isotopic ratios by negative ion mass spectrometry. *Anal. Chem.* 41 (6): 805 - 810.

Teichert, B. M. A., Eisenhauer, A., Bohrmann, G., Haase-Schramm, A., Bock, B. and Linke, P., 2003. U/Th systematics and ages of authigenic carbonates from Hydrate Ridge, Cascadia Margin: recorders of fluid flow variations. *Geochimica et Cosmochimica Acta* 67(20): 3845-3857.

Thompson, A. B., 1992. Water in the Earth's upper mantle. *Nature* 358(6384): 295-302.

Ulmer, P. and Trommsdorff, V., 1995. Serpentine stability to mantle depths and subduction-related magmatism. *Science* 268(5212): 858-861.

Underwood, M. B., and Pickering, K.T., 1996. Clay-mineral provenance, sediment dispersal patterns, and mudrock diagenesis in Nankai accretionary prism, southwest Japan. *Clays & Clay Minerals* 44: 339-356.

Underwood, M. B., Pickering, K., Gieskes, J. M., Kastner, M. and Orr, R., 1993. Sediment geochemistry, clay mineralogy, and diagenesis; a synthesis of data from Leg 131, Nankai Trough. *Proceedings of the Ocean Drilling Program, Scientific Results* 131: 343-363.

Vengosh, A., Kolodny, Y., Starinsky, A., Chivas, A. R. and McCulloch, M. T., 1991. Coprecipitation and isotopic fractionation of boron in modern biogenic carbonates. *Geochimica et Cosmochimica Acta* 55(10): 2901-2910.

Volpe, C., 1998. Stable chlorine isotope variations in the atmoshpere. *Ph.D. Thesis, Univ. of California, San Diego*.

Von Damm, K. L., 1988. Hydrothermal seawater-basalt-sediment interaction chemistry. *Applied Geochemistry* 3(1): 119.

Von Damm, K. L., 1990. Seafloor hydrothermal activity; black smoker chemistry and chimneys. *Annual Review of Earth and Planetary Sciences* 18: 173-204.

Von Damm, K. L., Bischoff, J. L. and Rosenbauer, R. J., 1991. Quartz solubility in hydrothermal seawater; an experimental study and equation describing quartz solubility for up to 0.5 M NaCl solutions. *American Journal of Science* 291(10): 977-1007.

von Huene, R., 1984. Tectonic processes along the front of modern convergent margins; research of the past decade. *Annual Review of Earth and Planetary Sciences* 12: 359-381.

von Huene, R. and Scholl, D. W., 1991. Observations at convergent margins concerning sediment subduction, subduction erosion, and the growth of continental crust. *Reviews of Geophysics* 29(3): 279-316.

Vrolijk, P., 1990. On the mechanical role of smectite in subduction zones. *Geology* 18(8): 703-707.

Wanke, H., 1981. Constitution of Terrestrial Planets. *Philosophical Transactions of the Royal Society of London. Series A, Mathematical and Physical Sciences.* 303: 287-301.

Warren, J. K., 2006. *Evaporites : sediments, resources and hydrocarbons*. Berlin ; New York :, Springer.

Wei, W., Kastner, M., Spivack, A. J., 2003. Halogen concentrations and stable isotopes (O, Sr, and Cl) in the Nankai Muroto Transect and their implication for fluid-sediment interactions and fluid flow. *Eos Trans. AGU, Fall Meeting Suppl., Abstract* 84(1459).

Wei, W., Kastner, M., Deyhle, A., and Spivack, A.J. , 2005. Geochemical cycling of fluorine, chlorine, bromine, and boron and implications for fluid-rock reactions

in Mariana forearc, South Chamorro Seamount. *ODP Leg 195. In Shinohara, M., Salisbury, M.H., and Richter, C. (Eds.), Proc. ODP, Sci. Results, 195*.

Wheat, C. G., Mottl, M. J. and Rudnicki, M., 2002. Trace element and REE composition of a low-temperature ridge-flank hydrothermal spring. *Geochimica et Cosmochimica Acta* 66(21): 3693-3705.

Whittaker, E. J. W. and Zussman, J., 1956. The characterization of serpentine minerals by x-ray diffraction. *Mineralogical Magazine* 31(233): 107-126.

Wicks, F. J. a. O. H., D.S., 1988. *Hydrous phyllosilicates : (exclusive of micas)*.

Xiao, Y. K. and Zhang, C. G., 1992. High-Precision Isotopic Measurement of Chlorine by Thermal Ionization Mass-Spectrometry of the Cs2cl+ Ion. *International Journal of Mass Spectrometry and Ion Processes* 116(3): 183-192.

Xiao, Y. K. Z., Y. M.; Liu, W. G. , 1995. Precise measurement of chlorine isotopes based on Cs2Cl+ by thermal ionization mass spectrometry. *Analytical Letters* 28(7): 1295-304.

You, C. F., Castillo, P. R., Gieskes, J. M., Chan, L. H. and Spivack, A. J., 1996. Trace element behavior in hydrothermal experiments; implications for fluid processes at shallow depths in subduction zones. *Earth and Planetary Science Letters* 140(1-4): 41-52.

You, C. F. and Chan, L.-H., 1996. Precise determination of lithium isotopic composition in low concentration natural samples. *Geochimica et Cosmochimica Acta* 60(5): 909-915.

You, C. F. and Gieskes, J. M., 2001. Hydrothermal alteration of hemi-pelagic sediments; experimental evaluation of geochemical processes in shallow subduction zones. *Applied Geochemistry* 16(9-10): 1055-1066.

You, C. F., Gieskes, J. M., Chen, R. F., Spivack, A. and Gamo, T., 1993. Iodide, bromide, manganese, boron, and dissolved organic carbon in interstitial waters of organic carbon-rich marine sediments; observations in the Nankai accretionary prism. *Proceedings of the Ocean Drilling Program, Scientific Results* 131: 165-174.

You, C. F., Spivack, A. J., Smith, J. H. and Gieskes, J. M., 1993. Mobilization of boron in convergent margins; implications for the boron geochemical cycle. *Geology* 21(3): 207-210.

Zhang, L., Chan, L. H. and Gieskes, J. M., 1998. Lithium isotope geochemistry of pore waters from Ocean Drilling Program sites 918 and 919, Irminger Basin. *Geochimica et Cosmochimica Acta* 62(14): 2437-2450.